8-27-2009

U-series dating, geochemistry, and geomorphic studies of travertines and springs of the Springerville area, east-central Arizona, and tectonic implications.

Eileen Hardy Embid

Eileen H. Embid
Candidate

Earth and Planetary Sciences
Department

This thesis is approved, and it is acceptable in quality and form for publication:

Approved by the Thesis Committee:

, Chairperson

Karl E Karlstrom

L. S. Crumpler

U-SERIES DATING, GEOCHEMISTRY, AND GEOMORPHIC STUDIES OF TRAVERTINES AND SPRINGS OF THE SPRINGERVILLE AREA, EAST-CENTRAL ARIZONA, AND TECTONIC IMPLICATIONS

BY

EILEEN H. EMBID

B.A., ART HISTORY
UNIVERSITY OF CALIFORNIA, SANTA CRUZ, 1979
B.S., EARTH AND PLANETARY SCIENCES
UNIVERSITY OF NEW MEXICO, 2005

THESIS

Submitted in Partial Fulfillment of the
Requirements for the Degree of

Master of Science

Earth and Planetary Sciences

The University of New Mexico
Albuquerque, New Mexico

August, 2009

ACKNOWLEDGMENTS

I would like to thank my advisors Dr. Laura J. Crossey and Dr. Karl E. Karlstrom for suggesting this project and for their help and support in all aspects of the work, including financial support. Thanks also to Dr. Larry S. Crumpler for taking the time to be part of my committee and for sharing his knowledge of the Springerville volcanic field. I owe my appreciation to him and to Dr. Jayne C. Aubele for organizing a wonderful tour of the field at the beginning of this study that provided the context for this investigation.

I also want to thank Dr. Yemane Asmerom for his generosity in allowing me the use of his laboratory and Dr. Victor J. Polyak for his patient and kind help with the U-series dating. Thanks also to Dr. Abdul-Mehdi S. Ali for the use of his laboratory and for his help with the water chemistry analyses.

Thanks to Brandi Cron and Euan Mitchell for help in the field and to the Department of Earth and Planetary Sciences for financial support through departmental scholarships.

.

U-SERIES DATING, GEOCHEMISTRY, AND GEOMORPHIC STUDIES OF TRAVERTINES AND SPRINGS OF THE SPRINGERVILLE AREA, EAST-CENTRAL ARIZONA, AND TECTONIC IMPLICATIONS

BY

EILEEN H. EMBID

ABSTRACT OF THESIS

Submitted in Partial Fulfillment of the
Requirements for the Degree of

Master of Science

Earth and Planetary Sciences

The University of New Mexico
Albuquerque, New Mexico

August, 2009

U-SERIES DATING, GEOCHEMISTRY, AND GEOMORPHIC STUDIES OF TRAVERTINES AND SPRINGS OF THE SPRINGERVILLE AREA, EAST-CENTRAL ARIZONA, AND TECTONIC IMPLICATIONS

by

Eileen H. Embid

B.A., Art History, University of California, Santa Cruz, 1979
B.S., Earth and Planetary Sciences, University of New Mexico, 2005
M.S., Earth and Planetary Sciences, University of New Mexico, 2009

ABSTRACT

High CO_2 springs and related travertine deposits of the Springerville area of east-central Arizona provide an exceptional field laboratory for understanding travertine-depositing spring systems. U-series dating of travertines provides an opportunity to unravel paleohydrologic and neotectonic histories near the southeastern edge of the Colorado Plateau. This interdisciplinary study combines water and gas chemistry data, travertine morphology and geochronology, analysis of geologic structures, basalt geochronology, and river incision studies to formulate an integrative model for both travertine formation and for landscape evolution of this region.

More than 70 individual travertine mounds and large platforms, formed from the coalesced deposits of multiple spring vents, cover a surface area of >33 km^2 near Springerville, Arizona. This area is at the intersection of the southeastern edge of the Colorado Plateau with the Jemez lineament, a northeast-trending zone of volcanic activity over the last 4.5 Ma. Travertine deposits occur in clusters near the Little

Colorado River (LCR) and along fault lineaments overlying the Springerville-St. Johns Dome, a faulted asymmetric anticline trapping a large natural CO_2 reservoir. This travertine and CO_2 system is bounded on the west by the Plio-Pleistocene Springerville volcanic field (SPV) which was active until 308 ka and on the east by the late Mio-Pleistocene Red Hill-Quemado volcanic field where volcanic activity continued until as recently as 71 ka.

Modern springs adjacent to the CO_2 field are actively degassing CO_2, have $C_{external}$ values of 50%, concentrations of TDS up to 2538 mg/l, and are currently depositing minor volumes of travertine. $^3He/^4He$ ratios from wells in the CO_2 field and adjoining springs range up to 0.58 R_A, indicating the presence of asthenospheric mantle-derived gases in modern spring waters (up to about 7% of the total helium). To explain the diversity of water chemistry in this small region, we hypothesize that deeply sourced fluids rise along NE- and NW-trending basement-penetrating faults that intersect at the SE end of the dome. These endogenic waters then mix with groundwater producing a complete mixing trend between meteoric and bicarbonate rich, high TDS end members.

Precise new U/Th dates indicate that travertine deposition began >350 ka, overlapping with waning volcanic activity in the Springerville and Red Hill-Quemado volcanic fields, and is still ongoing. Major times of accumulation at 350-300, 280-200, and 100-36 ka are interpreted to represent wetter paleohdrologic intervals. Synchronous outflow occurred from springs at different elevations above the LCR (from near river level up to 400 m above the river at ca. 200 ka) reflecting an unresolved combination of fluctuations in hydraulic head, gas pressure in the CO_2 reservoir, paleoseismicity, and partitioning dynamics of traps within the stacked CO_2 reservoir system. The life of one

major travertine mound system near the LCR that accumulated >20 m of layered travertine has been bracketed between 73 and 48 ka (25 ka). This mound formed from the sustained outflow of CO_2-charged spring waters from a central vent with a deposition rate of 0.94 m/ka.

Hiatuses of ~25-60 ka in the travertine rock record correlate with obliquity-forced warm interglacial peaks in the Devils Hole calcite $\delta^{18}O$ paleotemperature and global paleoclimate records. Periods of deposition also correlate with the five most recent volcanic episodes in the SPV and Red Hill-Quemado fields. Thus, the apparent ~70 ka cyclicity of travertine deposition appears to be due to a combination of increased climatically-modulated groundwater recharge during wet/glacial times and over-pressuring of the CO_2 / groundwater system due to the periodic influx of magmatically sourced fluids.

Dated travertines and basalts associated with elevated LCR gravel terraces in the region provide constraints on river incision and landscape denudation. Using the base of flows, basalt incision points indicate a long-term rate of 40-50 m/Ma. U-series dates on travertine that cements gravels directly above bedrock straths indicate incision rates of 100-150 m/Ma near Lyman Lake from 350-100 ka, increasing to 320 m/Ma in the last 100 ka.

TABLE OF CONTENTS

LIST OF FIGURES

LIST OF TABLES

INTRODUCTION

Travertine deposits provide insights and quantifiable information related to a wide range of earth system problems but their potential has been under-utilized. This paper presents an integrative study that investigates the spatial distribution and precise geochronology of travertine in the Springerville area of east-central Arizona. This area is a spectacular travertine occurrence located at the juncture of several regional provinces (Colorado Plateau, Basin and Range, and Jemez lineament) that provides an unparalleled opportunity to document links between groundwater and surface water chemistry, active faulting and magmatism, and economically important gas fields. Building on Crossey et al (2006; 2009), we also examine the potential use of travertines for paleoclimate and paleohydrology reconstructions; and to provide temporal constraints on regional landscape evolution, rates of incision, and denudation history (Pederson et al 2002; Karlstrom et al., 2007).

Modern springs can provide an analog for the types of water responsible for the large travertine accumulations. Springs, groundwater, and river water chemistries were characterized in order to develop an understanding of the modern hydrologic system. The modern Salado Spring waters within the Little Colorado River (LCR) corridor have high TDS, with concentrations up to 2538 mg/l. They are supersaturated with respect to calcite and aragonite, are actively degassing, and modern springs are rimmed by travertine mounds and cisterns that are similar to, although smaller in volume than, the adjacent older travertine mounds. About 5 km to the west, across a relatively sharp boundary locally referred to as the "badwater line" (Stone, 1979) (Fig. 1), chemistries of springs

are no longer supersaturated with respect to calcite or dolomite and have low CO_2 concentrations. This abrupt transition between zones of contrasting ground and surface water quality is demarcated by faults that appear to obstruct flow between gas-saturated waters mixed with deeply-sourced fluids from the CO_2 reservoir in the east and meteoric waters to the west. Thus, further chemical characterization of the modern groundwater system as presented below has important implications for understanding links between groundwater quality, the fault network, the distribution of travertines, and the origin of the gas field.

The travertine deposits near Springerville are one of the largest accumulations in the western United States covering >33 km^2 with >70 individual mounds and large coalesced platforms distributed over an area of ~800 km^2. Located near the southeastern edge of the Colorado Plateau, the Springerville area anchors the southwestern end of the Jemez lineament (Aldrich and Laughlin, 1984), an approximately 800-km long, 50-km wide NE-trending zone of basement-penetrating faults extending from the southeastern edge of the Colorado Plateau through the Jemez volcano of the Rio Grande rift, to the Texas panhandle. The lineament has been a zone of intense volcanism over the last 4.5 Ma. The travertines occur along the LCR where the river flows between two centers of late Cenozoic volcanism, the Plio-Pleistocene Springerville volcanic field (SPV) on the west and the late Mio-Pleistocene Red Hill-Quemado (RH-Q) volcanic field on the east (Fig. 1). A broad anticlinal fold straddles the Arizona / New Mexico border between the

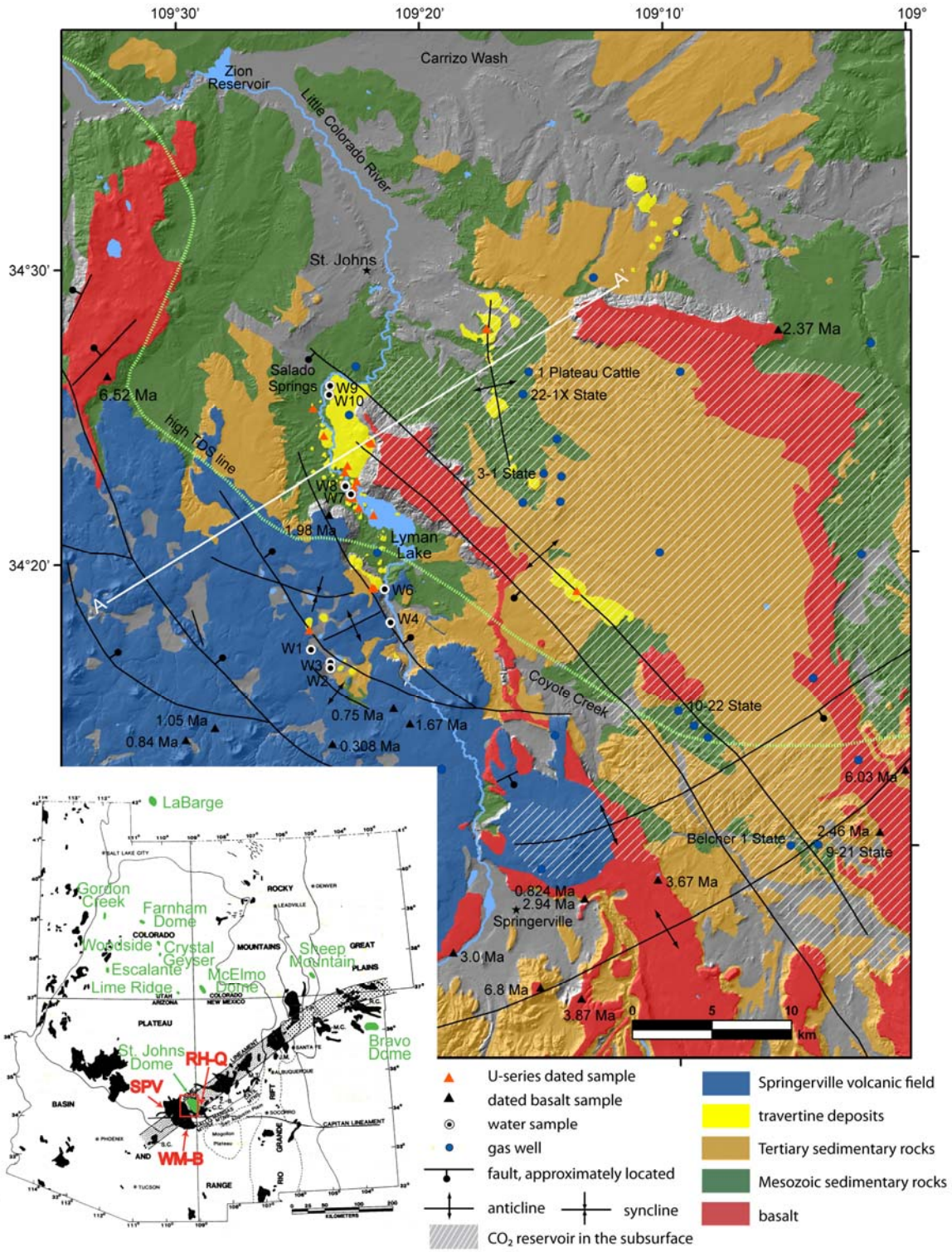

Fig. 1. Generalized geologic map of the Springerville area. Inset is an index map of the

Colorado Plateau region with late Cenozoic (≤11 Ma) volcanic fields and the Jemez lineament modified from Aldrich and Laughlin (1984). Area of this study is indicated surrounded by the Plio-Pleistocene Springerville (SPV), Mio-Pleistocene Red Hill-Quemado (RH-Q), and Miocene White Mountain-Baldy (WM-B) volcanic fields. Natural CO_2 reservoirs are indicated in green (from Allis et al., 2001)

two volcanic fields and hosts an 1813 km^2 natural CO_2 field (Rauzi, 1999). The travertines have been examined as part of a regional mapping effort (Condit et al., 1999), and in studies of the CO_2 field as a natural analog for carbon sequestration efforts (Moore et al., 2001; 2003), but this is the first study to concentrate on the age and significance of the travertines themselves.

The Springerville travertines have been used as natural examples of CO_2 leakage for carbon sequestration studies (Rauzi, 1999; Moore et al., 2003; Gilfillan et al., 2008; Haszeldine et al., 2005) and are important in understanding the origin of gas fields (Rauzi, 1999). Springerville-St. Johns Dome is one of several important gas fields in the Colorado Plateau region (see inset to Fig 1) (Allis et al., 2001). The gas reservoir is trapped in an asymmetric northwest-trending plunging anticline of Laramide age bounded on the southwest by the basement-penetrating Coyote Wash fault that offsets Mesozoic strata by 30-200 m and on the southeast by the NE-trending Salt Lake fault zone. Much of the gas comes from the Permian section, but new deeper exploration and discovery is taking place at the top of Precambrian crystalline rocks near the intersection of the two fault zones (T. White, personal communication). The reservoir has an estimated 445 billion m^3 of CO_2 beneath anhydrite and mudstone capping rock seals (Rauzi, 1999; Stevens et al., 2001).

In this study, we provide new high-precision U/Th ages for a suite of 41 travertine samples to determine periods of travertine deposition and accumulation rates. We integrate our data and field observations with insights developed by previous workers from studies that focused on distinct but interrelated aspects of the magmatic/hydrologic/gas systems (Condit, 1994; Rauzi, 1999; Crossey et al., 2009; Moore, 2003; Gilfillan, 2008). The new combined geochronologic framework from dated travertines and published K-Ar and $^{40}Ar/^{39}Ar$ basalt ages (McIntosh and Cather, 1994; Cooper et al,1990; Aubele et al, 1986; Condit and Shafiqullah, 1985; Laughlin et al, 1979; 1980) and the spatial patterns and relationships of these features to other elements in the landscape, make this location one of the best constrained areas for understanding travertine genesis and possible genetic linkages between volcanism, neotectonics, evolution of the LCR drainage system, and paleoclimate.

GEOLOGIC BACKGROUND

The Springerville area is an important locality to test models for Cenozoic evolution of the Colorado Plateau. The area exposes Eocene to Quaternary strata that place constraints on the interaction of uplift, volcanism, and the hydrologic system near the southern edge of the Plateau. Figure 2 is a geologic map of the Springerville area. The modern surface is formed by broad pediments of non-resistant Triassic Chinle Formation, remnants of a succession of Eocene and younger gravel terraces deposited during dry climatic aggradational cycles, windows of Cretaceous sandstone, and basalt flows and volcaniclastics from successive episodes of volcanism from the late Eocene-Oligocene

Datil-Mogollon volcanic field to the mid-Miocene White Mountain-Baldy complex, to the most recent eruptions at 308 ka in the SPV and 71 ka in the RH-Q volcanic fields.

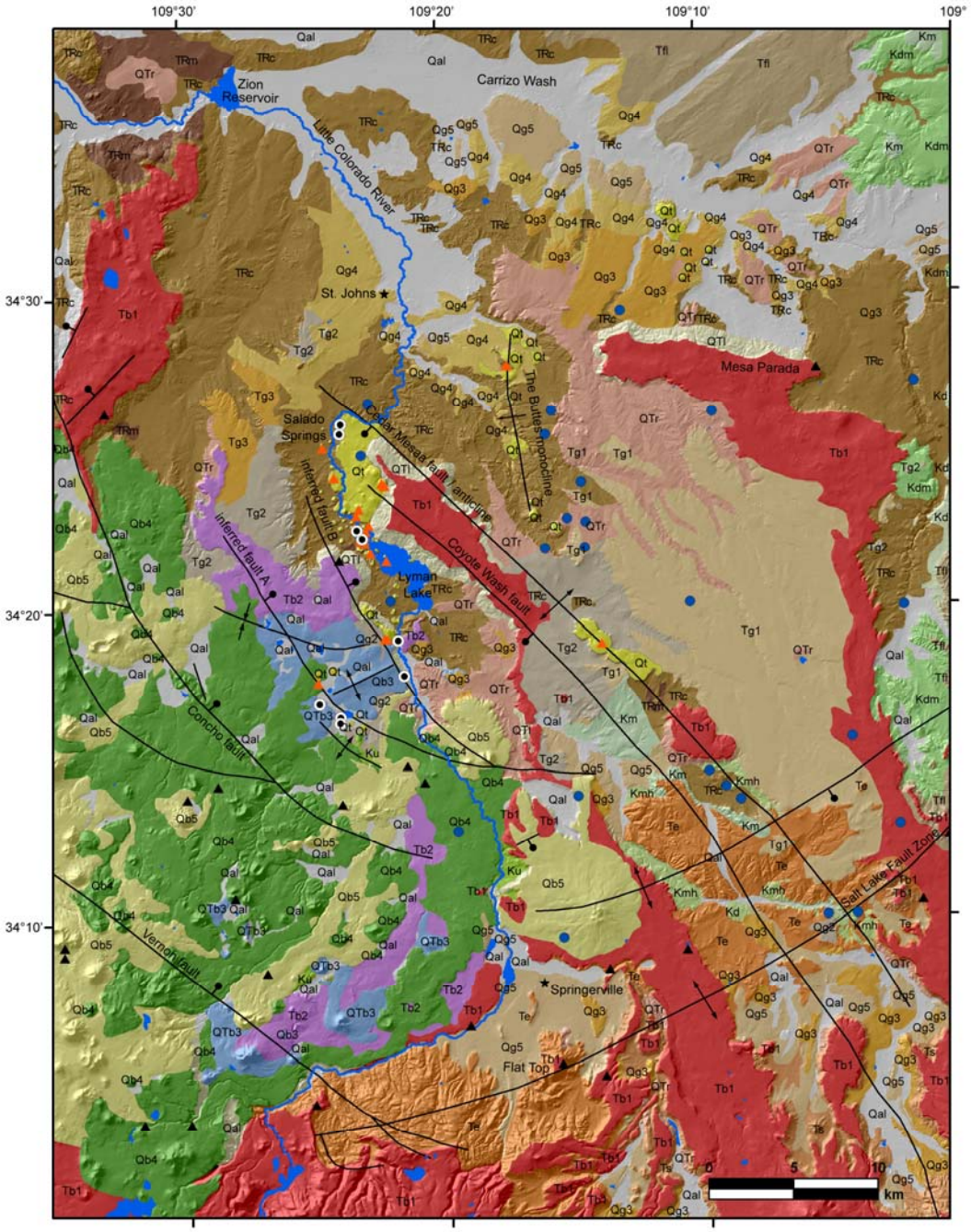

Fig. 2. Geologic map of the Springerville-St. Johns area and map explanation (below).

Explanation

- U-series dated travertine
- K-Ar dated basalt
- synclinal axis
- anticlinal axis
- monocline
- normal fault, ball on the downthrown side

Map Units

Quaternary

Qal	Alluvium and colluvium
Qt	Travertine deposits
Qg5	Gravel terrace 5 (Sirrine, 1958)
Qg4	Gravel terrace 4 (Sirrine, 1958)
Qb5	Basalt group 5 (0.00 - 0.97 Ma) (Condit et al., 1989)
Qb4	Basalt group 4 (0.98 - 1.67 Ma) (Condit et al., 1989)
Qg3	Gravel terrace 3 (Sirrine, 1958)

Quaternary and Tertiary

QTl	Landslide deposits
QTr	Richville Formation (Quemado) (Pliocene - Lower Pleistocene)
QTb3	Basalt group 3 (1.68 - 1.87 Ma) (Condit et al., 1989)

Tertiary

Tb2	Basalt group 2 (1.88 - 2.14 Ma) (Condit et al., 1989)
Tg2	Gravel terrace 2 (Sirrine, 1958)
Tb1	Basalt group 1 (2.15 -8.97 Ma) (Condit et al., 1989)
Tg1	Gravel terrace 1 (Sirrine, 1958)
Tfl	Fence Lake Formation (Miocene)
Ts	Spears Group (Upper Eocene - Oligocene)
Te	Eagar Formation (Eocene - Early Oligocene) (Baca Fm. correlative)

Cretaceous

Kd	Dakota sandstone (Upper Cretaceous)
Kdm	Intertongued Dakota sandstone and Mancos shale
Km	Mancos shale (Upper Cretaceous)
Kmh	Moreno Hill Formation
Ku	Cretaceous undivided

Triassic

TRc	Chinle Formation
TRm	Moenkopi

Several tectonic events have affected the area. Like much of New Mexico, the Paleozoic and Mesozoic stratigraphic column (Fig. 3) shows evidence for ancestral Rocky Mountain uplift in the region, as basal Paleozoic strata were removed and Permian rocks rest on basement. Northwest-trending faults in the region may have moved at this time (Karlstrom et al., 2000), perhaps reactivating older basement structures (Marshak et al., 2003). The Laramide orogeny also reactivated older faults and created compressional features such as monoclinal folding of Phanerozoic strata, including the broad northwest-trending asymmetric anticline, Springerville-St. Johns Dome, that warps Paleozoic and Mesozoic strata and is faulted by the basement-penetrating NW-trending Coyote Wash and the NE-trending Salt Lake fault zones (Fig. 4 cross section; Rauzi, 1999; Cather et al., 2008). Late Laramide-related uplift in the Mogollon highlands created the Baca basin with its axis running east-west through the Springerville area. Thick sequences of synorogenic coarse gravels with unroofed basement lithologies were deposited by a powerful eastward-flowing flashy stream. These gravels are referred to as Mogollon Rim gravels at the eastern end of the basin, the Eagar Formation in the Springerville area in the central basin, and the Baca Formation in the western basin in New Mexico. Regional paleoslope shifted during the deposition of the Mogollon Rim / Eagar Formation / Baca Formation. Flow was toward the ENE as the basal member was deposited, sourced in the contemporaneously uplifted Mogollon highlands (Potochnik, 1989). As the middle and upper members were deposited, drainage rotated toward the NW off of the Morenci lineament to the SE (Cather and Johnson, 1986). The Eagar Formation gravels form a wedge that thins towards the north with outcrops preserved in the southern portion of the

study area at elevations from 2225 to 2408 m (7300-7900 ft) underlying mesas including a 145 m-thick section beneath the 6.80±0.02 Ma basalt capping Flat Top (McIntosh and Cather, 1994). The contact with the underlying Cretaceous sandstone is an angular unconformity with up to 100 m of relief along Coyote Creek (Cather, 1994).

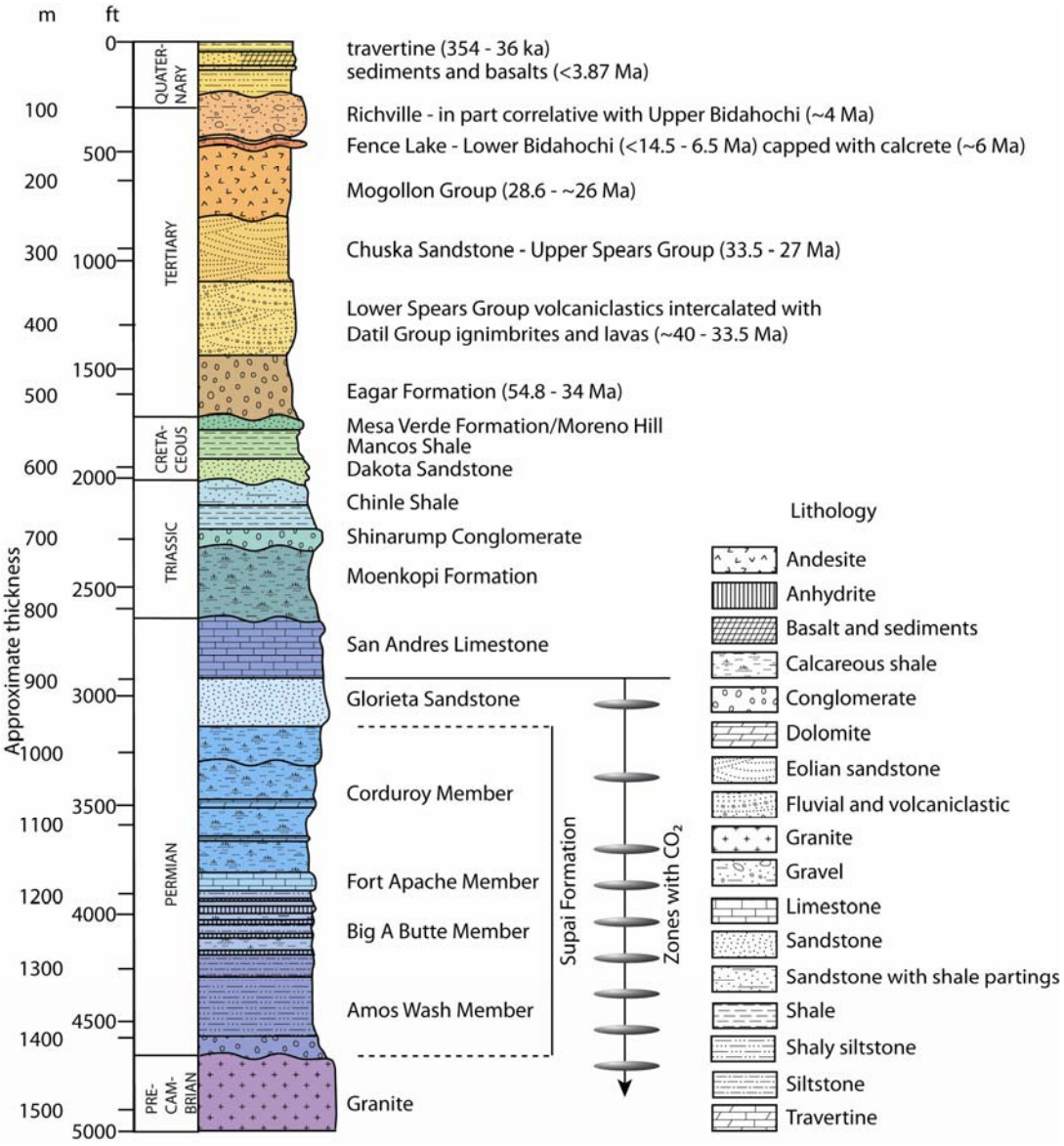

Fig. 3. Stratigraphy of the Springerville area showing zones of CO_2 (modified from Rauzi, 1999)

Magmatism started in the area with the Mogollon-Datil ignimbrite flare up at the end of the Laramide orogeny and continued from ~40-24 Ma (Cather et al., 1994b). The Datil Group is composed of ignimbrites and lavas deposited before a regional disconformity that marks a 31.4-29.0 Ma hiatus in volcanism. Above the disconformity, basaltic and andesitic deposits, including the Bearwallow Mountain Andesite, form the Mogollon Group. Volcaniclastic deposits intercalated with the ignimbrites comprise the Spears Group (McIntosh and Chamberlin, 1994). The fluvial and debris-flow deposits of the Lower Spears Group, with increasing proportions of volcanic fragments up-section, was deposited from ~34–33.5 Ma, thinning toward the north and indicating a shift in drainage direction (Cather and Johnson, 1984; Potochnik, 1989). The unit is preserved in the southern part of the field area at ~2286 m (~7500 ft) as a thin bed between the Eagar Fm and capping basalts. The Upper Spears Group consists of eolian sandstones up to 250 m thick that were deposited in the area as part of the Chuska Erg, a regional sand sea, from 33.5–27 Ma (Cather, et al, 2008) and are preserved in the subsurface at the southern edge of the field area.

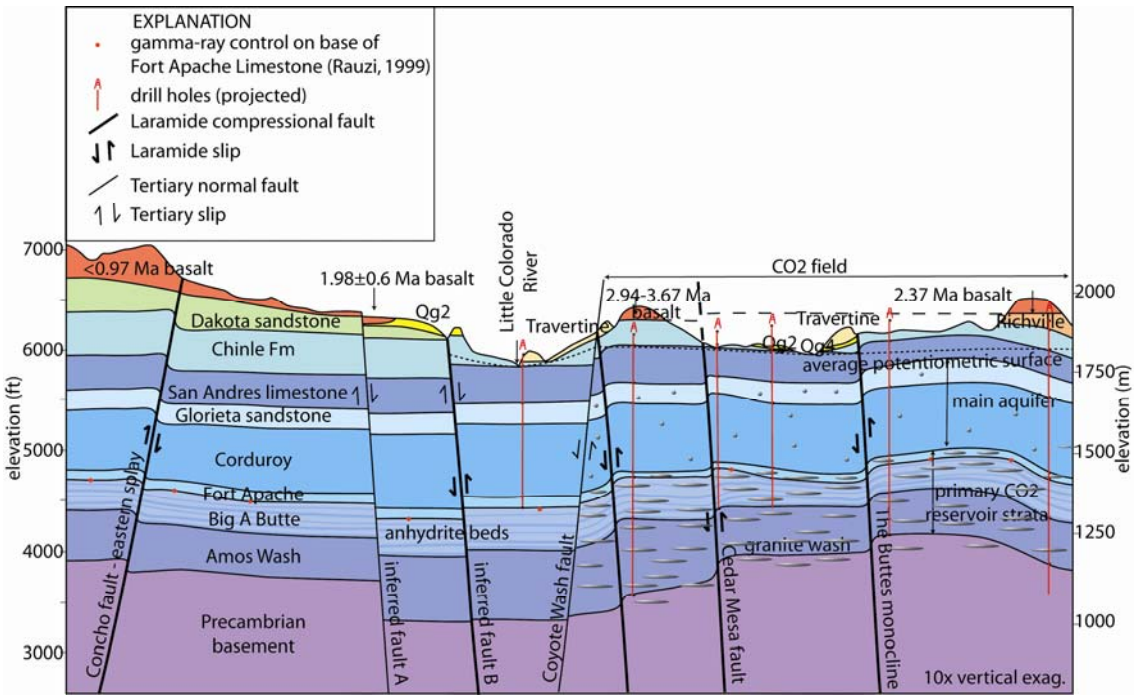

Fig. 4. Generalized cross-section across Springerville-St. Johns gas reservoir along line shown on Fig. 1, modified from Rauzi 1999, Condit et al. 1994, and Sirrine 1958; lithologies explained further in Fig.2 and Fig. 3.

Basin and Range extension began at 24.8 Ma (Faulds et al., 2001) and is expressed in the area as normal slip on older reverse faults. Major faults within the SPV, such as the Concho and Vernon faults, that show normal slip since emplacement of the young basalts, are arcuate, subparallel to the margin of the Colorado Plateau with a few ~perpendicular ENE-trending structures (Condit et al., 1992). Figure 4 (cross section) is based on our interpretation of the locations of faults (Fig. 2) from drillhole data, and gamma-ray data for the position of the base of the Permian Fort Apache Limestone in the subsurface (Rauzi, 1999). Faults are interpreted to be a combination of Laramide reverse

faults and Tertiary (and still active) normal faults. For example, normal offset across the Coyote Wash fault ranges from 30 m (100 ft) at Salado Springs to 200 m (600 ft) 25 km to the SE at the apex of the anticline (Rauzi, 1999); much of this displacement is Tertiary as shown by more than 30 m of displacement along a 13 km segment of a Pliocene basalt flow. Dip on the faults is not constrained.

The deposition of the Chuska sandstones was followed by a period of intense erosion from the late Oligocene to early Miocene, creating a regional angular unconformity with the exhumation of at least 1230 m caused by major uplift in the area (Cather et al., 2008). From 14.5 - ~6.5 Ma the area was at the southern edge of the shallow Bidahochi depositional basin (Scarborough, 2001; McIntosh and Cather, 1994) with a stable local base level. Aggradation of sediments began backfilling paleovalleys with coarse fluvial Fence Lake gravels deposited by high energy streams flowing from the east. These gravels are correlative with the lower Bidahochi Formation (McIntosh and Cather, 1994) and are preserved inset against basalt mesas at 2225 m (7300 ft) at the eastern edge of the study area and form a broad terrace covering the northeastern section.

The White Mountain-Baldy complex became active in the mid-Miocene with a shift in dominant tensional stresses to the west (Aldrich and Laughlin, 1984). The main pulse of activity was from 9-6 Ma. Basalt flows from this complex underlie the younger SPV and are exposed around the perimeter of the field, including Flat Top in the south-central part of the study area, and a 6.52±0.01 Ma flow from a NNE-trending alignment of fissure vents at the northeastern edge of the Springerville volcanic field.

This Miocene pulse of volcanic activity was followed by another period of incision that was less intense than the post-Chuska, pre-Bidahochi period, exhuming ~520 m in this area until the present and interrupted only by aggradation of the Richville Formation from ~4 Ma, correlative with the Quemado Formation (Cather et al., 2008).

Volcanism then migrated toward the north from the White Mountains to the SPV where 409 predominantly monogenic volcanoes in an area of ~4800 km^2 (3000 mi^2) erupted from 2.1–0.308 Ma. Early flows were extensive ~5 m-thick sheets of tholeiitic basalts (Condit et al., 1989) and the volume of magma decreased with time as compositions became more alkalic. Figure 2 shows the basalts of the SPV divided into age groups according to the classification of Condit et al. (1989) shown in the map explanation (Fig. 2B). Activity migrated generally from west to east at a rate of 2.9 cm/yr with an average recurrence rate of ~3000 yrs (Crumpler et al., 1994). Vents occur in 10-20 km diameter clusters generated from many discrete magma batches with intense localized activity lasting <250 ka. Eruptions increased from 2.1-1.5 Ma, maintained steady state from 1.5-0.75 Ma, and then waned (Condit et al., 1996). Volcanic cones are closely-spaced in alignments oriented WNW in the western part of the field and ENE in the eastern portion adjacent to the LCR, reflecting the continuing evolution of stress in the area (Condit et al., 1996; 1989; Connor et al., 1992). Phenocrysts from SPV basalts indicate that they are derived from prolonged storage of magmas at two depth intervals, 0-12 and 23-30 km (Putirka and Condit, 2003).

Magmatism in the Red Hill-Quemado area 40 km west of the LCR also occurred in two distinct intervals, from 7.9-5.2 Ma and 2.5-0.071 Ma, overlapping with White

Mountain-Baldy and SPV volcanism, also with younger activity in the north. The alignment of vents and faults shifted over time from N60°E in the late Miocene, similar to the average trend of the Jemez lineament, to N35°E in the more recent interval (McIntosh and Cather., 1994).

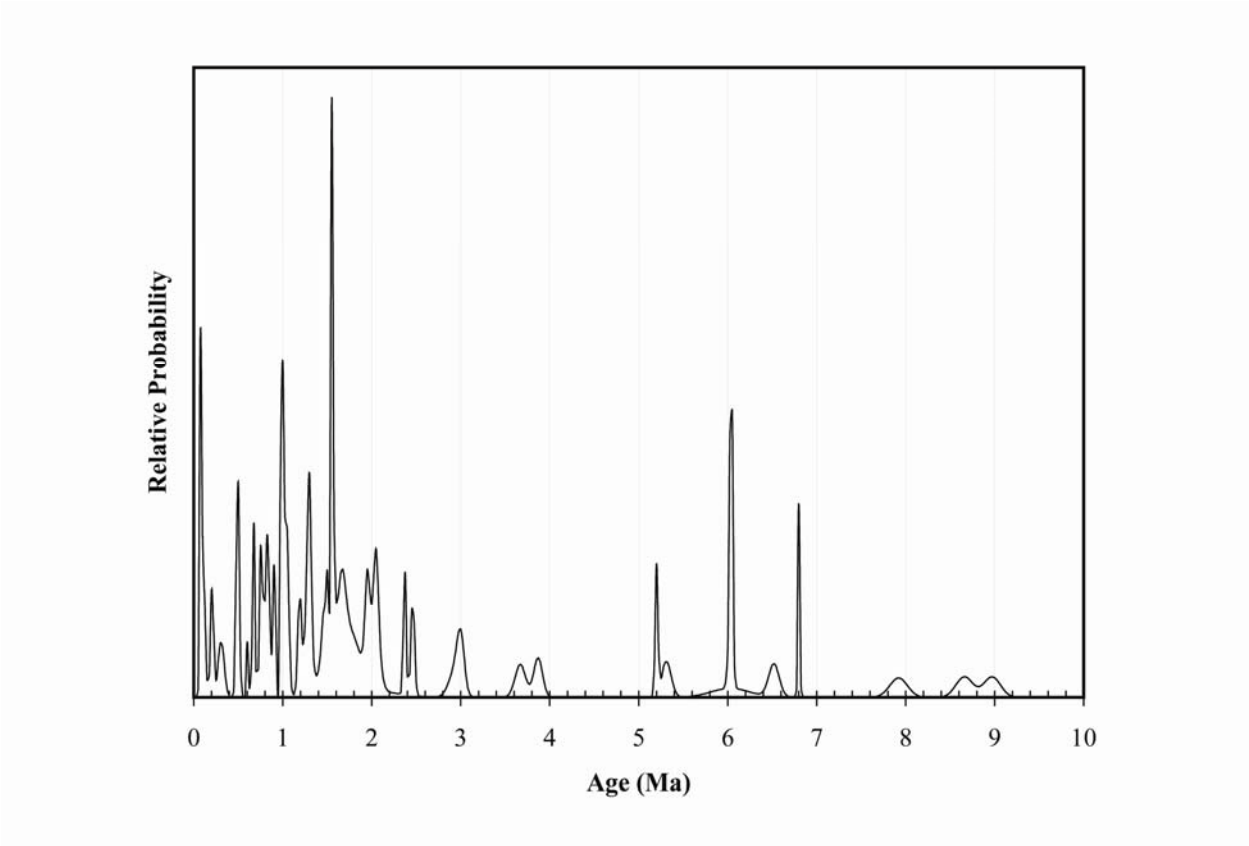

Fig. 5. Age probability diagram of dated basalts of the Springerville and Red Hill-Quemado volcanic fields.

Following the 6 Ma integration of the Colorado River across the Kaibab uplift (e.g. Karlstrom et al., 2008), the Little Colorado River began incising through Bidahochi and older strata and cut broad valleys in the relatively non-resistant strata. Streams have incised a network of deep narrow channels in the resistant basalts, for example the LCR and Coyote Creek have cut 37 m deep slots in a 1.67 Ma basalt flow. We see no evidence

in the Springerville area to support McKee and McKee's (1972) suggestion that the ancestral LCR (pre-6 Ma) flowed SE. Instead aggradation was in a northerly direction since the Eocene, post-lower Eagar Formation deposition, due to northerly-flowing river systems.

The course of the modern LCR, 45 km north of its headwaters on Mt. Baldy, lies at the eastern edge of the SPV. Distal basalt flows from the surrounding White Mountain and Red Hill-Quemado volcanic fields mark pre-established drainages and paleo-surface elevations and now stand as high northwest-trending elongate mesas (Fig. 2). Elevated remnants of a series of younger gravel terraces were mapped by Sirrine (1958) and are designated Tg1 through Qg5 in this study (Fig. 2). These are interpreted to be the record of post-4 Ma incision of the LCR into the SVF.

Faults

The Springerville-St. Johns Dome formed at the intersection of two major regional structural fabrics that reflect different stress regimes that have affected the area. The Coyote Wash fault that bounds the anticline on the west is part of a discontinuous system of northwest-trending faults and small undulations superimposed on the broad fold. The axis of the Cedar Wash anticline parallels the Coyote Wash fault and is faulted at depth at least in segments. Open fractures that are concealed at the surface have been encountered in drilling (Rauzi, 1999; T. White, personal communication, 2009). Strata between wells in Coyote Creek at the southern end of the dome are offset by 38 m down-to-the-SW (Rauzi, 1999) while exposed segments in Antelope Valley and at the northern

end of the dome northeast of Salado Springs show offsets of 45 m (Sirrine, 1958) and 30 m respectively. The offset of Permian strata along the Coyote Wash fault increases from 30 m at the northwestern end at Salado Springs to 183 m at the apex of the anticline (Rauzi, 1999). The Coyote Wash / Cedar Mesa fault zone intersects the NE-trending Salt Lake fault zone / regional anticlinorium that parallels the Jemez lineament but that is often not shown on Arizona maps since its identification on the New Mexican side of the field area during the mapping of the Quemado 30' x 60' quadrangle (Cather et al., 2008; Anderson, 1994). The dip on the faults is not constrained. The highest concentration of CO_2 gas in the Springerville-St. Johns Dome has recently been discovered near this intersection 60 m beneath the Permian strata in granite wash (T. White, personal communication), suggesting the possibility of enhanced influx and trapping of deeply-sources fluids at the juncture of the two fault zones.

The intersecting trends of these fault zones are also seen in volcanic vent alignments within both the Springerville and Red Hill-Quemado volcanic fields. In the SPV, the intersection of the WNW alignment that is prominent in the generally older western portion of the field and the dominant ENE alignment of the eastern section is located in the south-central part of the field and is the locus of the most enduring magmatism and the highest concentration of volcanoes of the field, ranging in age from 1.30–0.61 Ma (Connor et al., 1992; Condit et al., 1994).

Crumpler et al. (1994) observed a left-lateral shear component to faults in the SPV and on the Coyote Wash fault which created pull-apart basins in the northwestern section of the field, including the basins occupied by the town of Concho and Lyman

Lake. Movement in the left-lateral sense on the Coyote Wash fault may also explain the long-term travertine deposition at that location that constructed the large platform (Hancock et al., 1999).

WATER CHEMISTRY

The motivation of this section is that the modern hydrologic system can provide insight into past travertine deposition. The model proposed by Crossey et al. (2006; 2009) is that travertine depositing springs tend to be warm, saline, have high pCO_2, high $C_{external}$, and have other geochemical tracer evidence for input of endogenic fluids containing mantle-derived He and CO_2 and deep crustally derived Sr and CO_2 fluid components. This section builds on data presented by Crossey et al (2009) that suggest that the modern Springerville springs are analogs for the types of springs that precipitated past travertine deposits over the last >350 ka.

Results of water analyses

Ten water samples from eight springs adjacent to travertine deposits and two LCR river samples from up- and down-stream of Lyman Lake were collected and analyzed using techniques described in Appendix A and Crossey et al. (2006) to characterize the chemistry of the modern spring/groundwater/surface water systems. Sampling locations are shown on Fig. 1. Samples from the LCR 2 km upstream of Lyman Lake and from the outflow below the dam were collected for comparison with spring waters from Nielson Spring, 24 Ranch Spring, The Cienaga, Wiltbank Spring, Salado Springs cistern and

marsh, and an unnamed spring 0.7 km downstream from the Lyman Lake dam. Springs were sampled as close to source outlets as possible.

The composition of river water and waters from the western springs fall within the calcium-bicarbonate facies while Salado Springs waters and water from the unnamed spring have higher sodium (Drever, 1997). The water from Salado Springs and the adjoining marsh had the highest total dissolved solids (TDS), alkalinity, and Ca, Na, and SO_4 concentrations. Other springs located along the LCR and the outflow from Lyman Lake show intermediate values for these constituents while the river itself and waters from springs located west of the river have low concentrations. Salado Springs water had higher concentrations of trace elements, particularly Al, B, Ba, K, Li, and Sr. Waters from springs and seeps along the LCR, including Salado Springs, are supersaturated with respect to calcite and aragonite while those from springs located west of the current river course are not, despite their proximity to travertine mounds.

Regional groundwater flow is towards the north-northwest with recharge in the White Mountains and porous basalts of the SPV. A discontinuous system of faults, including the Coyote Wash fault, obstructs groundwater flow between the volcanic and CO_2 fields. A high TDS or "badwater" line (Stone, 1979; Figs. 1 and 5) defines the southwest limit of a zone of poor quality groundwater and roughly coincides with the western edge of the gas field (Rauzi, 1999). North-flowing groundwater in the Glorieta Sandstone aquifer (analogous to the C-aquifer of Cooley, 1969) mixes with lateral flow from the CO_2 reservoir. Both waters are affected by deeply-sourced fluids coming up the faults, but this study provides better understanding of the badwater line. We propose that

it is co-located with the Coyote Wash fault. In this model, the trapped high TDS gas field waters have a dynamic interaction with meteoric recharge that depends on paleohydrology and microseismicity. This interaction is documented by the travertine accumulations that mark the upward leakage of the high TDS waters along the faults that serve as high permeability pathways for mixing between deeply-derived fluids and shallow recharge and also serve as barriers to flow between the CO_2 reservoir and meteoric groundwaters to the west of the structure.

Our new data expands and corroborates existing water chemistry studies and the spatial distribution patterns in the extreme water quality variability in the region surrounding the CO_2 field (Moore et al., 2005). Results for select parameters for samples from this study are plotted with groundwater analyses from the USGS National Water Information System in Figures 6A-F to demonstrate the surrounding geographic context of our study area. A striking pattern emerges of high TDS, sulfate, bicarbonate, and $C_{external}$ concentrations clustered in the area of the CO_2 field and toward the NW of the field. Another area of high concentrations of these constituents also occurs along highway I-40 east of Holbrook.

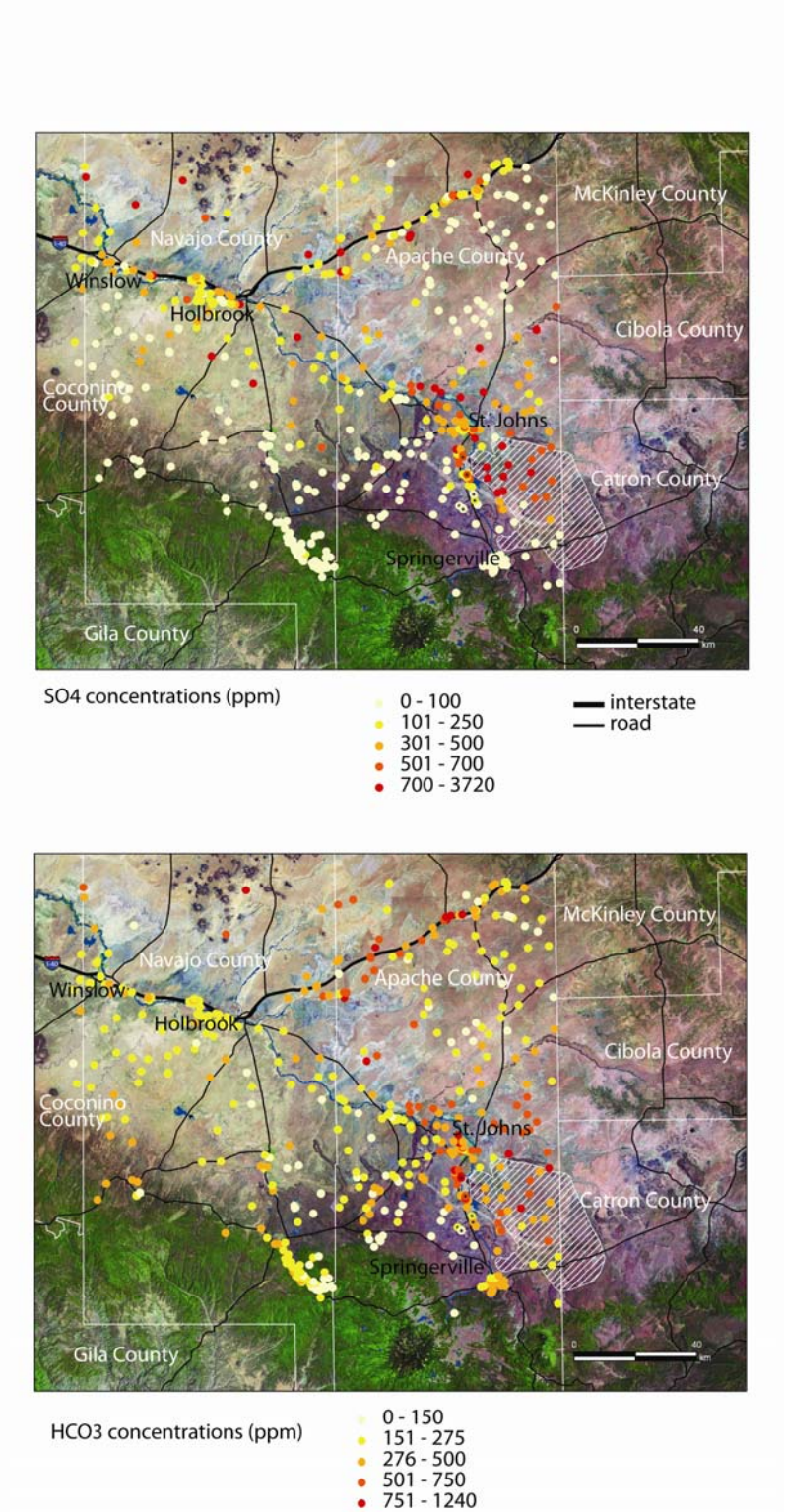

Fig. 6. Spatial distribution of selected chemical constituents in groundwaters in region of the study (Hatched area indicates CO_2 reservoir in the subsurface.).6A) Sulfate concentrations. 6B) Bicarbonate concentrations.

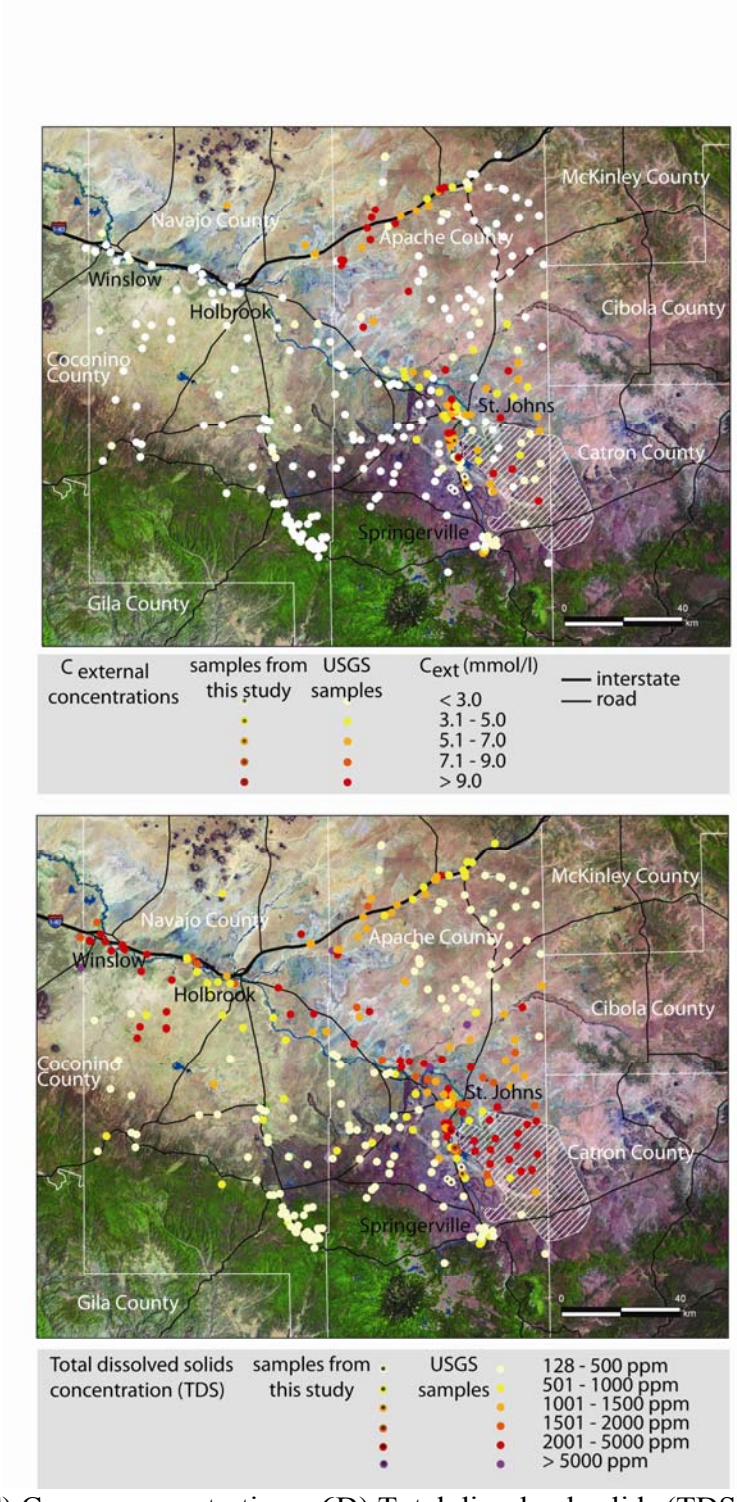

Fig. 6C) $C_{external}$ concentrations; 6D) Total dissolved solids (TDS) concentrations. Concentrations >500 ppm TDS exceed the EPA secondary maximum contaminant level guideline for drinking water.

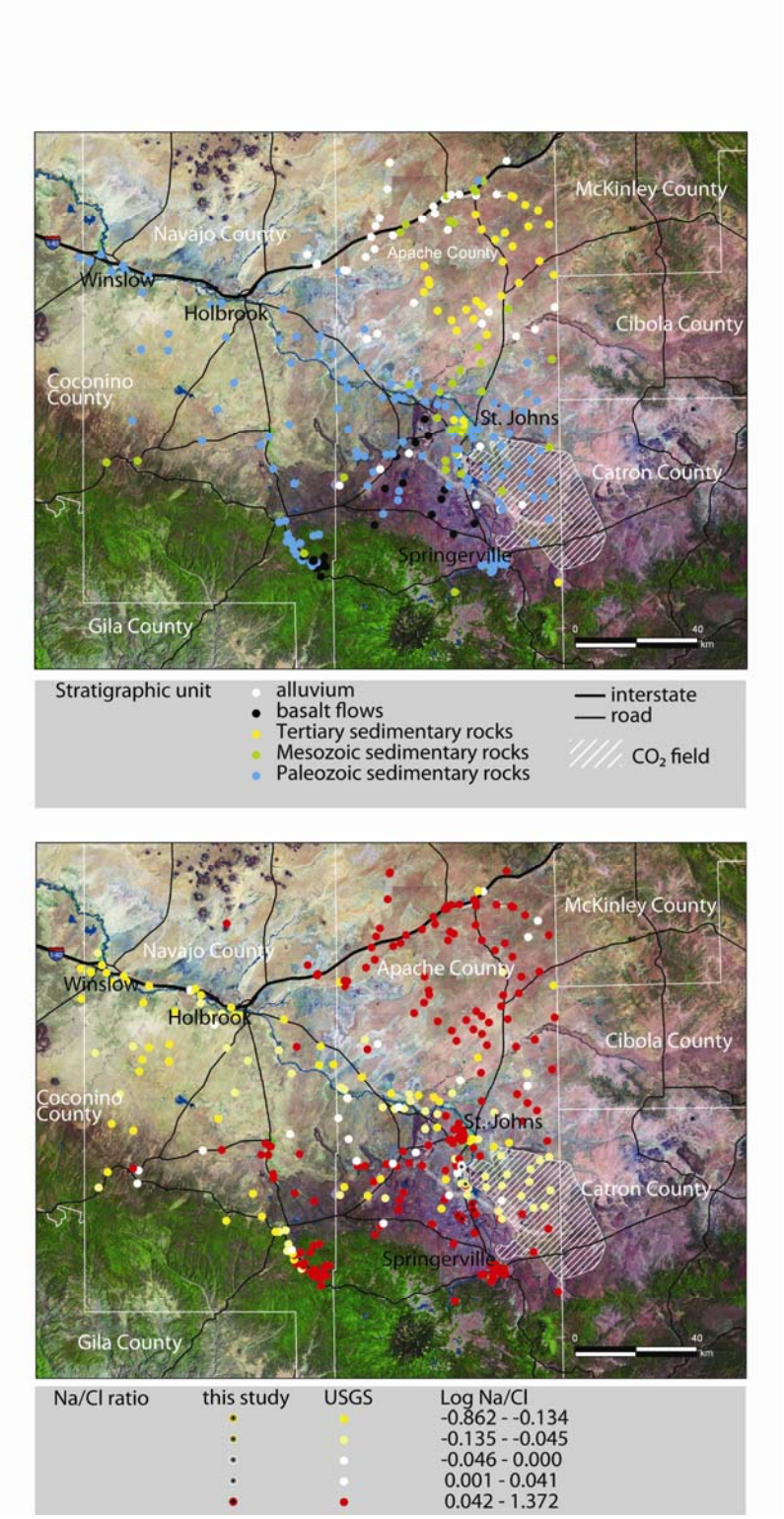

Fig. 6E) Stratigraphic unit in which groundwater wells used in the data compilation are completed; 6F) Na/Cl ratio reported as log Na/Cl.

A piper diagram of the collective data shows a wide range of compositions for the entire area with various degrees of intermixing (Fig. 7). Waters range from Ca-Mg HCO_3 type with high TDS to Cl-SO_4 type. A primary mixing trend is defined between a meteoric endmember (left side of the quadrilateral) and one or more high TDS endmembers similar to that seen in the Colorado Plateau (Crossey et al., 2009) and Rio Grande rift (Newell et al., 2006). End member values are described below (W2, W3 and Zion of Fig. 7), as well as the water chemistry of Salado Spring (W9, W10) that represents the largest active travertine-depositing spring in the area.

Waters that plot closest to the meteoric endmember are low TDS samples (W2 and W3 of Fig. 7) that are interpreted to be dominated by meteoric recharge from the White Mountains but, like all of the groundwaters in Figure 7, have mixed somewhat with older waters in the Glorieta sandstone or perched aquifers and hence are themselves mixtures. Some of our lowest TDS samples, with concentrations of 314, 288, and 187 mg/l respectively, are 24 Ranch Spring, Wiltbank Spring and The Cienaga, all from within the Springerville volcanic field (Samples W1,W3,W2 of Table 1). The spring at 24 Ranch issues from beneath the base of a 0.97-1.67 Ma basalt at 1920.2 m (6300 ft), with a flow of 1.96 l/s (ref). Two km southeast of 24 Ranch Spring, Wiltbank Spring and The Cienaga issue from alluvium in a basin surrounded and underlain by <1.87 Ma basalts including the youngest dated 0.308±0.07 Ma flow in the field (Aubele et al., 1986). Although extinct travertine mounds occur near these springs, these modern spring waters are near-meteoric, flowing from a perched aquifer in the basalt and are undersaturated with respect to calcite, dolomite, and aragonite. These are not the type of

waters that can deposit large volumes of travertine as shown by calcite saturation values of -0.1 to -1.12 and pCo_2 of -2.01 to -2.84. Calcite-cemented basalt breccia and brecciated sandstone clasts in a basalt matrix at the southern edge of the travertine mound north of 24 Ranch spring suggest that an annealed fault runs beneath these western travertines.

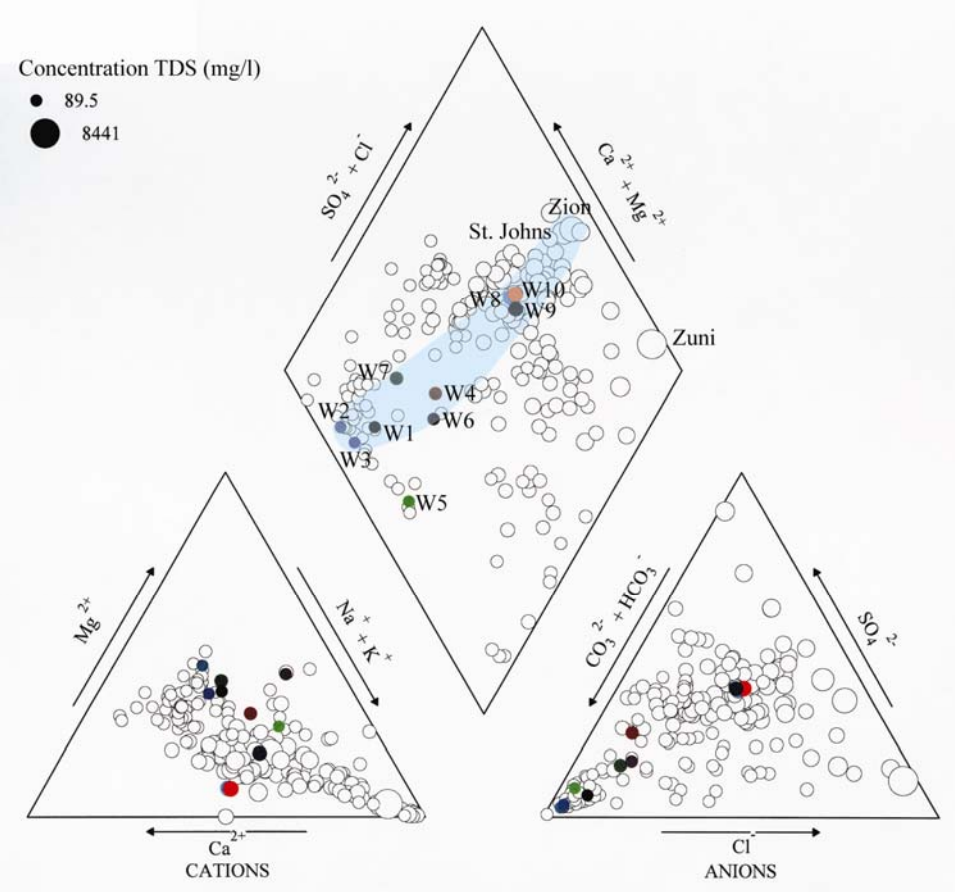

Fig. 7. Piper diagram of groundwater and spring water samples between Springerville and Zion Reservoir from this study (solid circles) and from the USGS (open circles) (Appendix B). Symbol size is proportional to TDS concentrations. Labels W1-W10 are keyed to Table 1. Blue swath indicates a mixing trend between meteoric waters from the SPV and high TDS waters of Zion Reservoir. Salado Springs (W9, W10) plot closer to the high chloride+sulfate endmember. Groundwater wells near the Zuni River that joins the LCR just north of the reservoir is a high chloride endmember.

Sample#	Sample ID	Description	Sample Date	UTM- E	UTM- N	Temp °C	pH	TDS
W1	EE06-AZ-SP4	24 Ranch Spring outflow	3/17/06	646000	3794750	ND	7.70	314
W2	EE06SW-TC1	The Cienaga Spring	4/23/06	647232	3793939	13.1	7.59	288.2
W3	EE06SW-WB1	Wiltbank Spring	4/23/06	647225	3793605	12.5	7.06	186.7
W4	EE06-AZ-SP3	Nielson Springs outflow	3/17/06	651000	3796430	ND	8.10	1025
W5	LC04-SPV-2	Springerville west	11/29/04			13.8	7.62	296.5
W6	EE06LL-101	LCR upstream of Lyman Lake	11/18/06	650636	3798519	7.6	8.11	469.9
W7	LC04-SPV-1	LCR downstream of Lyman Lake	11/28/04	648500	3804500	9.1	6.95	1179
W8	EE06LL-100	unnamed spring	11/18/06	648169	3805004	12.5	6.85	1924
W9	EE06-AZ-SP1	Salado Springs cistern	3/16/06	647199	3811280	18.1	6.79	2492
W10	EE06-AZ-SP2	Salado Springs marsh	3/16/06	647137	3810714	17.2	6.98	2538

Table 1A. Water sampling locations and field parameters. ND = not determined.

Sample	Alk.	Ca	K	Mg	Na	Cl	Br	SO_4	Balance	Saturation Indices			C_{ext}	pCO_2
										Calcite	Dolomite	Aragonite		
W1	213.56	26.22	10.74	17.51	21.92	11.59	0.00	12.50	-1.84	-0.10	-0.13	-0.25	0.0023	-2.84
W2	215.39	23.98	7.26	18.73	13.86	4.00	0.03	5.00	-3.33	-0.29	-0.52	-0.44	0.0022	-2.33
W3	131.19	18.55	6.78	10.96	12.42	2.78	0.05	4.00	4.00	-1.12	-2.31	-1.28	0.0013	-2.01
W4	555.25	74.17	35.60	46.17	100.40	50.93	0.42	162.10	-4.54	0.99	2.03	0.84	0.0070	-2.45
W5	199.16	18.21	5.63	12.08	41.15	5.24	0.06	15.00	0.56	-0.40	-0.80	-0.56	0.0025	-2.39
W6	286.78	15.14	3.53	26.31	51.79	34.13	0.13	53.20	-12.44	0.01	0.33	-0.15	0.0038	-2.77
W7	702.92	101.92	19.95	77.02	96.98	66.54	0.70	113.20	0.70	0.13	0.43	-0.01	0.0070	-1.17
W8	594.92	153.40	18.06	52.66	256.90	316.61	0.39	531.60	-11.62	-0.08	-0.44	-0.23	0.0093	-1.20
W9	707.80	328.50	42.74	36.05	357.70	392.84	0.30	626.10	0.25	0.31	-0.09	0.16	0.0084	-1.05
W10	683.39	335.00	45.27	36.69	375.40	412.48	0.32	649.40	0.98	0.47	0.23	0.32	0.0081	-1.26

Table 1B. Major ion concentrations reported in mg/l, alkalinity as mg/l HCO_3

Sample#	Al	B	Ba	Cu	Fe	Li	Mn	SiO2	Sr	V	Zn
W1	0.04	0	0.15	0.01	0	0.03	0.02	28.37	0.33	0.05	<MDL
W2	<MDL	0.04	0.04	<MDL	0.2	<MDL	<MDL	53.74	0.34	0.08	<MDL
W3	0	0.02	0.04	<MDL	<MDL	<MDL	<MDL	48.97	0.23	0.12	<MDL
W4	0.1	0.14	0.2	0.01	<MDL	0.08	0	47.13	1.7	0.05	<MDL
W5	2.09	0.11	1.85	<MDL	0.62	1.69	0.97	32.4	3.41	<MDL	<MDL
W6	0.01	0.16	0.01	0.02	<MDL	0.07	<MDL	23.45	0.29	<MDL	<MDL
W7	1.75	0.8	3	<MDL	0.67	2.12	0.96	37.62	7.67	<MDL	<MDL
W8	<MDL	0.61	0	0.02	<MDL	0.35	<MDL	13.85	1.78	<MDL	<MDL
W9	0.48	0.58	0.55	0.01	<MDL	0.96	0.02	15.2	4.61	0.01	0.01
W10	1.47	0.98	0.27	0.01	0.57	1.02	0.03	16.42	4.84	0.01	<MDL

Table 1C. Trace ion concentrations reported in mg/l. <MDL = below method detection limit.

In contrast, the highest TDS endmember (Zion of Fig. 7) comes from analysis of the groundwaters at St. Johns and the Zion Reservoir reported by the USGS NWIS that flow from the gas field. These waters have TDS up to 8441 mg/l, are high in Ca + Mg and bicarbonate, have pCO_2 of up to -1, and modeled calcite saturation indices of 0.99 (nearly pure CO_2). $C_{external}$ values, the percentage of the CO_2 not derived from the dissolution of carbonate and gypsum minerals in the aquifer ($C_{external}$ = Ca + Mg - SO4; Chiodini et al., 2002) range up to 0.016.

Waters from Salado Springs and the unnamed spring plot closer to the high TDS endmember. Salado Springs (W9, W10 on Fig. 7), also with high TDS, includes several springs at the base of a large travertine platform with a combined flow of 15 l/s (Moore et al., 2005). The present spring is at the edge of the marshy floodplain of the LCR. The spring emerges in cisterns rimmed by 0.5 m of travertine ~3 m above river level. Active degassing of CO_2 is evident by the bubbling nature of the cistern pools. This spring system may be the best modern analog for past travertine-depositing waters, although water volume and artesian head must have been substantially higher in the past and groundwater data suggest that past geochemical endmembers could have had higher TDS concentrations and been more supersaturated with respect to CO_2. Water chemistry of Salado Spring (analyses W9, W10 of Tables 1) shows these waters are warm (T= 18 C), have pH of 6.8-6.9, and are brackish, with TDS up to 2538 mg/l (sea water is 35,000 mg/l; Table 1). $C_{external}$ values range up to 0.05. Water chemistry of Sample W9 from Salado Springs indicates that these waters contain about 70% $C_{carbonate}$ (CO_2 derived from dissolution of carbonate and gypsum) and 30% $C_{external}$. Using C isotopes, Crossey et al

(2009) calculated that, of the 30% $C_{external}$, 4% is derived from soil and organic gases (4% $C_{organic}$) and 26% is derived from deep sources (26% $C_{endogenic}$).

Comparison of gas isotope analyses

Chemical analysis of a gas sample collected from a Salado Spring cistern shows a high helium concentration of 3×10^{-6} cc (Crossey et al., 2009). Nearby gas wells show helium values ranging from 2-4 orders of magnitude higher (9.42×10^{-4} cc to 1.34×10^{-2} cc; Gilfillan et al., 2008). Interestingly, although the reported helium concentrations are higher in the gas field than the springs, the helium isotopic data from Salado Spring has a $^3He/^4He$ value of 0.58 R_A (Crossey et al., 2009) compared to a mean value of 0.43 R_A for the gas field analyses (Gilfillan et al, 2008). These values are some of the highest values reported for the Colorado Plateau and indicate the presence of mantle-derived helium in the modern spring gases (Crossey et al., 2009; Gilfillan et al., 2008). Assuming MORB values of 8 R_A (Graham, 2002), this indicates that about 7% of the helium is from the MORB asthenosphere and that the flux of mantle gases is recent and probably related to the 3 Ma-0.3 Ma Springerville magmatic activity and/or the 2.5-0.71 Ma activity in the Red Hill-Quemado field. Mixing models using carbon isotope and $CO_2/^3He$ values for this sample suggest that 2-6% of the CO_2 may also be derived from the asthenosphere (Crossey et al., 2009).

Sample#	Sample ID	CO_2	He	Ar	N_2	CH_4	R_c/R_A
G1	EE06-AZSP-1	92.4	2.94E-06	1.40E-02	0.6	1.71E-05	0.58±0.01
G2	22-1X	82.9	1.34E-02	2.59E-03	16.0	1.20E-01	0.455±0.008
G3	3-1	91.7	7.06E-03	1.17E-03	8.0	6.34E-02	0.433±0.009
G4	10-22	98.9	9.42E-04	2.52-04	1.0	1.20E-02	0.394±0.008

Concentrations in vol % water free normalizations
All errors reported to 1 σ level
R_c = measured $^3He/^4He$ corrected for air contamination; $R_A = {}^3He/^4He$ in air (1.4×10^{-6})
G1 from this study and Crossey et al., 2009; G2-G4 from Gilfillan et al., 2008; 2009.

Table 1D. Gas chemical data comparing samples from Salado Springs and the CO_2 reservoir.

The Springerville-St. Johns Dome gas reservoir, itself, is a world class gas reservoir; its origin and location are closely linked to the badwater line and the location and distribution of the travertines. As shown in Figure 3, the predominant CO_2-containing strata within the gas field are the folded and faulted Fort Apache, Big A Butte, and Amos Wash members of the Permian Supai Formation with impermeable anhydrite and mudstone capping layers and the fractured and highly weathered Precambrian granite wash at the base of the Supai. Gas in the reservoir is mainly in a free gas state but corrosive carbonated waters are found in the overlying aquifer in the Glorieta Sandstone and karstified San Andres Limestone as well (Rauzi, 1999). The average production zone thickness of the stacked reservoir is 100 m with an average depth of 600 m (Allis, 2001). Source rock porosity and permeability varies considerably across the field as does the effectiveness of seal rocks (Moore, 2005; Allis, 2001; Rauzi, 1999). Gases from wells in the CO_2 field show a range of concentrations from 78.7-93.1% CO_2, 6-18.5% nitrogen, 0.17-0.81% helium, 0.001-0.1% methane, and 0.1-0.3% argon with concentrations varying laterally (Rauzi 2003). Recent studies by Gilfillan et al (2008) conclude that the gas is largely of mantle origin, infilling along the Coyote Wash fault and migrating

toward the northwest of the trapping structure to points where the folded and dipping gas-bearing strata intersect the surface along faults at the gas-groundwater contact. This interface is marked on the surface by travertine mounds, helping document the link between mantle-derived fluids and travertine deposition (Crossey et al., 2006).

Well pressures vary vertically and laterally within the reservoir from 8-33 bars in the Fort Apache, 25–36 bars in the Big A Butte/Amos Wash, and 13–48 bars in the granite wash, reflecting localized areas with more efficient confining seals within the same stratigraphic units and/or increased gas volume. In at least one well, 10-22 State (Fig. 1), 1999 data collected before significant commercial development showed that pressure does not necessarily increase with depth. It increased from 8 bars in the Fort Apache member at 266.9 m (1860 ft) to 29 bars in the Big A Butte at 480.1 m (1575 ft) and dropped to 13 bars in the granite wash at 626.1 m (2054 ft). Pressure is highest at the southern and northern ends of the reservoir, in the 9-21 State well, at the intersection of the Coyote Wash and Salt Lake fault zones, and in 1 Plateau Cattle and its replacement well 22-1X State on The Buttes anticline (Rauzi, 1999). Recent deeper drilling of a new well near the 9-21 State well has encountered a large deep reserve of gas in the granite wash at the base of the Amos Wash member, further evidence of a deep source.

Moore et al (2005) determined from mineralogical evidence that pCO_2 in the Big A Butte member of the Supai Fm in well 22-1X at the NW end of the dome was higher in the past and was later reduced.

Modeling of the noble gas isotopes from samples collected from three wells in the CO_2 field indicates a dominantly magmatic source for the gas with infilling takes place

from the SW and flowing toward the north (Gilfillan et al., 2008). The $^3He/CO_2$ ratio is highest in gases representing the earliest phase of reservoir filling (Ballentine et al., 2000). In the Springerville-St. Johns reservoir the highest value is in the north (1.02×10^{-8} decreasing to 5.24×10^{-10} in the south) (Gilfillan et al. 2009) (Table 1D). $CO_2/^3He$ ratios show a drop of an order of magnitude between wells 10-22 State at the SE end of the field to 3-1 State and then a drop of another order of magnitude from 3-1 State to 22-1X State and Salado Springs. These values suggest CO_2 loss or dilution relative to ^3He as the gases mix with groundwater and migrate toward the northwestern boundary of the reservoir (Gilfillan et al., 2009). The influence of this CO_2 loss into ground and surface water flowing north is reflected in the maps of the distribution of HCO_3, $C_{external}$, high TDS, and high sulfate waters downstream (Fig. 6).

TRAVERTINE OCCURRENCE

Distribution

Extensive travertine deposits covering a total area of >33 km^2 occur in four groups (Fig. 1). The spatial distribution of travertines is controlled both by the evolution of hydrologic base level controlled by river incision through time and by faults. Like volcanic vents in the surrounding volcanic fields, travertine mounds are preferentially located in lineaments along the trace of basement-penetrating faults with the major concentration where the modern river crosses major faults. Recent models hypothesize that these faults serve as conduits for CO_2-charged deeply-sourced fluids to rise from the mantle into gas-trapping folds or to escape under pressure from depth, degassing and

precipitating calcite or aragonite as the spring waters equilibrate to atmospheric pressure and CO_2 levels (Crossey et al., 2006; 2009). The faults also serve as barriers to groundwater flow from the recharge zone beneath the SPV, restricting mixing and dilution of the high TDS waters northeast of the badwater line.

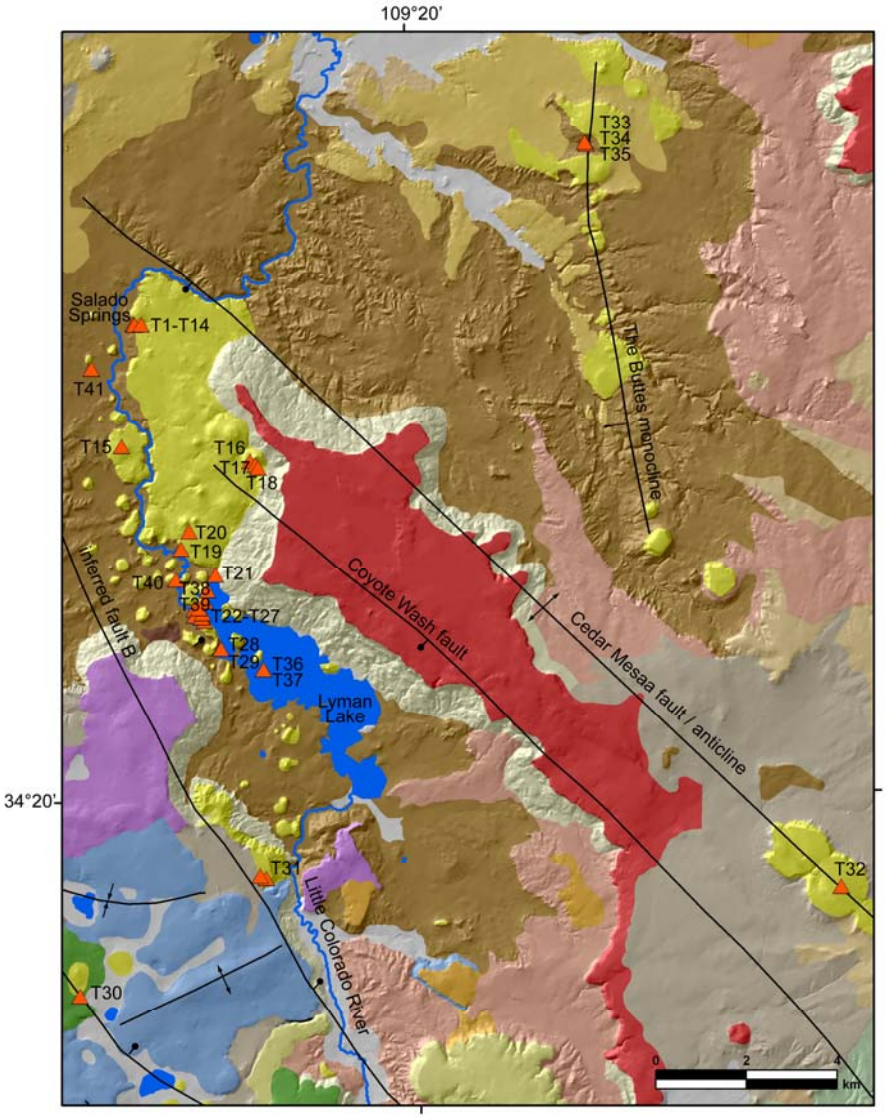

Fig. 8. Map showing travertine sample locations. Sample numbers are keyed to Table 2. Group D which consists of 8 mounds located 3-7.5 km to the NE is not shown.

Group A is the cluster of mounds along a 20 km-long stretch of the present course of the Little Colorado River and includes the platform that extends from the north end of Lyman Lake to Salado Springs, formed from more than 12 large mounds that are clustered so closely that their laminated deposits overlap into the 6.4 x 3.2 km platform. Mound vents along the LCR range in elevation from 1804-1957 m (5920-6420 ft) with bases buried in more than 4 m of modern alluvium (Sirrine, 1958) to 20 m above the current river elevation. The surface of the platform retains several preserved vents on both sides of the LCR as the river has incised its course through the deposit, isolating two large segments on the west bank of the river. Salado Springs, at the northern end of the group, consist of several springs issuing from the alluvium into a marsh ~3 m above the current river level. These springs lie at the base of a 22.3 m scarp formed at the eroded edge of the northernmost mound of the platform. The platform straddles and conceals the Coyote Wash fault and is dissected at the north by the Cedar Mesa fault. The highest vent is at 1956.8 m (6420 ft) just below the basalt flow lobe that caps the mesa along the Coyote Wash fault and that is interpreted to mark the paleoriver channel elevation at 2.94-3.67 Ma. The platform base is elevated 30 m above the river at 1828.8 m (6000 ft) at the southern end and is obscured by alluvium below current river level at 1786.1 m (5860 ft) at the northwestern end.

Group B follows a 33 km-long arcuate configuration 10-15 km to the east and subparallel to the present LCR. These travertine mounds overlie the northward-plunging Springerville-St. Johns anticline and are significantly higher at the southern end, stepping down 90 m where the dome splays into the Cedar Mesa and The Buttes anticlines (Rauzi,

1999; Sirrine, 1958). Base elevations range from 2103.1 m (6900 ft) for the southeastern-most Voight Mesa mounds to 1859.2 m (6100 ft) at the northern end at the Salt Lake Road. Vents range from 1908-2125.1 m (6260-6972 ft). The southeastern mounds are the highest and largest with diameters up to 1.4 km with two distinct mounds coalescing into a 2.5 km-long ridge. The arc of travertine mounds is aligned with the axis of the folds, suggesting spring migration tracking lateral propagation of fissures along fold axes. Two large mounds at the SW end of this group that were shown on maps in 2001 (Moore et al, 2001) have since been removed for development of the power plant and half of a mound on the north side of the Salt Lake road has been quarried by the Apache County Engineering Department.

Group C is a cluster of five mounds 5 km west of the LCR, where travertines follow the trace of an inferred concealed arcuate fault parallel to the Vernon and Concho faults that step down-to-the-northeast (Fig. 1). These western mounds, like the Voight Mesa mounds, have broad low-relief morphologies. Bases are from 1920-1932.4 m (6300-6340 ft) and tops of the highly weathered mounds range from 1928.8-1944.6 m (6328-6380 ft). Calcite-cemented sandstone breccia and basalt fragments between 24 Ranch Spring and the mound to the north may indicate possible annealing of an underlying fault and the chemistry of adjoining springs indicates that, in spite of the proximity of the travertine mound cluster, CO_2 is no longer leaking in this area. A 2.7 x 0.5 km remnant of an originally much larger travertine platform with fossilized stromatolites is perched at 1938.5 m (6360 ft) 5 km NE of these mounds, 91 m above the

LCR at the western edge of Richville Valley. Large toreva blocks of the platform have slumped downslope toward the river.

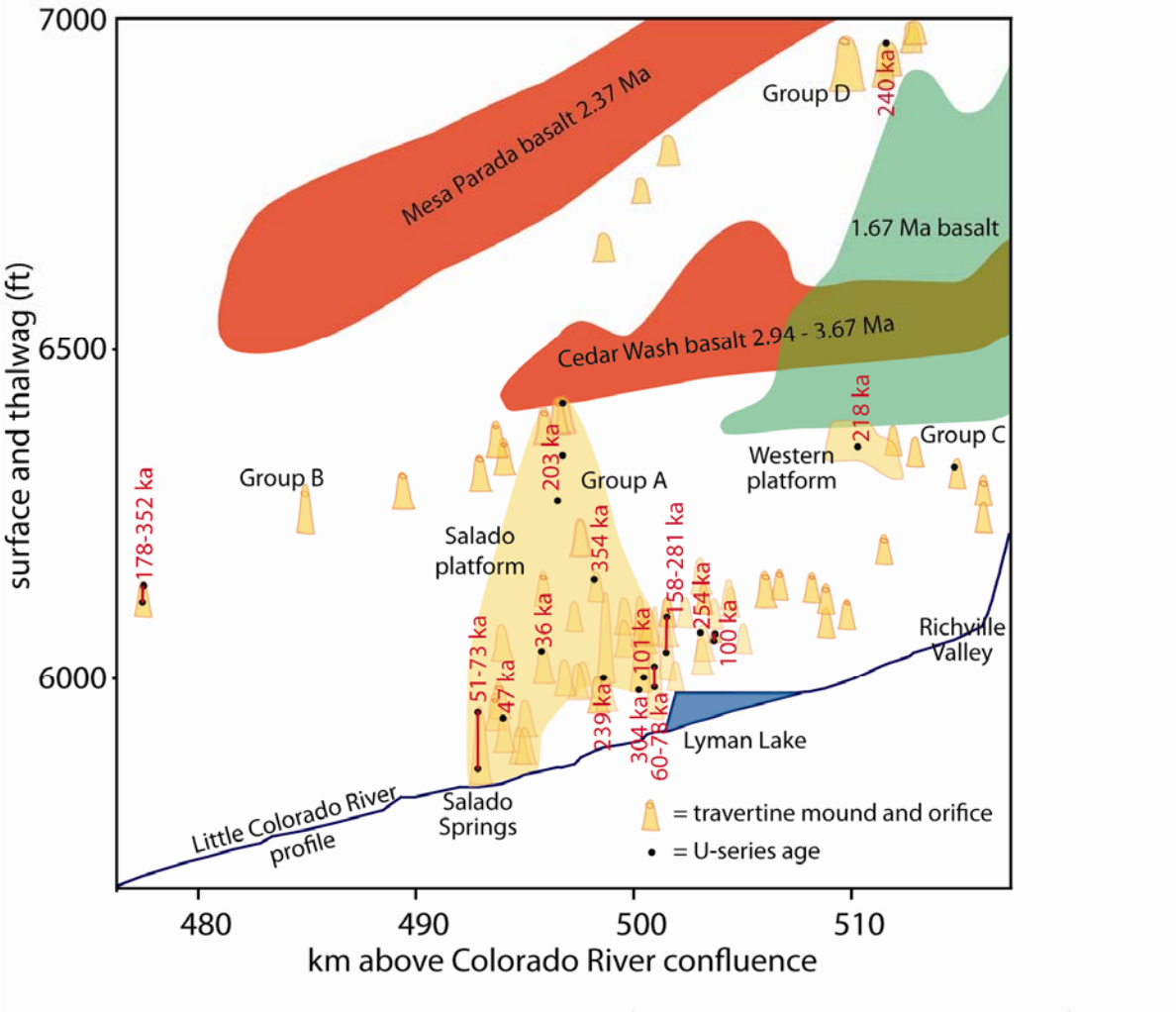

Fig. 9. Profile of the Little Colorado River with projected elevations of dated travertine samples.

Group D is located ~20 km east of the LCR, south of Carrizo Wash (Fig. 1). Mound bases are at 1828.8 m (6000 ft) and vents are from 1861.4-1867.8 m (6107-6128 ft). These travertines were not dated as part of this study.

Travertine facies

Individual travertine accumulations build up through time with morphologies and stratigraphies that reflect episodicity in rates and style of flux from spring orifices. The mounds in the Springerville area are erosional remnants of originally more voluminous deposits that, in most instances, are perched above the elevation of the modern potentiometric surface. Unlike travertine deposits found in many locations globally that form as a series of terraced pools and draped slopes precipitated from spring waters flowing down a stream channel or along a fissure, the Springerville deposits are predominantly once-symmetric cones of horizontally laminated travertine, each formed from long-term sustained outflow expelled under artesian conditions from the point source of a central spring vent (Fig. 10A). Steep-sided cones with radii between 122-400 m (10B) are clustered along the LCR near Lyman Lake and are perched 3-30 m above the valley floor, exposing bases of up to 10 m of river gravel fill on bedrock straths (10C). Broad, low-relief mounds with radii up to 1.4 km (10D) are located 5-10 km to the west and to the east of the river. The bases of several mounds are obscured by alluvium (10E). Heights of individual mounds vary from <3 m-~60 m (Moore et al., 2005).

Variations in depositional facies record paleoconditions during precipitation that can be compared to facies classifications from modern cool and thermal travertine-depositing systems (Fouke, et al., 2000; Chafetz and Guidry, 2003; Chafetz and Folk, 1984; Fouke et al., 2003) to provide clues in reconstructing the evolution of the ancient Springerville spring system. Facies include vents, ponds, waterfalls, proximal- and distal-slopes, channels, and vegetated marshes.

Travertine mound morphologies	Description
	Aerial view of the top of part of the Salado travertine platform formed by the coalesced deposits of twelve mounds. Three distinct mounds are visible, two of which have preserved open vents. Photo courtesy of Larry S. Crumpler.
	Steep-sided, smaller diameter travertine mound typical of deposits found adjacent to the Little Colorado River. Individual mound heights range from <3 to 60 m and diameters range from 122 to 400 m.
	Travertine mound near Lyman Lake perched 24 m above the LCR atop Chinle Formation strath and 3 m of river gravel and fine sediments.
	Broad, low-angle travertine mound of the type found overlying the CO_2 field and west of the LCR. Diameters range up to 1.4 km.

Travertine mound morphologies	Description
	The base of the northwestern end of the Salado Springs platform buried in alluvium.
	Salado Springs cistern. Spring waters are slowly exsolving CO_2 and He.
	A preserved domal vent covering of a small, young mound.
	One of the Salado platform mounds with a preserved vent open to a depth of 20 m.

Travertine lithofacies	Description
	A medium diameter mound with a collapsed and partially filled vent.
	A large-diameter vent, completely filled with sediment.
	Mudcracked micrite from the top of an eastern mound with casts of calcified bubbles, indicating dessication of a pond.
	Crystallized salt casts in a micritic sample from a western mound.

Travertine lithofacies	Description
	A mound that has been dissected by undermining of the LCR. The interior travertine is stained by Fe- and Mn-rich waters. Vertical laminae line conduits to the vent.
	Vertical white calcite veins and Fe- and Mn-stained travertine irregular laminae from a dissected mound exposed venting system.
	The interior of a mound near the spring vent showing the thick sequence of dense, light-colored horizontally-laminated travertine that is typical of exposures of large mounds throughout the Springerville area.
	Travertine laminae intercalated with poorly sorted silt and gravel deposited during flooding events and/or hiatuses in travertine deposition. Scale of clastic beds ranges from several centimeters to 14 m.

Travertine lithofacies	Description
	20 m high prograding vertical laminae precipitated from abundant CO2-charged spring waters cascading over an elevated scarp of horizontal travertine.
	Chaotically-oriented laminar deposits created by abundant, turbulent spring outflow. Individual laminae are thick and very dense.
	Botryoidal 1.5-cm-thick calcite spar lining a spring vent.
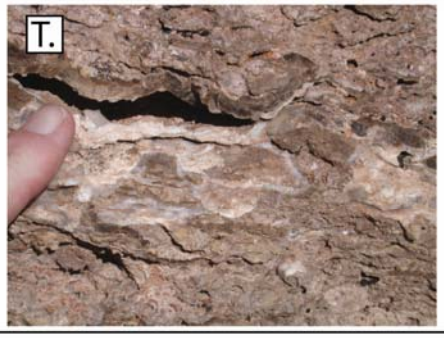	Secondary spar deposited by infiltration of spring waters into cavities in older travertine.

Travertine lithofacies	Description
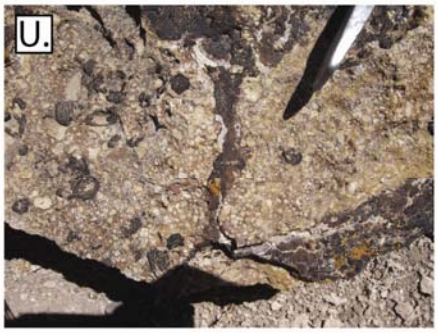	Pisolitic Fe- and Mn-stained deposit with angular travertine intraclasts and calcite-lined fractures formed in the energetic environment of a spring vent. (Black spots are lichen.)
	A calcite raft sheet that once floated on the surface of a pond. Dark concentric rings of calcite formed on clumps of bacteria radiate out to an outer ring of clear spar.
	Raft sheets and calcified bubbles from microbial degassing in a pond environment with cemented gravel.
	Porous travertine with large solution cavities lined with cm-thick, iron-stained, secondary shrub clusters similar to a pond morphotype found in thermal systems (Fouke et al., 2000), suggesting that the cavities were fluid-filled when crystals formed, possibly by higher-temperature water than the modern springs.

Travertine lithofacies	Description
	Successive layers of proximal slope microterracettes with 3-cm-high dams formed of arcuate needle shrubs on the scalloped prograding edge (Fouke et al., 2000).
	Layers of dendritic shrubs on a proximal slope.
	Ridged network formed by precipitation of travertine on filamentous bacteria in shallow water flowing toward the left and grading into smooth flowstone.
	Stromatolitic laminae (block has fallen out of place and is now upside-down) with thick layers at the center base transitioning abruptly to fine laminae.

Travertine lithofacies	Description
 CC.	Calcified filamentous bacteria.
 DD.	Rimstone and low dams creating shallow pools on a low angle distal slope.
 EE.	Vuggy unstratified travertine with chaotically-oriented plant casts formed in a marshy environment.
 FF.	Brecciated basalt fragments encased in cm-thick calcite spar with calcite cement infilling.

Vents in the study area show a range of scales and degree of preservation. The modern Salado Springs consist of several active springs, most of which are submerged in a marsh. One issues from a weakly developed travertine cistern that rises 0.5 m above the surrounding floodplain and modern water table (10F). The vent extends to a depth of several meters below the surface alluvium. The waters in the marsh and cistern contain significant concentrations of dissolved CO_2 and He gases but only bubble when disturbed. A few young mounds nearby that rise 30 m above the current river level have preserved domed vent coverings (10G). An older mound has a small diameter open vent chamber extending to a depth of 20 m (10H). More highly eroded mounds throughout the study area, when a vent location can be determined, have collapsed vents partially (10I) or completely filled with sediment (10J) and occasional micritic travertine, perhaps indicative of dissolution of laminated travertine and reprecipitation under quiet pond conditions (Lu, 2000). In some locations the micrites show tension cracks, mud cracks (10K), and salt crystal casts (10L), suggesting evaporation of highly saline standing pools after spring influx ceased. Other mounds are so highly eroded on the surface that they preserve very little morphological information. However, excavation by the Apache County Engineering Department of one highly-eroded mound on the Salt Lake Road exposes ~20 m of a stacked sequence of laminated travertine similar to what has been exposed by erosion at Salado Springs and in a mound near Lyman Lake dam. These exposures help constrain a significantly higher estimate of the volume of travertine deposited in the area than what would otherwise be suggested by what is now visible at the surface of most of the mounds.

The river has undermined and eroded large portions of individual cones (10M), in a few cases exposing internal plumbing systems. These allow for detailed examination of internal structures and evidence of the evolution of a mound. Some mounds have iron and manganese oxide-hydroxide-stained storage chambers and central conduits lined with vertically laminated deposits (10N). Parasitic vents that emerge from between older laminae on some mounds and layers exposed at the top of eroded mounds are also sometimes Fe- and Mn-stained.

Travertine deposits in the Springerville area are predominantly horizontally laminated, dense, white to beige, with 0.5 mm- to 20 cm-thick laminae (10O) precipitated radially near a central spring source. Highly porous laminae with vugs oriented randomly or in fenestral-style, parallel to lamination, are also common. Episodic hiatuses in deposition signifying dry periods or the migration of springs are marked by beds ranging in thickness from a few centimeters to 14 m of gravel and silt intercalated with travertine (10P). Periods of abundant spring outflow are evident in drapes and waterfalls, also varying in scale from 1-20 m (10Q). The chaotically-oriented, thick, dense laminated deposits at the northwestern edge of the Salado platform reflect a time of renewed abundant, turbulent spring outflow (10R).

Vent facies include dense laminae of coarse spar 1–4 cm-thick (Chafetz and Guidry, 2003), sometimes in botryoidal clusters (10S), and ranging from opaque white to semi-translucent beige and grey. Spar can also be found as secondary deposits precipitated into cavities by spring waters infiltrating through crevices in established mounds (10T). These dense crystalline samples provide low-detritus samples for robust

U/Th dating but they provide the age of the last stage of travertine deposition in the mound. Pisolitic laminae and deposits rich in intraclasts form near the energetic environment of the vent when spring waters are vigorously erupting under pressure from the subsurface (10U) (Chafetz and Guidry, 2003). Raft sheets (10V) form on the surface and bacterial shrubs and mats of ridged cyanobacterial mats (10AA) (Farmer, 2000) form on the floor of calmer adjoining pools where calcite and/or aragonite crystallize on microbial substates. Calcified bubbles from bacterial outgassing (10W) (Chafetz and Folk, 1984) and spherules formed by nucleation on organic material (Farmer, 2000) develop in shallow ponds and terraces. Secondary solution cavities can also be lined with hemispherical shrubs (10X) and may indicate precipitation in high temperature waters (Fouke et al., 2000), although similar morphologies have been observed in modern ambient-temperature deposits at Havasu Canyon in the Grand Canyon regions as well (O'Brien et al., 2006).

Microterracettes (10Y) and terracettes on a range of scales from 1-40 cm are preserved both on the modern surface of proximal slopes and between layers recording prograding deposition with spring vent migration and modulations in flow. Microterracettes are formed of arcuate needle shrubs (10Z) (Fouke et al., 2000). Crenulated laminae, networks of filamentous bacteria and smooth flowstone (10AA), and stromatolitic (10BB) morphotypes occur on proximal and distal slopes (10DD). Channel deposits include laminated and wedge-shaped deposits of cemented travertine intraclasts, sediments, and gravel, as well as unstratified, porous deposits rich in plant casts. Distal slopes also include the highly porous, unstratified bryophyte faces (Bonny and Jones,

2003), with abundant plant casts formed where spring waters flowed into a mossy, vegetated marsh environment (10EE).

The only currently-depositing travertine observed in the area today occurs at a small spring between Lyman Lake and Salado Springs 4.5 m above river level. A thin encrustation of travertine is precipitating on soil and vegetation as small volumes of water flow downslope from the spring to the river.

Brecciated basalt fragments next to the mound north of 24 Ranch spring are cemented in a calcite matrix, with cm-thick calcite spar encasing the fragments and suggesting that an annealed fault may run beneath the mound.

U- Series geochronology of travertines

The next section provides one of the first detailed geochronologic studies of the life of a travertine system in the southwestern USA. We use precise U/Th dating on geologically well constrained samples. Travertine samples were collected at key locations (Fig. 8) with an emphasis on samples that help constrain paleohydrology and landscape evolution of the region.

Geochronology methods

Powdered samples were drilled parallel to laminations with a 0.5 mm-diameter bit from the least porous laminae avoiding discolored and oolitic layers to minimize detritus. Sample powders were digested in 15N HNO_3 and spiked with a $^{236}U/^{229}Th/^{233}U$ mixed-spike, fluxed at low heat for one hour, dried down, and dissolved with 5-10 drops of 15N HNO_3 and 2 drops of perchloric acid. After drying, the samples were dissolved in

Sample#	Sample ID	UTM (X)	UTM (Y)	elevation (ft)
T1	EE07-60*#	647071	3810865	5863
T2	EE07-60R*#	647071	3810865	5863
T3	EE07-61	647071	3810865	5871
T4	EE07-62	647071	3810865	5881
T5	EE07-62R	647071	3810865	5881
T6	EE07-63	647071	3810865	5895
T7	EE07-63R	647071	3810865	5895
T8	EE07-64	647071	3810865	5904
T9	EE07-64R#	647071	3810865	5904
T10	EE07-65#	647071	3810865	5915
T11	EE07-65R*	647071	3810865	5915
T12	EE07-66	647087	3810841	5930
T13	EE07-67	647087	3810841	5936
T14	EE07-70	647237	3810846	5950
T15	K04-SPV-4	646804	3808152	6040
T16	EE07-72	649636	3807822	6271
T17	EE07-73*	649758	3807736	6340
T18	EE07-74*#	649816	3807678	6413
T19	EE07-84A	648121	3805876	6000
T20	EE07-83A	648295	3806272	6150
T21	EE07-81A#	648881	3805304	5983
T22	EE06LL-	648585	3804373	6060
T23	EE09-7#	648514	3804561	6060
T24	EE07-79#	648598	3804451	6065
T25	EE07-78#	648574	3804356	6058
T26	K04-SPV-5C	648653	3804711	6055
T27	EE06LL-51B	648637	3804286	6098
T28	K04-SPV-2#	649005	3803665	6069
T29	K04-SPV-6	648706	3804956	6080
T30	EE06SW-	645896	3796000	6320
T31	EE06LL-	649867	3798654	6460
T32	EE09-3B	662694	3798429	6972
T33	EE09-4C	657061	3814825	6217
T34	EE09-5A	657024	3814874	6240
T35	EE09-5B	657024	3814874	6240
T36	EE07-76	649938	3803215	6068
T37	EE07-75AR#	649938	3803215	6058
T38	EE06LL-	648428	3804396	5985
T39	EE06LL-52B	648417	3804532	6020
T40	EE06LL-	648008	3805196	6000
T41	K04-SPV-3	646137	3809871	5940

Table 2A). Geochronology sample locations and elevations. 2B) (below) Geochronology results. # denotes low $^{230}_{Th}/^{232}Th$. * denotes low ^{238}U concentrations. Errors reported are 2σ confidence interval. Assumed initial $^{230}Th/^{232}Th$ activity ratio of 0.8 ± 0.4.

sample#	^{238}U	error	^{232}Th	error	$[^{230}Th/^{232}Th]$	error	$[^{230}Th/^{238}U]$	error	$\delta^{234}U_m$	error	$\delta^{234}U_i$	error	uncorr age	+ error	- error	corr age	+ error	- error
T1*#	52.32	0.21	125168.19	301.8	3.38	0.020	2.65	0.018	1263.1	11.8	3668.1	216.6	392,938	20,699	18,668	377,197	20,046	18,112
T2*#	53.52	0.13	90263.07	216.3	3.00	0.022	1.66	0.012	1570.4	3.7	1977.9	48.6	99,190	1,079	1,071	81,636	8,553	8,052
T3	292.63	0.75	275.83	45.5	2784.34	459.398	0.86	0.004	1323.5	2.3	1516.1	2.9	48,094	248	247	48,084	248	247
T4	285.62	0.66	209.14	37.7	5007.20	903.499	1.20	0.005	1478.1	1.4	1787.0	2.4	67,146	337	336	67,139	337	336
T5	213.90	0.55	18133.41	71.5	46.53	0.250	1.29	0.006	1486.0	3.3	1825.0	5.2	73,586	457	456	72,710	630	627
T6	256.78	0.71	7711.03	32.3	111.67	0.578	1.10	0.004	1392.6	1.6	1661.2	2.5	62,738	315	315	62,410	354	354
T7	271.87	0.71	10336.50	61.6	92.64	0.792	1.15	0.008	1411.4	2.8	1699.4	4.5	66,118	579	577	65,707	613	610
T8	185.67	0.45	16337.21	53.6	37.85	0.179	1.09	0.005	1337.0	1.8	1598.3	3.5	64,148	351	350	63,159	604	601
T9#	172.32	0.44	82625.55	216.6	6.02	0.031	0.94	0.005	1296.5	2.3	1489.4	12.3	54,806	356	355	49,081	2,852	2,793
T10#	199.45	0.49	42401.79	111.4	15.81	0.071	1.10	0.005	1317.4	2.0	1575.1	6.1	65,652	379	377	63,228	1,262	1,250
T11*	59.00	0.16	2639.04	41.2	111.05	1.798	1.63	0.008	1213.5	3.6	1792.0	7.1	115,715	980	973	115,248	1,003	996
T12	173.10	0.59	5690.18	40.2	81.70	0.654	0.88	0.004	1213.5	5.0	1406.2	6.0	52,550	363	361	52,152	412	410
T13	219.09	0.65	8376.50	51.1	71.09	0.557	0.89	0.005	1254.2	3.6	1451.4	4.5	52,120	381	380	51,665	442	441
T14	296.72	1.01	565.04	44.7	1440.28	114.069	0.90	0.005	1296.1	4.7	1499.0	5.7	51,487	354	353	51,465	354	353
T15	538.83	1.44	5366.65	53.3	198.39	2.070	0.65	0.003	1243.1	1.9	1375.6	2.2	35,951	176	176	35,829	186	186
T16	184.89	0.47	6984.36	43.3	88.45	0.667	1.09	0.005	237.1	1.8	420.5	4.7	203,533	2,890	2,829	202,757	2,897	2,835
T17*	25.33	0.07	1936.65	47.1	55.32	1.425	1.38	0.012	370.2	5.4	845.5	33.1	293,456	12,737	11,765	292,244	12,625	11,669
T18*#	8.41	0.05	12407.42	55.2	3.47	0.050	1.67	0.025	525.9	18.8	1538.9	279.5	397,987	67,214	48,649	379,915	57,985	43,541
T19	309.49	0.76	41992.67	111.9	41.37	0.167	1.84	0.007	836.7	1.6	1645.6	13.7	240,807	2,784	2,732	239,306	2,853	2,797
T20	500.16	1.48	20035.59	77.6	146.19	0.719	1.92	0.008	738.9	3.7	2008.1	52.7	354,146	9,026	8,578	353,758	9,001	8,555
T21#	263.88	0.70	586012.78	1384.0	2.54	0.010	1.85	0.008	706.3	2.7	1669.4	67.8	330,998	7,051	6,755	304,331	14,019	12,744
T22#	141.01	0.46	399795.55	922.8	2.55	0.011	2.37	0.011	959.6	6.7	6724.1	4120.1	699,966	189,899	97,316	688,883	169,093	91,694
T23#	269.13	0.65	712340.13	1724.6	2.15	0.010	1.86	0.009	734.0	1.3	1623.2	76.9	313,890	6,205	5,945	280,792	16,368	14,603
T24#	105.14	0.25	62191.63	147.0	8.73	0.034	1.69	0.007	973.1	2.2	1519.3	16.3	164,666	1,339	1,327	157,654	3,688	3,591
T25#	144.96	0.38	133921.89	312.7	7.54	0.033	2.28	0.010	1248.0	3.2	2363.4	33.8	234,155	2,976	2,920	225,924	4,942	4,779
T26	175.75	0.58	3056.04	35.9	607.89	7.577	3.46	0.018	2359.1	4.5	4444.7	39.0	224,210	3,017	2,960	224,117	3,015	2,958
T27	155.48	0.43	624.49	46.0	2834.13	208.829	3.72	0.015	2367.2	4.4	5091.9	51.8	271,028	3,517	3,443	271,009	3,517	3,443
T28#	199.62	0.44	301960.87	932.6	5.62	0.027	2.78	0.012	1587.0	1.5	3258.4	57.7	265,264	3,481	3,401	254,534	6,200	5,944
T29	243.54	0.82	1896.26	149.2	1200.62	27.618	3.06	0.014	2091.9	5.8	3753.4	27.0	206,891	2,335	2,302	206,843	2,334	2,302
T30*#	62.78	0.16	17282.01	70.1	16.10	0.117	1.45	0.010	410.6	3.0	969.4	27.9	308,082	9,809	9,201	303,949	9,720	9,118
T31#	153.92	0.44	250090.15	688.7	2.77	0.015	1.47	0.008	505.6	2.6	937.2	36.4	245,426	4,398	4,270	218,361	13,346	12,102
T32	647.74	1.56	9946.61	51.1	195.12	1.333	0.98	0.005	80.3	0.8	158.4	2.5	240,591	4,411	4,253	240,205	4,400	4,242
T33	440.55	1.05	47466.19	135.7	53.15	0.261	1.87	0.009	1089.4	1.3	1800.5	9.6	178,882	1,773	1,751	177,758	1,846	1,821
T34	598.63	1.48	12700.54	52.0	361.31	1.838	2.51	0.010	1219.1	1.5	3155.9	52.5	336,698	5,830	5,612	336,549	5,824	5,606
T35	420.92	1.02	12368.08	74.1	255.22	2.162	2.45	0.016	1156.8	1.9	3130.1	99.7	352,387	11,093	10,315	352,180	11,077	10,301
T36	270.00	0.64	47241.47	117.0	45.36	0.178	2.60	0.010	2908.0	6.8	3861.1	12.7	101,360	626	624	100,309	812	808
T37#	168.22	0.41	588289.29	1454.5	2.02	0.009	2.31	0.010	2010.5	2.7	2646.7	112.4	128,375	932	926	97,280	14,713	13,320
T38#	143.74	0.36	89725.10	212.4	11.19	0.045	2.28	0.009	2998.3	4.7	3739.1	21.8	82,011	477	476	78,126	1,984	1,957
T39	158.18	0.47	3404.99	45.3	280.26	3.850	1.97	0.009	3404.5	7.1	4030.1	9.4	59,812	355	355	59,687	360	359
T40	101.01	0.25	302.82	46.4	2619.75	401.60	2.57	0.010	2871.6	6.3	3822.7	10.8	101,232	630	628	101,214	630	628
T41	148.84	0.39	180.49	35.7	4563.85	902.797	1.81	0.007	3919.1	4.3	4476.6	5.8	47,065	235	235	47,058	235	235

500 μL of 7N HNO_3 and added to Teflon columns containing 500 μL of Bio-Rad AG® 1W-x8 200-400 mesh chloride form resin. Thorium fraction was collected with 6N HCl and uranium fraction was collected with 1N HBr. Samples were dried down and dissolved in 3% HNO_3 for analysis on a Neptune MS-ICPMS in the Radiogenic Isotope Laboratory at the University of New Mexico to establish absolute, high-resolution ages of periods of travertine deposition.

Calculations used the following decay constants: λ^{230} of 9.1577±0.0278 x 10^{-6} $year^{-1}$ and λ^{234} of 2.8263±0.0057 x 10^{-6} $year^{-1}$ (Cheng et al., 2000). Errors reported are 2σ confidence intervals. Two laboratory blanks, analyzed for quality assurance, had measured values of <30 pg of ^{232}Th and ^{238}U. Ages were corrected using an initial $^{230}Th/^{232}Th$ activity ratio of 0.8 ± 0.4.

Geochronology results

U/Th dating of the 41 travertine samples collected is summarized in Table 2. We discuss dating results in terms of the following groups of samples: 1) Life of a mound: a stratigraphic sequence of 9 samples from the 22.3 m scarp of laminated travertine in one prominent platform deposit that gives information about the life of a travertine mound spring; 2). Paleohydrology: samples were taken at the tops of mound vents from both individual mounds and coalesced platforms that date the high stand of paleo-groundwater tables throughout the field area; 3) Incision points: we sampled the base of several travertine accumulations where travertine was deposited atop river gravels that, in turn, rest on bedrock straths at different elevations above the LCR that give new incision rate

data points.

Most analyses have sufficiently high ^{238}U concentrations and give precise results with 2 sigma errors. However, low ^{238}U concentrations <100 ppb in 6 samples indicated by * in Table 2, is probably due to uranium leaching and the calculated ages are not considered robust. Samples with high concentrations of detrital thorium, probably incorporated into the travertine with suspended clay particles, are indicated by #. Sample designations ending in R are replicate samples drilled from different laminae of the same hand sample as a quality control. Calculated ages range from 36-354 ka. These data indicate that conditions needed for voluminous travertine deposition persisted at least episodically in the Springerville area for more than 350 ka. Map locations for each sample are shown in Figure 8; and heights in the landscape are projected onto the profile of Figure 9.

Lifecycle of a travertine mound

The largest travertine accumulation in the Springerville-St. Johns area is the 6.4 x 3.2 km Salado platform just east of the LCR that was constructed from at least 12 coalesced mounds (Fig. 8). The platform base extends from below 1780 m (5840 ft), the current ground surface at the northwestern edge at Salado Springs, to 1816.6 m (5960 ft) at the southeastern edge and 1827.3 m (5995 ft) at the southern edge. The upper surface is formed of 12 domes developed around discrete spring vents. The mounds range in diameter from ~200-900 m with the elevation of the top of the highest mound at 1956.8 m (6420 ft), an overall range in elevation from base of the platform to the top of >176.8

m (580 ft). This spring system was apparently the ancestor of the modern Salado Spring system in the sense that it was the predominant spring system along the LCR at the time of its formation.

We collected a vertical suite of 9 samples for radiometric dating from the northwestern edge of the platform next to Salado Springs, a cross sectional stratigraphic section of flat lying travertine that is exposed because of fracturing at the edge of the mound. The sample suite was collected from the base of the 22.3 m-thick cliff exposure up to the nearest vent (Fig. 11). The top of the stratigraphic succession has intermittently been the location of travertine drapes that formed as abundant spring waters cascaded over the cliff into the river (Fig. 10Q, 10R). Our suite was collected back from any drapes and sampled only flat lying layers and hence provides stratigraphic context for the development of this thick accumulation and perhaps a timeframe for typical rates of accumulation of the most active mounds.

Field evidence of disconformities in the horizontally laminated section is preserved in the form of beds of mud and gravel between travertine layers ranging in thickness from a few centimeters to 0.5 m in this section and occasional wedge-shaped deposits indicate hydrologic changes. Like modern systems, the accumulation of travertine was undoubtedly irregular because of migration of the sites of deposition as spring flow shifted direction across the mounds, similar to the life of a building volcanic edifice.

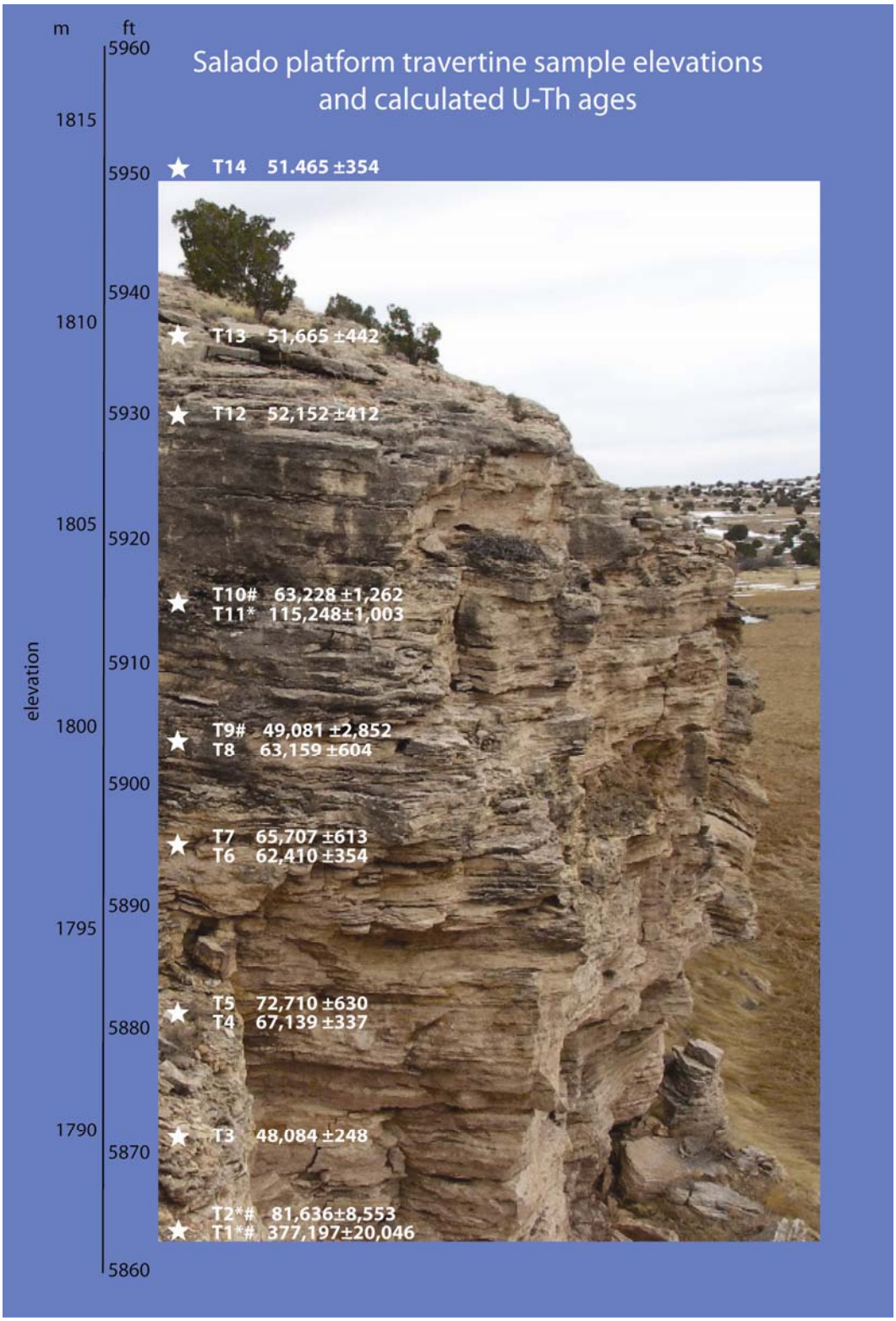

Fig. 11. Sample elevations and calculated U/Th ages for the Salado platform.

Dense “flowstone” was considered potentially most suitable for U/Th dating because of its lack of porosity and less potential for detrital contamination. These layers occur in bedding-parallel infillings and in small voids and cavities within the horizontal laminations (7T). Some of these have botryoidal textures similar to speleothems and, like sills and dikes, clearly crystallized secondarily to the laminae within which they were deposited. In an effort to establish which types of samples would give the most dependable data about the travertine occurrence, we examined the question of the extent to which these infillings can be used to date the sequential accumulation of the mound. From the geochronology, most appear to be approximately synchronous with layer deposition but some are tens of thousands of years later. Two of the samples from the Salado platform suite give calculated ages that are inconsistent with their stratigraphic locations but are similar to each other, in spite of their vertical separation of 10 m. The clean, white, crystalline calcite texture of these samples, T3 (flowstone) and T9 (calcite needle shrubs) contrasts with the porous beige laminae above and beneath them and indicates a change in depositional facies consistent with cavity infilling. The calculated ages of the samples, T3: 48,084±248; T9: 49,081±2,852 (within 2σ error of each other), suggests that secondary deposition occurred ~48 ka with the infiltration of CO_2-saturated spring waters, 2000-3000 years after primary deposition of the top layers of the mound. These ages are considered valid indications of a period of travertine deposition in the area but not of the timing of the main mound construction. In addition, rather than continuous infiltration, the ages indicate that the secondary infilling occurred in a pulse late in the lifespan of the mound. Sample T41, from a nearby small vent across the river and at a

slightly higher elevation than T9 at 1810.5 m (5940 ft), was also deposited at nearly the same time, at 47 ka.

A graph of age vs. elevation for the platform mound (Fig. 12) indicates that spring flux and travertine accumulation were fairly constant (R^2=0.91) throughout the 22 ka interval from 73-51 ka depositing 15.8 m with a rate of deposition of 0.94 m/ka. This calculation is based on the sample ages that are considered robust, excluding T1 and T2 from 1 m and T11 from 15.9 m above the base because of low uranium concentrations, and samples T3 and T9 because their anomalously young ages as discussed above.

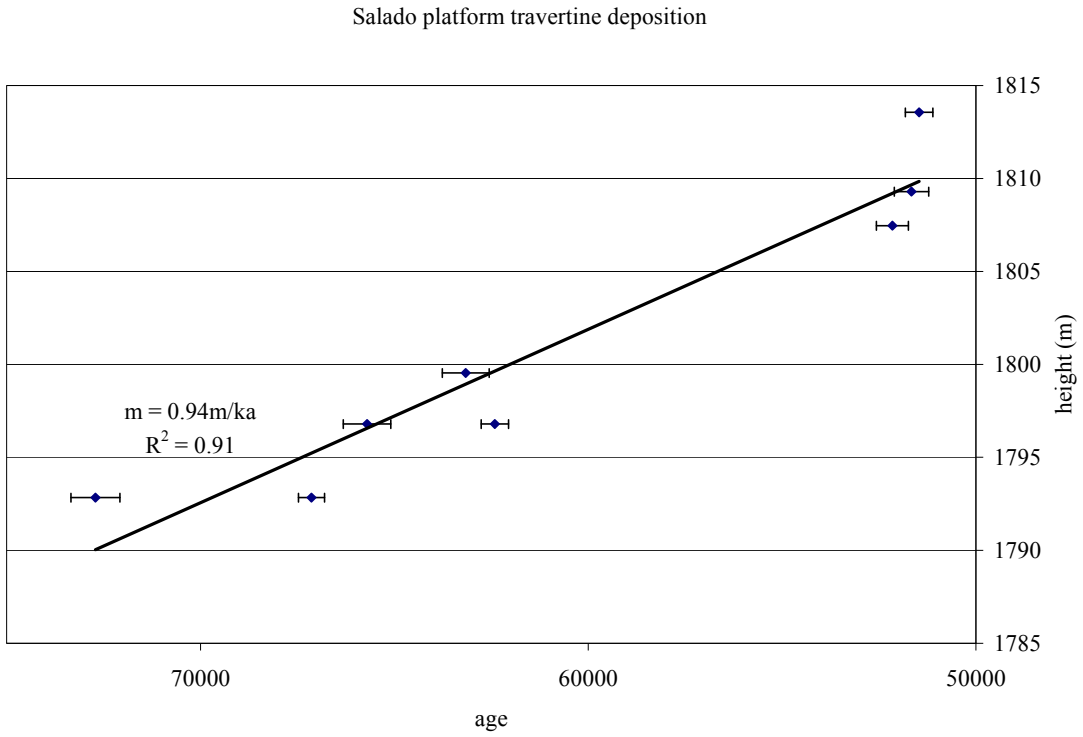

Fig. 12. Plot of elevation vs. age for Salado platform sample suite which indicates that deposition occurred at a fairly constant rate of 0.94 m/ka for at least 22 ka of the total accumulation.

Transitions in depositional regimes such as from thickly-bedded to finely laminated deposits or travertine-cemented gravel horizons within a mound sequence indicate a change in flow rates and river base flow but in dated sequences were found to sometimes occur without interruptions in depositional continuity. Drapes of laminated travertine cascading over the eroded edge of previously deposited layers in some localities indicate a lapse of time before resumption of deposition from the same spring orifice or from another nearby with drapes ranging from 2 m on mounds adjoining Lyman Dam to >22 m at Salado Springs. Parasitic vents perched at lower elevations on the side of thick sequences of older laminated travertine, in addition to cavity-filling facies, demonstrate secondary infiltration through porous and fractured deposits. However, the major mode of accumulation of travertine in the area is typified by the exposure at Salado Springs, with fairly dense horizontal laminae extending laterally for tens to hundreds of meters that were deposited by steady outflow from a central spring vent.

Older spring platform systems

Travertine deposition started in the area ~350 ka. Older spring vent systems developed at different elevations over time and tracked fluctuations in the potentiometric surface. As today, artesian head was higher toward the east above the dome, with a difference in elevation of 27.5 m between travertines deposited synchronously during the first pulse of activity. The oldest samples with robust ages are T20, deposited 384 ka by a spring flowing at 1874.5 m (6150 ft), and T35 deposited 352 ka at 1902 m (6240 ft), at

the southern end of the Salado platform and the north end of The Buttes monocline, respectively. The youngest sample, T15 from the western edge of the platform, was deposited 36 ka at 1841 m (6040 ft) when the equipotential surface was 61 m above the current river level.

Formation of the Salado platform spanned the entire time period of travertine deposition found throughout the study area, from 354-36 ka. A total of 21 samples were collected from representative locations around the main platform including the base at 3 laterally-separated locations, mounds at the highest elevations on the eastern side of the platform, a sample from a large segment of the platform on the west side that has been separated from the main deposit by river incision, and the suite of samples from Salado Springs. Build-up of the platform apparently started from the southern and eastern edges from ~350-200 ka and then migrated toward the north and west ~80-36 ka, generally, but not consistently, dropping in elevation over time.

The Buttes was also an active area of deposition for an extended period from 354-178 ka and western and southeastern mounds were deposited from 240-218 ka. Other distinct mounds located near the LCR range in age from 281-48 ka. Deposition of a mound next to Lyman Lake dam occurred from 281-158 ka. Morphological features such as a drape overlying inset river gravels and a parasitic vent suggest at least one hiatus in the depositional sequence that is not thoroughly characterized by the current sample suite.

Hiatuses spanning 25-60 ka occur in the travertine record with periods of continuous accumulation lasting ~70 ka, from ~270-200 ka and from ~100-36 ka (Fig.

13A). An older period of deposition from ~380-300 ka is less well constrained in the current dataset, partly because of uranium leaching and detrital thorium contamination leading to less precise calculated ages than younger samples and partly because of limited sampling in the eastern and western extremes of the study area.

Main conclusions of the analysis of the older platform systems are that: 1) Springs within the modern LCR corridor in the vicinity of the Salado Springs area have been active for at least the last 350 ka; 2) Hydrostatic pressures have fluctuated over time across the Coyote Wash fault zone with a difference of potentiometric head of ~35 m at 350 ka, 300 m at 250 ka, and 60 m today (Moore et al., 2005). 3) Life of each mound spring system ranges from 20-180 ka with resumed outflow from the same or nearby vents occurring in some locations after hiatuses spanning 25-60 ka. Accumulated total thicknesses of >22 m suggests deposition rates of 0.94 m/ka; 4) Major periods of continuous accumulation lasting ~70 ka occurred from ~270-200 ka and from 100-36 ka.

PALEOHYDROLOGY AND PALEOCLIMATE IMPLICATIONS

Under artesian conditions, spring elevations can be as high above the water table as the pressure head of the confined system. Faults, a network of crevices, or permeable strata can also provide flow paths at lower elevations than the potentiometric surface for lateral outflow. Presumably, the volume of travertine precipitated from springs fluctuated according to the degree of over-pressuring of the system due to the dynamic feedback between increases in groundwater volume due to fluctuations in climatically-related

recharge and increases in gas volume due to seismic pumping and/or volcanically-related influx of CO_2. This section explores possible climate connections.

Although travertine can be deposited in an interglacial climatic period as evidenced by modern travertine-depositing springs in the region (Crossey et al., 2006) and globally (Pedley et al., 2009), dating of the Springerville system suggests that large-volume accumulations of travertine were episodic and raises the question of whether these travertine episodes were related to times of large water volumes recharging the hydrologic system and resulting higher head.

Continuous travertine deposition occurred in pulses that lasted ~70 ka. Hiatuses of ~25-60 ka coincide with warm interglacial climatic peaks. Periods of accumulation correlate with cooler periods in the Devils Hole calcite $\delta^{18}O$ time series that records regional paleotemperatures (Landwehr et al., 1997; Winograd et al., 1997) and global paleoclimate curves (Raymo and Ruddiman, 2004; Shackleton and Pisias, 1985) (Fig. 13A-C). An age probability plot (Fig. 13D) shows that significantly more of the calculated ages of dated travertine samples fall between 100-36 ka than at other times but this reflects, in part, a shift between large platform-style and large-diameter mound accumulations throughout the field to smaller cones in the central section and the high-resolution sampling of one young mound, rather than an increase in volume of deposition with time. However, the five most recent episodes of magmatic activity in the SPV and Red Hill-Quemado fields which are within 5-45 km of the travertines also coincide with periods of travertine deposition and the relative influence of paleoclimatic fluctuations and volcanism is unresolved.

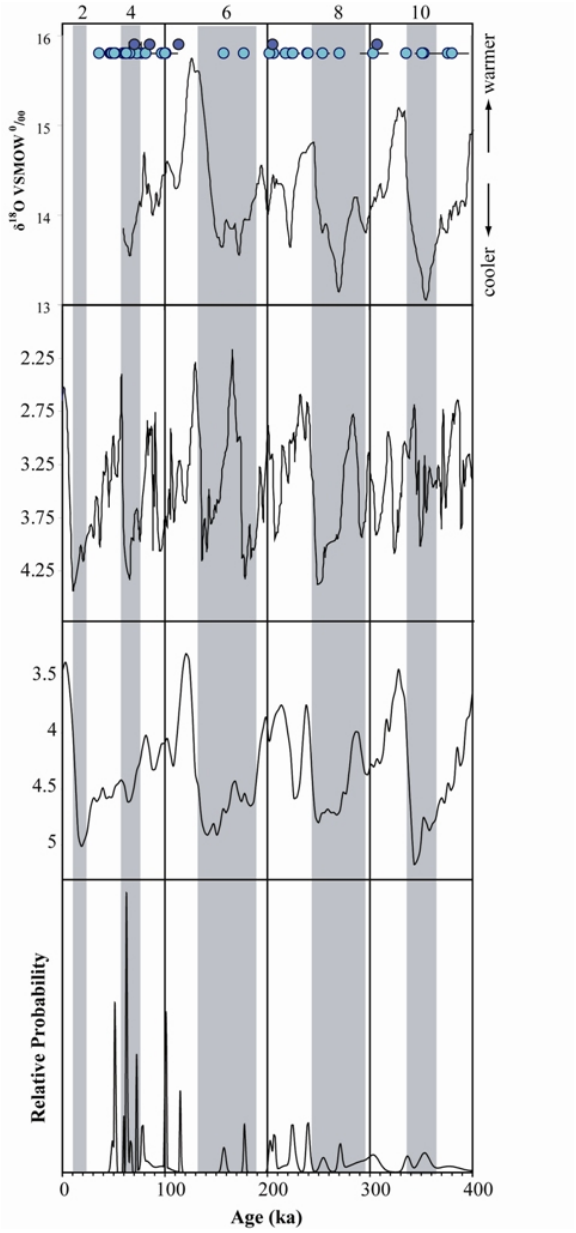

Fig. 13. Correlation diagram of dated Springerville travertine (turquoise dots) and basalts (blue dots) of the Springerville and Red Hill-Quemado volcanic fields with: A) regional paleotemperature records based on the Devils Hole calcite $\delta^{18}O$ time series (Landwehr, et al., 1997); global paleoclimate records from B) Raymo and Ruddiman, 2004, and C) Shackleton and Pisias, 1985; and D) travertine age probability diagram. Shaded intervals indicate glacial stages (modified from Anders et al., 2005).

DISCUSSION OF POSSIBLE SEISMIC CONTROLS ON TRAVERTINE ACCUMULATION

The Springerville system is exceptional because it involves an economically important He and CO_2 gas field (445 billion m^3 of CO_2) that is associated in time and location within Quaternary volcanic activity and massive travertine accumulations. These associations allow some inferences and speculations about the origin, conduit system, and depositional setting of CO_2-rich fluids. Based on He isotope and other tracers we infer the rise of CO_2-rich fluids with magma from depth. These gas-rich fluids ascend along regionally important faults and accumulate in structural and stratigraphic traps. The Springerville travertines are in close proximity to long-lived and recent episodic magmatism in the SPV and Red Hill-Quemado volcanic fields and U/Th dating of travertine samples indicates an overlap in periods of travertine deposition and active volcanism. Mineralogical evidence from St Johns Dome suggests that CO_2 partial pressures were higher in the past (Moore, et al., 2005) as is also required by the heights of observed travertine mound springs and this over-pressuring may be a requirement for significant travertine deposition. Volcanism continued until 0.308±0.07 Ma in the SPV and until 0.071±0.012 Ma in the Red Hill-Quemado field (McIntosh and Cather, 1994). Travertine deposition in the area continued until 36 ka. The discontinuity in ages of the current dataset suggests cyclicity in deposition alternating with episodic prolonged hiatuses rather than continuous slow leakage of gases input during volcanic activity.

Episodic seismic reactivation of faults that allowed an influx of deeply-sourced fluids is another potential cause of pulses of travertine deposition. Swarms of recent

shallow microearthquakes nearby and upwarped basalts are evidence of on-going tectonic activity (Eagar and Fouch, 2007; Crumpler et al., 1994). U/Th dating of additional travertine samples and additional basalt age determinations would be required to achieve the necessary resolution to definitely determine the relative influence of climatic fluctuations and pulses in tectonic activity.

LANDSCAPE EVOLUTION

The Colorado Plateau-Rocky Mountain region is an erosional landscape (Dutton, 1882) which was uplifted from sea level in late Cretaceous time, and likely has undergone additional uplift events in the Tertiary (Karlstrom et al., 2005). A key question in addressing the uplift and denudation history of different parts of the region is the time of "tectonic turn around" (McMillan, et al., 2006), defined as the time of transition from deposition and building of stratigraphy on the Colorado Plateau to erosional denudation and stripping. The Springerville area, located on the southern edge of the Colorado Plateau is an important case area because it contains an excellent record of Tertiary deposition. As shown in Figure 2, the exposed Mesozoic sedimentary section of Triassic Chinle to Cretaceous rocks is unconformably overlain by a >1 km-thick succession that includes the fluvial Eagar Formation (correlative with the "Rim" gravels of Potochnik, 2001), lacustrine/fluvial Bidahochi Formation (Fence Lake and Richville), Mio-Pleistocene Springerville and Red Hill-Quemado volcanics, gravels, and travertines. "Turn around" from deposition to denudation first occurred in this area at the end of Mogollon-Datil volcanism ~26-24 Ma (McIntosh and Cather, 1994). Aggradation

continued from <14.5-6.5 Ma during deposition of the Fence Lake Formation and ~4 Ma with infilling of Richville Formation gravels. The erosional history of the region is discussed in 4 steps: 1) pre-6.5 Ma "initial" condition, 2) 6.5–2 Ma, 3) 2-0.5 Ma, and 4) post-0.5 Ma.

Our analysis of incision and denudation of the Springerville region uses the modern LCR profile as the local reference base level. Figure 14 is the first of a series of longitudinal profiles of the LCR that illustrate the evolution of landscape features through time. It shows the modern Little Colorado River profile from the northern slope of Mt. Baldy to Zion Reservoir (not shown on the figure) with the projected elevations of modern remnants of adjoining 6 Ma and older basalts and terraces. This profile was taken from USGS topographic maps. It shows that the river drops from an elevation of 3475 m at its headwaters on Mt. Baldy to 1804.7 m (5921 ft) at Lyman Lake, to 1689 m at Zion Reservoir, a total vertical drop of 1786 m over 120 km horizontally. It has an overall slope of 15 m/km and a major knickpoint where the river flows through a steep gorge cut in young basalts of the Springerville volcanic field. The slope of the river channel varies from 45.6 m/km at the knickpoint in basalt to 0.003 m/km through the non-resistant Triassic Chinle shale. The LCR flows north from Mt. Baldy until it is diverted to the east around 3.0 Ma and younger basalts of the SPV. It meanders across the flat alluvium- and Qg5-covered floor of Round Valley near the town of Springerville before converging with Nutrioso Creek and flowing into a 2 km-long, 36.6-61 m (120-200 ft) -deep narrow gorge cut partway through consecutive layers of basalt at Coyote Hills. The river emerges briefly from the gorge into Hooper Valley and then flows through another 8 km-long

gorge through 1.67±0.09 Ma basalt to Richville Valley at the confluence with Coyote Creek from the east and Vigil Run from the west. Lyman Lake and Salado Springs are located downstream of this valley.

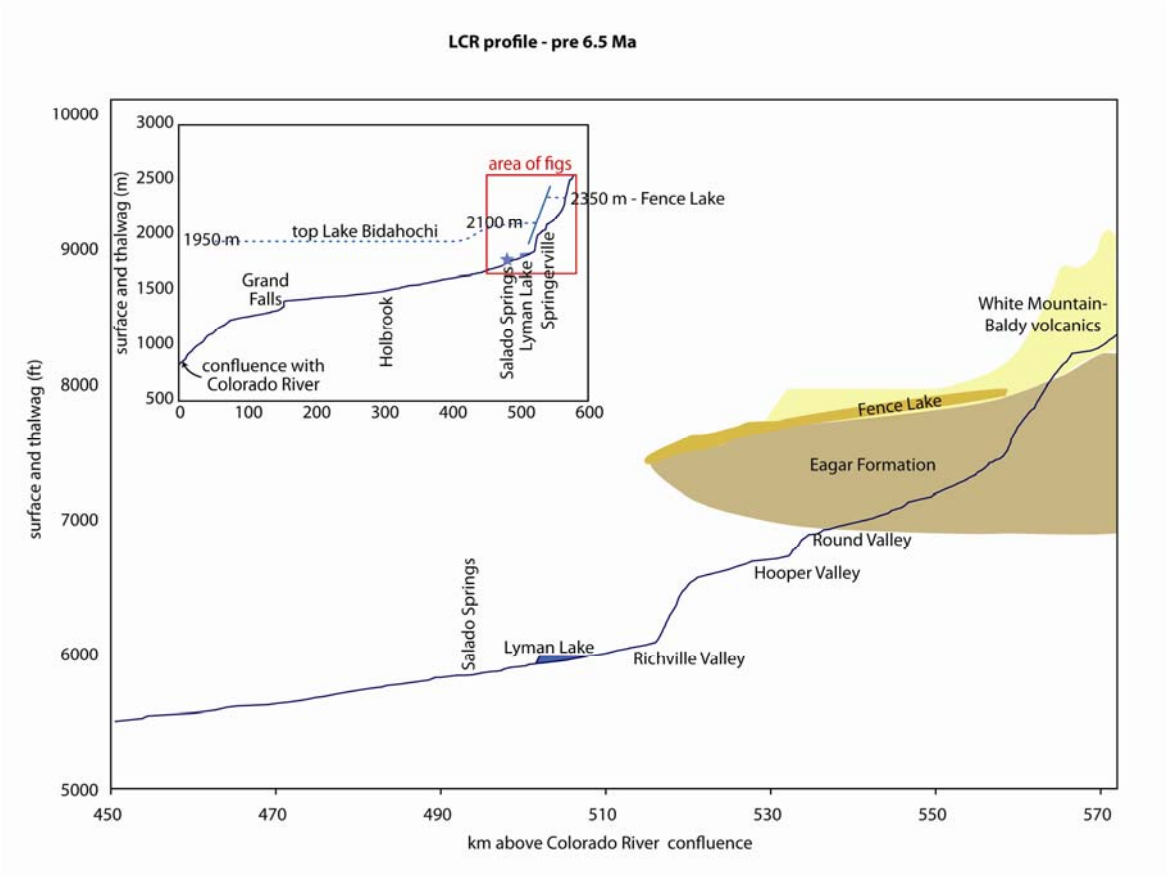

Fig. 14. Pre-6.5 Ma time slice for landscape evolution discussion. Tectonic turnaround took place ~6.5 Ma in the study area after deposition of the Fence Lake gravels. Inset shows section of the LCR profile discussed in this study in the context of the entire length of the river from the headwaters on Mt. Baldy to the confluence with the Colorado River.

Pre-late Miocene landscape evolution—pre-6.5 Ma

As mentioned earlier, the Springerville region was the site of net deposition of sedimentary units until about 4 Ma. The region was near sea level during deposition of the upper Mesa Verde Group at about 80 Ma. Laramide uplift about 70 Ma created the

Mogollon highlands to the south and west which resulted in rivers that flowed northwards onto the Colorado Plateau and eastwards into the Baca Basin and deposited the Mogollon Rim Formation of Potochnick (2001), called the Eager Formation in this area (55-34 Ma). These rocks are disconformably overlain by the volcanogenic rocks of the Spears and Datil Groups (~40-24 Ma) that record an episode of voluminous caldera-related volcanism to the south in the Mogollon-Datil volcanic field (Cather et al., 1994). During this time, the region was alternately the depositional site for the Chuska Erg sands from the north and continued volcanic debris from the south. Reversal of drainage from N- and E-flowing rivers to south-flowing streams (e.g. the Salt River) took place in the middle Miocene as a result of Basin and Range extension and collapse of the Mogollon highlands after 14.8 Ma (Potochnick, 2001). This event set the stage for a period of internal drainage on the southern Colorado Plateau (Bidahochi/ Fence Lake Formations).

The Fence Lake Formation sits atop the Eager Formation and represents deposition in Lake Bidahochi until about 6.5 Ma. A prolonged dry period produced a thick 1.5-2 m-thick calcrete layer at the top of the Fence Lake Formation (Cather et al., 1994) which was overlain by the Richville Formation. These fluvial sediments are correlative with the Quemado Formation to the east and, in part, with the upper Bidahochi Formation and were deposited in this area until ~4 Ma (McIntosh and Cather, 1994), suggesting a continued aggradational setting until that time.

Pliocene basalts cap thick sequences of Eagar Formation and thin beds of Fence Lake deposits in the southern section of the study area where large patches of Eagar Formation are exposed. Large terraces of Fence Lake are exposed in the northern section

(Fig. 2). In most places the early basalt flows (6.03-6.8 Ma) are clearly atop the sedimentary sequence and can be thought of as low areas (the paleo- LCR?) within a continued aggradation period for the landscape. Later flows (2.94-3.87 Ma), atop Richville Formation gravels, seem to be inset and are thus a record of the turn around and a shift to a denudational/incisional regime, as discussed below. Long term average incision rates calculated from the ca. 6 Ma flows are 40-50 m/ Ma for this region of the LCR (Fig. 19).

6.5-2 Ma time slice

Regional erosion followed the end of late Miocene volcanism after 6.5 Ma when Lake Bidahochi overtopped its depositional basin and the Little Colorado River began incising its gorge and draining into the Colorado River (Scarborough, 2001; Karlstrom et al., 2008).

Post- Eager Formation gravels, as mapped by Sirrine (1958), are projected into the river profile in Fig. 15. These gravels show typical inset relationships, with older gravels higher than inset younger gravels. Remnants of the oldest gravel (Tg1 terrace; Fig. 2) are inset into Eagar Fm along Coyote Creek at elevations of 2165-2195 m (7100-7200 ft). The gravels are also found at 2070-2100 m (6800-6900 ft) apparently underlying the southeastern Voight Mesa travertine mounds and are preserved as high-standing islands in younger Tg2 gravels as well as in Richville Formation to the north.

Up to 50 ft of Tg2 gravel underlies much of the SPV basalt field at elevations 60-100 m (200-300 ft) higher than the LCR riverbed. This terrace gravel is preserved on the

surface in large patches west of the Salado travertine platform, east of Richville Valley, and underlying the northwesternmost travertine mounds on Voight Mesa. There are no dates available for the gravels, and correlation of gravels is difficult, but based on their heights and comparison to dated basalts we estimate that Tg1 may be >2 Ma; and Tg2 ~ 1-2 Ma. West of the LCR, Tg2 appears to underlie travertine and basalts as old as 1.98±0.6 Ma. Tg2 gravels range in height from about 100 m (300 ft) west of the LCR and as high as 200 m (600 ft) east of the LCR. Both Tg1 and Tg2 show convexities that are similar in shape to the modern knickpoints in the LCR and are interpreted to be paleoknickpoints.

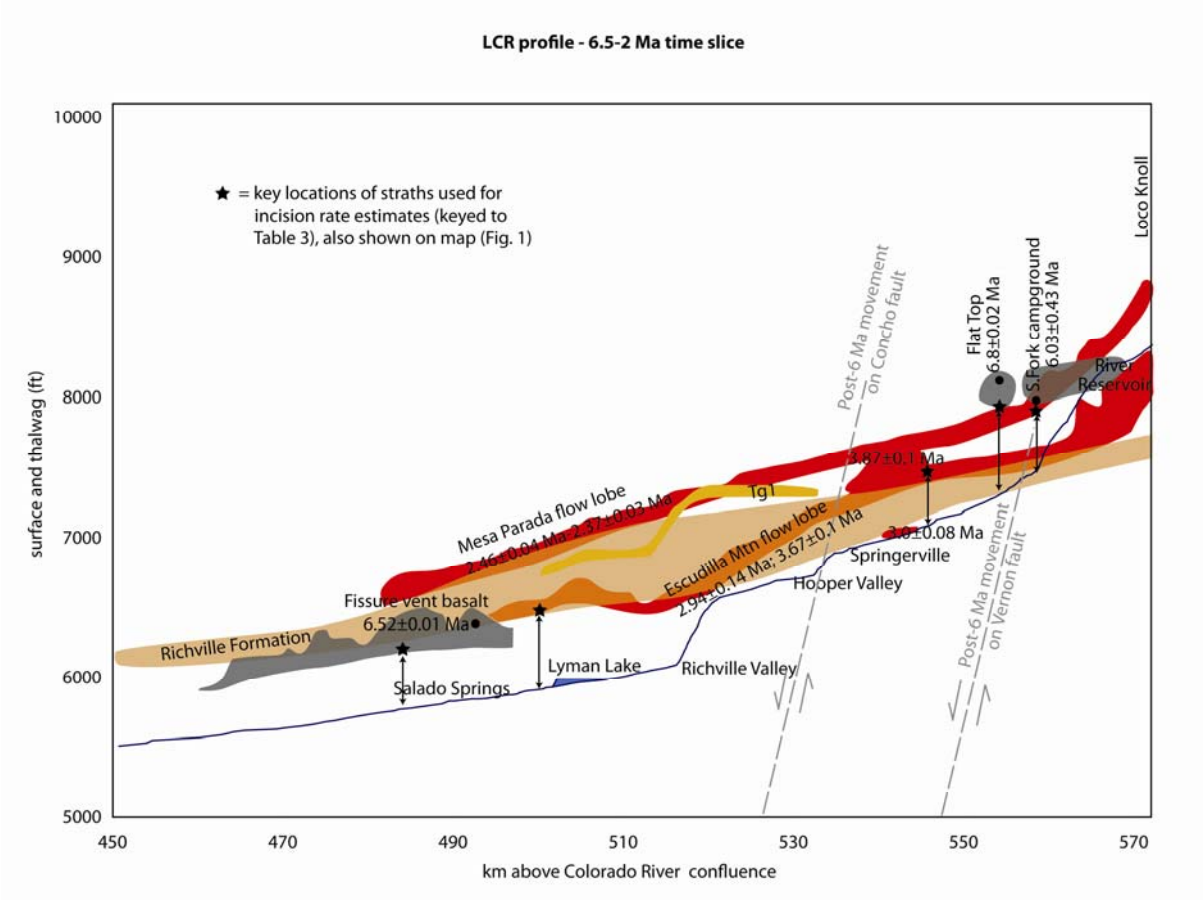

Fig. 15. 6.5-2 Ma time slice.

Bases of dated basalts are projected at their exposed elevation perpendicular to river. These basalts are classic examples of inverted topography, where basalts flowed into the lowest topography they could reach. The fact that the basalt flows are now the highest units in the landscape is due to their resistence to erosion relative to surrounding rocks. Thus, the long, thin nature of the Coyote Wash and Mesa Parada flows suggests they followed paleodrainages. Based on the present map, we infer that the 2.94±0.14-3.67±0.12 Ma Coyote Wash flow (just E of Lyman Lake) from Escudilla Mountain, part of the White Mountain-Baldy complex, marks the paleochannel of the LCR at ~ 3 Ma. This basalt now forms the resistant cap of an elongate, northwest-trending mesa that is faulted on the SW by the Coyote Wash fault that bounds the broad anticline. The lobe shows an uneven height above the modern river profile (Fig. 15) compatible with a graben between the Coyote Wash fault and inferred fault A or B, with the LCR valley lying in the graben. The height of the base of the flow at Lyman Lake is 1950.7 (6400 ft.), giving an incision rate of 52 m/Ma, similar to post- 6 Ma rates.

A second prominent flow lobe, the 2.46±0.04-2.37±0.03 Ma Mesa Parada flow, originated in the Red Hill-Quemado area to the east and filled a paleostream valley cut into older basalts (McIntosh and Cather, 1994). It flowed toward the northwest in an arc around St. Johns Dome into a channel cut in Fence Lake, Tg1, and Richville gravels from 7500-6500 ft at the eastern edge of the study area. A smooth gradient is preserved in the profile to the present. The difference in height between the flows from Red Hill and Escudilla Mountain might be explained in terms of preservation of 2-3 Ma paleotopography with the Escudilla Mountain flow in the lowest channel and Red Hill

flow on the other side of the anticline, in a different and higher local channel. Thus, the Mesa Parada flow is interpreted here to be a paleotributary to the LCR that was emplaced on top of the St Johns dome. Tg1 gravels were mapped by Sirrine beneath/ adjacent to both flows, but additional study of the gravels will be needed to verify this interpretation. Projection of the 2000 m (6560 ft.) height of the base of the Mesa Parada flow at the extreme NW tip of the preserved flow to the present river yields an apparent incision rate of 100 m/Ma, but because the projection is farther and the paleodrainage a possible tributary or relict topography, this rate is interpreted to be a maximum rate. Further use of these basalt paleoprofiles will require additional dating and mapping in key locations, but this method shows promise for evaluating the progressive evolution of an erosional landscape in that the LCR river profile is the main mechanism for incision/denudation now and has been so since before 4 Ma.

2-0.5 Ma time slice

The terrace mantled by 10-15 ft of Qg3 gravel was the next erosion surface ~30 ft below Tg2 (Sirrine, 1958). It is preserved in Big Hollow Wash beneath 1.68-1.87 Ma basalts which constrains its age, in Richville Valley atop Richville Formation, and upstream along Coyote Creek. Undated travertines along Carrizo Creek are deposited on this surface.

The next youngest gravel in the area was cut in the Richville, Chinle, and Shinarump outcrops in the northern part of the study area and is capped with coarse Qg4 gravel. Qg4 is 10-15 ft thick and consists of coarse gravel and sand with some angular

boulders of older travertine and basalt deposited by strong streams (Sirrine, 1958). Many travertine mounds are deposited on a base of Qg4 gravel on The Buttes anticline and near Carrizo Wash. Remnants of the terrace are exposed west of the Salado platform at 6000 ft and are preserved at the base of many of the travertine mounds in that area ranging in age from 350-78 ka. Large blocks of basalt slumped from the mesas onto the Qg4 terrace indicate a period of massive erosion and landslides postdating deposition of the gravels (Sirrine, 1958).

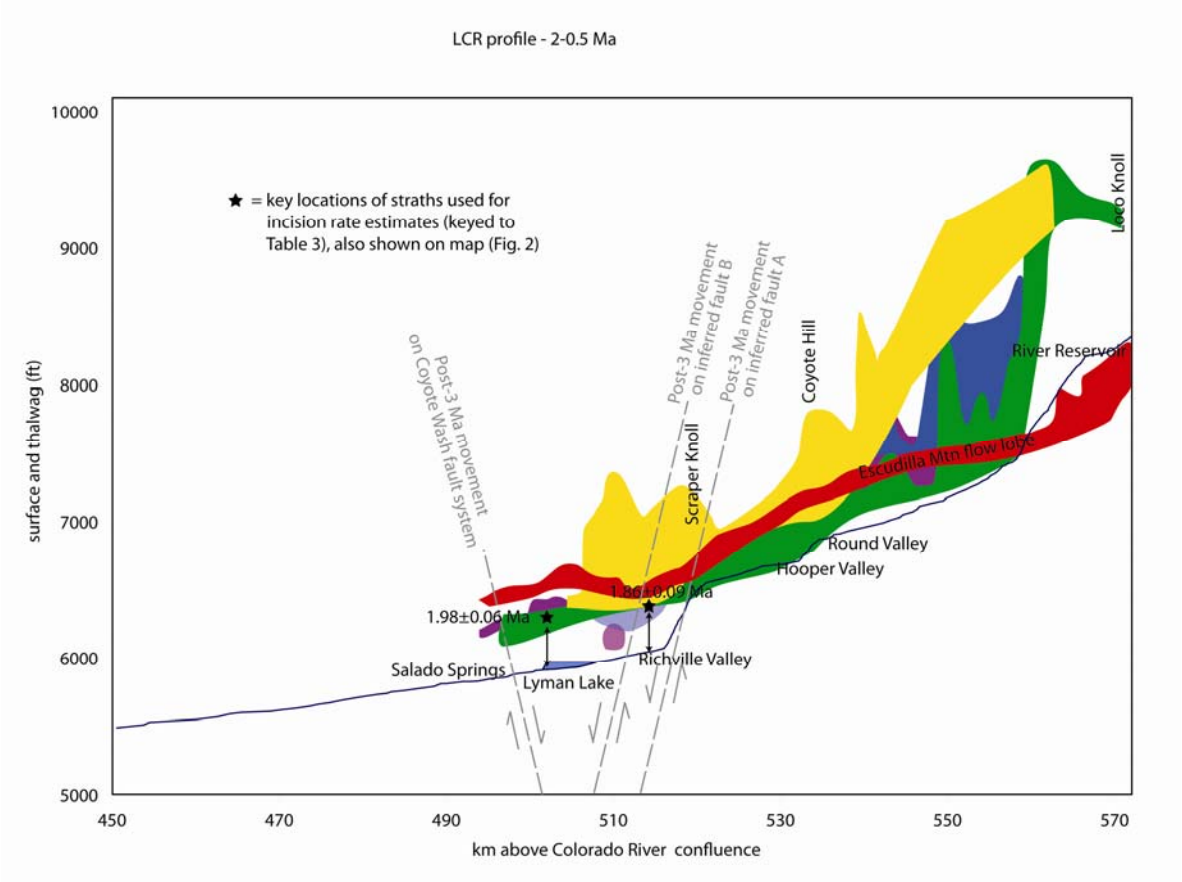

Fig. 16. 2-0.5 Ma time slice. Basalt classifications are based on Condit et al. (1999) age groups: yellow 0-0.97 Ma, green 0.98-1.67 Ma, blue 1.68-1.87 Ma, purple 1.88-2.14 Ma, red >2.14 Ma (shown on Fig. 2).

Late Quaternary (post- 500 ka) landscape evolution using straths, gravels, and travertines

This section uses travertines that directly overly gravels that, in turn overlie bedrock straths to date incision and denudation in the region in the late Quaternary. Incision rates based on ages and elevations of the bases of basalt flows along the LCR from south of Springerville to St. Johns average 42 m/Ma for the period from 6.8-1.67 Ma. Dated travertine samples from a subset of the mounds are evidence of long-term accumulation beginning >350 ka. Our method is to map bedrock straths that are overlain by LCR gravel that in turn are overlain by datable travertine. The U-series age on the travertine is thus taken as a proxy for the age of the strath (see also Pederson et al., 2002 and Karlstrom et al., 2007 for application of this method for Grand Canyon incision points). The best incision points are discussed below and are tabulated in Table 3.

Approximately 4 m of modern alluvium fills the river channel (Sirrine, 1958). This has been factored into our calculation of total river incision. The oldest dated sample that also dates a strath, is the 304 ka T21 sample from the southern end of the Salado platform. It is from the base of the travertine at an elevation of 1823.6 m, overlying 1 m of gravels that in turn rest on a strath 22.3 m above the LCR. Because this sample had low ^{238}U concentration and the calculated age may therefore be less reliable, we averaged the incision rate for this point at the base of the Salado platform with the rate calculated for T19 which was also collected just above river gravels at the base of the southern end of the platform. This sample was from 5.5 m higher. The calculated incision rates for the 2 points are 73.2 and 121.2 m/Ma and the average is 109.2 m/Ma.

One nearby mound next to Lyman Lake dam (sample T23) dated at 281 ka formed 60 m higher atop river gravels on a well exposed strath. This sample gives an incision rate of 166.2 m/Ma. Sample (T28), also from the northern end of Lyman Lake, with a younger calculated age, 255 ka, formed 9 m higher at the base of another mound and gives a slightly lower incision rate of 146.1 m/Ma. These relationships show that there was some topographic relief at the time that the travertines developed but that on average incision rates increased considerably from the long-term average by the time travertine deposition began in the area.

Samples from a more recent pulse of travertine accumulation ~100 ka provide an even higher average rate of incision. Samples T37, T38, and T40 are all from the bases of individual mounds between Lyman Lake and Salado Springs overlying river gravel/strath contacts and are dated 97, 78, and 101 ka respectively. They show that the average river incision rate in the last 100 ka increased to 320 m/Ma.

Sample #	Sample elevation	River elevation	age (Ma)	incision rate (m/Ma)
T23	6060	5920	0.281	166.2
T28	6069	5960	0.255	146.1
T37	6058	5960	0.097	349.5
T38	5985	5918	0.078	313.5
T40	6000	5915	0.101	296.5
avg. T19, T21	5992	5908	0.272	109.2
UAKA 82-194	6320	5940	1.98	60.5
AWL-5-77	6300	6080	1.67	42.6
801C	6300	5760	6.52	25.9
AWL-7-77	8400	7500	6.03	46.2
AWL-8-77	7700	7000	3.87	56.2
AWL-40-74	6400	5910	2.94	52.2
AWL-42.74	7020	6980	3	5.4
SMC-5	7980	7000	6.8	44.5

Table 3. Summary of best incision points used in incision rate estimates. Sample numbers with T are travertine samples shown in Fig. 18. Other samples are basalts shown on Fig. 15 and 16.

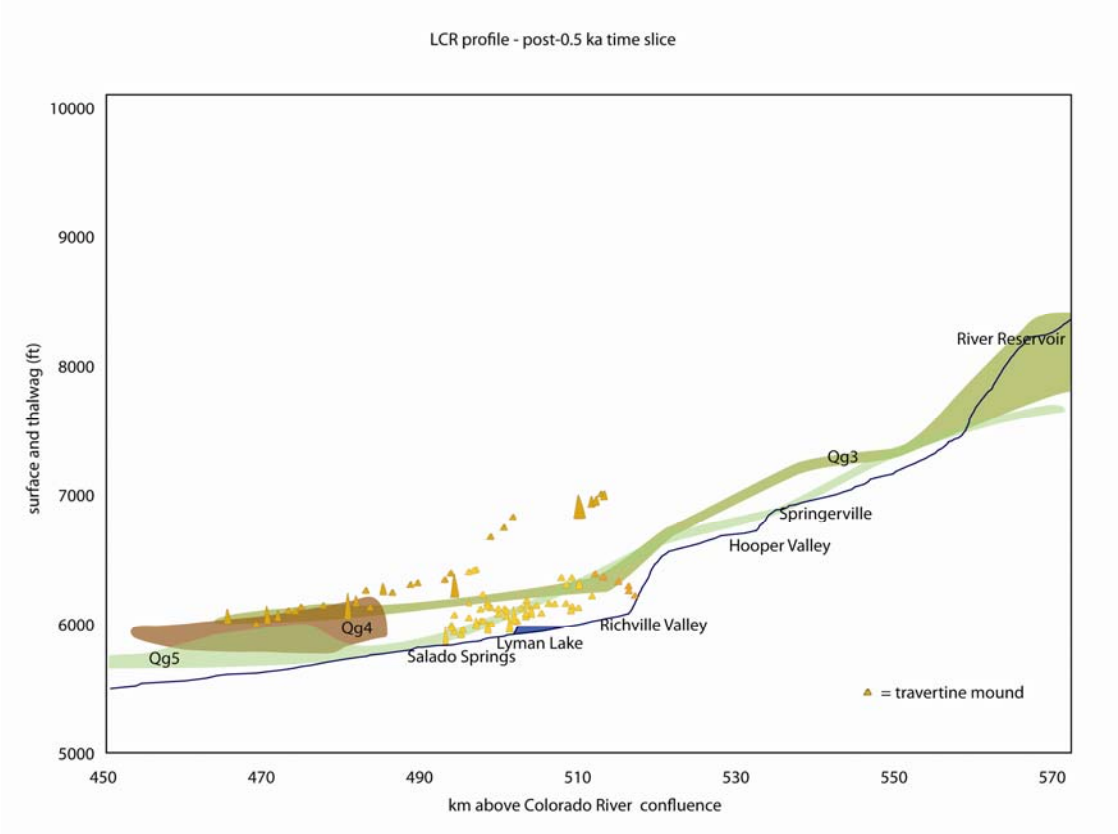

Fig. 17. Post-0.5 Ma time slice with relative elevations of young gravel terraces and travertine deposits.

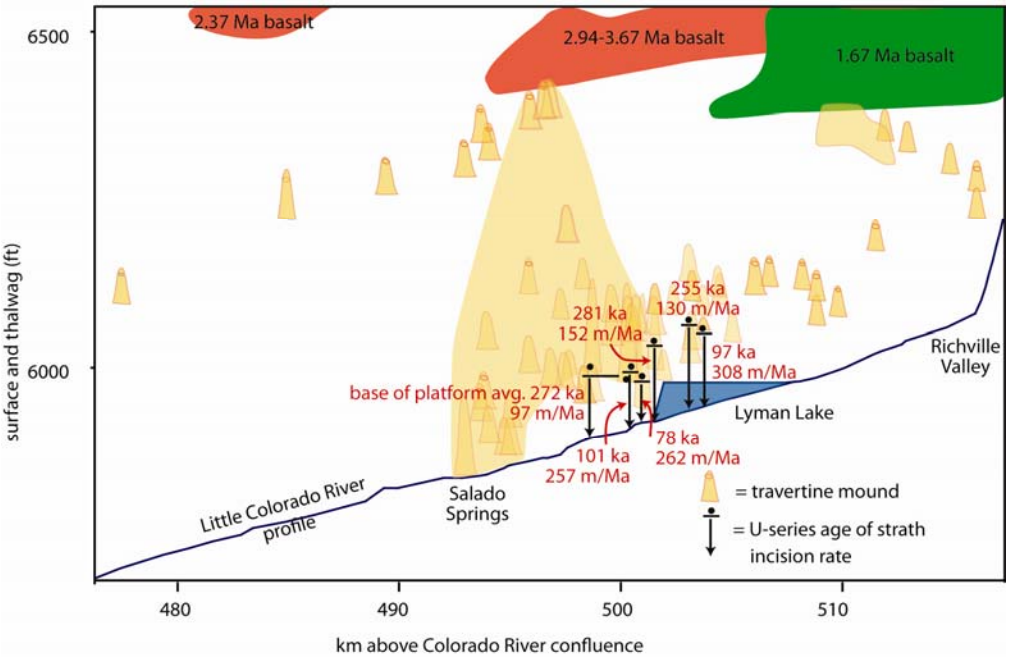

Fig. 18. Incision rates based on dated travertine samples deposited on straths.

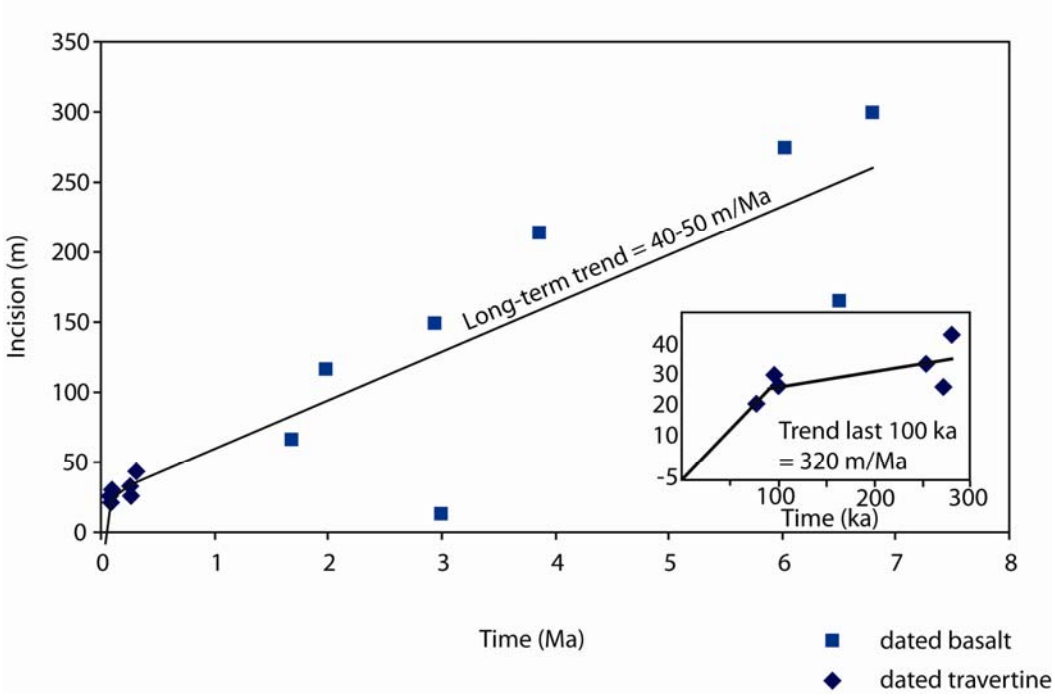

Fig. 19. Summary of incision rates through time based on elevations of basalt and travertine dated samples. Inset shows the increased rate over the last 300 ka.

Figure 19 is a summary of the variation in incision rate through time. Average incision rates of 40-50 m/Ma from 7 Ma persisted until sometime after 2 Ma, increased to 100-150 m/Ma in the Lyman lake area ~350-100 ka, and to 320 m/Ma in the last 100 ka.

SUMMARY OF MAIN FINDINGS

Waters in the modern Springerville spring system can explain the concentration of past travertines in the Salado Spring area. The geometry of the deposits indicates deposition of voluminous travertine along the same fault system for >350 ka. Analyses of the modern spring and groundwater show that the badwater line is related to the main travertine-depositing tectonic structures. Mixing trends indicate endogenic water

endmembers that are moderate T (20° C at surface), highly saline, with high CO_2, and $C_{external}$ concentrations up to 0.016.

The modern CO_2 field offers insights into the somewhat independent nature of water and gas. The average modern hydrostatic pressure intercept in the CO_2 field is at ~1830 m (6004 ft) with depths shallowing to the north with the plunging structure (Moore et al., 2005). Proportions of constituent gases, depth of producing zones, and groundwater flow rates vary across the field due to variability in permeabilities and porosities in the heterogeneous Permian reservoir rocks and differing efficiencies of local anhydrite and mudstone capping seals (Rauzi, 1999). The CO_2 reservoir is vertically stacked with perched high-pressure pockets and local differences of >60 m in the depth to water (Moore et al., 2005). Gas is now being found in basement, flow is steady but heterogeneous well to well. The potentiometric surface is not a smooth planar feature and, instead, higher-pressure fluids are forced to higher elevations within the reservoir along faults. Lateral migration allows leakage at different exposed elevations on the steeply-dipping flank of plunging anticlines with synchronous travertine precipitation at multiple elevations down to the current river level. Episodic seismically-related CO_2 influx or minor reactivation along faults created differential displacement and reorganization of hydrological flowpaths.

Gas chemistry, like the water chemistry, indicates the presence of asthenospheric- and deep-lithosphere derived fluids. $^3He/^4He$ ratios indicate that He is 7 % from the asthenosphere. $CO_2/^3He$ and C isotopic data suggest that CO_2 may be 2-6 % from the asthenosphere (depending on mixing models). Little methane suggests the gas field is not

related to oil fields. Our interpretation is that the deep CO_2, along with the other components of the endogenic fluid are derived from a compound history of mantle degassing (Crossey et al., 2009).

Modern flux of deeply derived CO_2 can be estimated from $C_{external}$ and spring discharge data. A large volume of gas is still stored in the CO_2 reservoir and high bicarbonate waters with a mantle-derived gas component flow from area springs.

The lifecycle of a mound spring accumulation is best represented by the study of the >73-51 ka Salado platform sample suite. The deposition rate for this 22.3 m accumulation averaged 0.94m/ka.

The combination of factors that allowed these spectacular accumulations of travertine in the past included wetter times, higher equipotential surface, possibly increased seismicity of CO_2 degassing. Compared to regional climate curves and the marine O isotope record, the wetter times appear to correlate well with the transition from glacial to interglacial times at the ends of O isotope stages 4,6,8, and 10. Past accumulations at different heights indicate higher water/gas head, especially at ~200 ka and 350 ka. The precise ages obtained by this technique indicate pulses of travertine accumulation from >354-36 ka and add to the limited continental paleohydrologic and paleoclimate record from directly datable materials.

Incision history- Overall, flowing spring elevations progressively dropped over time as the river incised a deeper channel and the water table dropped. However, this simple trend is also complicated by climatically-related fluctuations in groundwater recharge and tectonically-related modulations in gas influx from depth that could have

episodically over-pressured the hydrologic system and elevated the subsurface gas/water interface thereby raising spring outflow elevations.

This study uses precise dates on travertine to examine climatic, tectonic, and geomorphic controls on CO_2 flux and important interplay between volcanism, faulting, seismicity, paleoclimate, and landscape evolution in controlling CO_2 leakage, the migration of spring activity, and the detailed record preserved in travertine.

APPENDICES

APPENDIX A - METHODS

Water sampling and analysis methods

Spring temperature, pH and conductivity were measured in situ using an Oakton 1066 Series pH / ion / °C portable meter. Spring coordinates (latitude/longitude) were collected with a GPS unit. Two samples from each locality were collected in nalgene bottles; one bottle was collected without head space for alkalinity measurements and the other was filtered and acidified with HNO_3 for preservation until cation analysis. Water samples were preserved on ice and analyzed for major and minor element composition within 2 weeks in the Diagensis and Analytical Chemistry Laboratories at the University of New Mexico using standard methods (American Public Health Association, 1995). Anion concentrations were analyzed on a Dionex 500X Ion Chromatograph. A Perkin Elmer Optima 5300 DV Optical Emission Spectrometer was used for major cations and minor elements. Alkalinity determinations were made using the standard titration method described in Standard Methods, Procedure 2320, with a titration buret and a pH meter.

The pH meter was calibrated before analyzing each batch with pH 7 and pH 10 standard buffers. Resultant chemistries were then assessed with a computer speciation program (PHREEQC) and the saturation indices for selected minerals were determined (Table 1B). In addition, the CO_2 level with which the sample pH and alkalinity are consistent was computed.

Data from 431groundwater quality analyses from the USGS National Water Information System (NWIS) (http://waterdata.usgs.gov/nwis/qwdata) (Appendix B) were compiled for samples within an area defined by the latitude 35.3°- 33.87°, longitude 110.8°, and 108.3° that had been analyzed for Ca, Mg, K, Na, Cl, SO_4, and HCO_3 for comparison.

Mapping and GIS analysis

Mapping was done combining data from maps by Condit, et al.(1994) and Sirrine (1958) with modifications based on additional published Ar basalt ages (Laughlin et al., 1979; 1980; Aubele et al., 1986; Cooper et al., 1990; McIntosh and Cather, 1994) and structural and geologic data from Rauzi (1999), Allis, et al. (2005), digital datalayers from the Arizona and New Mexico Geological Surveys, ALRIS and RGIS, USGS topographic maps, and Landsat satellite imagery.

APPENDIX B - USGS NIWS WATER CHEMISTRY DATA

Concentrations are reported in ppm; $C_{external}$ values are in mol/L.

sample ID	date	lon	lat	Ca	Mg	Na	K	HCO3	Cl	SO4	TDS	Cext
A-07-28 06DBB2	7/24/74	-109.429	34.029	7.9	1.8	48	0.7	145	5.6	8.2	217.2	0.002
A-08-31 31ADD	12/19/74	-109.107	34.046	1.7	0.3	110	1.2	187	10	12	322.2	0.003
A-08-31 34ABB	12/19/74	-109.062	34.052	44	13	20	0.9	218	4.5	19	319.4	0.002
A-08-23 22ABB	8/7/92	-109.903	34.080	27	13	9.5	1.1	163	1.5	0.4	215.5	0.001
A-08-29 16CBC	8/16/66	-109.300	34.086	3.2	1.4	182	6.7	412	11	39	655.3	0.007
A-08-29 16CBC	8/13/74	-109.300	34.086	4.7	2	190	6.6	467	10	39	719.3	0.008
A-08-29 16BDC	11/1/74	-109.295	34.089	7.8	2.5	170	5.6	462	11	32	690.9	0.007
A-08-29 16BAA	8/13/74	-109.293	34.096	4.2	1.6	200	4.8	350	93	44	697.6	0.006
A-08-23 10CAA	12/11/70	-109.903	34.104	21	9.5	12	1.9	138	1.8	1.5	185.7	0.001
A-08-29 09BDD	8/14/74	-109.293	34.104	40	23	40	3.2	307	8.2	12	433.4	0.003
A-08-23 09ACC1	7/21/71	-109.918	34.105	15	7.6	6.3	2	99	1.5	1.3	132.7	0.001
A-08-29 07BCB	8/18/66	-109.334	34.106	49	14	8	0.1	236	3	8	318.1	0.002
A-08-29 07BCB	8/4/92	-109.334	34.106	48	13	8.3	1	223	0.8	1.4	295.5	0.002
A-08-29 11ADA	9/25/74	-109.249	34.107	24	26	54	5.7	314	7.3	19	450	0.004
A-08-29 07ABD	8/18/66	-109.323	34.108	43	19	19	0.1	244	13	10	348.1	0.002
A-08-29 07ABD	8/4/92	-109.323	34.108	48	20	22	1.3	273	13	12	389.3	0.003
A-08-23 11ABC	7/22/71	-109.884	34.109	13	7.9	6.3	4.3	97	1.4	3	132.9	0.001
A-08-23 11ABC	8/4/92	-109.884	34.109	15	8.9	5.7	1.5	96	3	4.6	134.7	0.001
A-08-23 10BAD1	12/11/70	-109.905	34.108	21	9.5	12	1.9	138	1.8	1.5	185.7	0.001
A-08-29 11BBC	8/15/74	-109.264	34.109	47	27	55	2.4	320	21	42	514.4	0.003
A-08-23 05DDC	6/27/72	-109.933	34.112	24	10	16	2.2	159	5	7	223.2	0.002
A-08-29 04DCC	8/16/66	-109.290	34.113	42	24	41	2.7	320	17	18	464.7	0.003
A-08-29 04DCC	8/14/74	-109.290	34.113	40	26	29	1.5	281	16	14	407.5	0.003
A-08-23 02CBA	8/3/71	-109.891	34.117	11	6	13	1.8	102	1.3	1.5	136.6	0.001
A-08-23 04BCC	8/7/92	-109.927	34.120	33	15	8.9	1.7	181	5	3.3	247.9	0.002
A-08-23 04ABD	7/20/71	-109.917	34.122	32	16	12	1.9	200	2.7	0.3	264.9	0.002
A-08-23 05BDA	7/14/71	-109.938	34.122	29	10	15	2.3	179	6.2	2	243.5	0.002
A-08-29 02ABA	8/15/74	-109.253	34.125	36	19	42	1.1	290	5.7	13	406.8	0.003
A-08-29 03BBA	8/15/74	-109.279	34.125	38	19	34	6.5	296	7.7	9.3	410.5	0.003
A-09-23 32DCC	7/14/71	-109.927	34.126	14	8.2	6.3	1.8	97	2	0.8	130.1	0.001
A-09-23 32CDC	8/3/71	-109.931	34.126	25	15	12	1.5	161	7.2	8	229.7	0.001
A-09-22 36CCA	7/21/71	-109.968	34.128	36	14	18	3.3	195	16	4	286.3	0.002
A-09-23 32DCB	7/20/71	-109.927	34.129	18	9.7	7.3	1.9	122	2.6	2.5	164	0.001
A-09-23 32DBC	7/14/71	-109.927	34.129	14	8.2	6.1	1.6	96	1.7	1.8	129.4	0.001
A-09-22 36CBB	1/11/72	-109.972	34.131	63	23	21	3.1	305	25	7.8	447.9	0.003
A-09-29 33CBA	8/17/66	-109.283	34.133	28	18	64	8.2	312	11	16	457.2	0.004
A-09-29 32BDC2	8/15/74	-109.300	34.133	57	20	37	2.5	306	19	17	458.5	0.003
A-09-29 32BDC1	8/15/74	-109.301	34.134	50	19	26	1.6	275	17	13	401.6	0.003
A-09-29 33BDA	8/17/66	-109.281	34.136	40	19	64	8.6	304	10	17	462.6	0.003
A-09-29 33BDA	8/6/92	-109.281	34.136	27	15	50	6.2	288	9.8	8.5	404.5	0.004
A-09-23 34ABD1	10/15/71	-109.889	34.138	19	14	7.3	0.6	143	3.4	2	189.3	0.001
A-09-23 34ABA	12/13/70	-109.889	34.139	5.3	1.5	30	1.8	100	2	4.3	144.9	0.001
A-09-23 34ABA	10/15/71	-109.889	34.139	5	1.5	30	1.7	104	2.4	2.3	146.9	0.002
A-09-22 25DDC	4/6/72	-109.873	34.139	19	11	6.3	1.6	117	3	5.8	163.7	0.001
A-09-22 25CDC	1/11/72	-109.965	34.141	37	19	17	4.1	244	6.2	4.5	331.8	0.002
A-09-22 26CBC	8/4/92	-109.989	34.146	68	15	7.1	1.3	241	6.4	37	375.8	0.002
A-09-22 25ACD	1/27/71	-109.961	34.149	55	16	19	2	118	16	104	330	0.001
A-09-22 22DBC	10/15/71	-109.998	34.159	170	33	22	0.7	344	160	69	798.7	0.001
A-09-30 14CCB	3/20/75	-109.147	34.171	48	15	27	2.6	237	10	20	359.6	0.002

sample ID	date	lon	lat	Ca	Mg	Na	K	HCO3	Cl	SO4	TDS	Cext
A-09-22 15DCB1	8/3/71	-109.997	34.171	68	14	3.9	1.2	252	3	22	364.1	0.002
A-09-22 15BCD	10/20/71	-110.003	34.176	71	14	3.8	1.3	272	6.3	32	400.4	0.002
A-09-22 14ADB	10/15/71	-109.975	34.179	67	18	8.5	1.6	276	4.3	45	420.4	0.003
A-09-23 18ADB	7/13/71	-109.940	34.180	15	8.7	6.2	2.2	99	2.1	4	137.2	0.001
A-09-23 18ADB	4/15/72	-109.940	34.180	16	8.2	5.3	1.9	88	2	7	128.4	0.001
A-09-22 09CCC	7/21/71	-110.022	34.184	74	19	4.4	1.3	240	5.4	77	421.1	0.002
A-09-22 04CBD	7/20/71	-110.006	34.188	49	13	3.7	1.6	177	3.5	48	295.8	0.002
A-09-27 01DDB	12/20/74	-109.431	34.200	16	8.1	11	2.3	108	3.5	3.2	152.1	0.001
A-09-23 05DCC	10/15/71	-109.928	34.201	23	16	11	3	172	5.4	4.8	235.2	0.002
A-09-23 04DBD	10/15/71	-109.907	34.204	14	10	10	2.8	122	3.1	1.8	163.7	0.001
A-09-22 04CAA	7/21/71	-110.018	34.204	79	19	4.4	1.1	238	5.3	85	431.8	0.002
A-10-25 29DDD	2/18/77	-109.711	34.230	14	8.6	6.6	1.8	89	2.9	10	132.9	0.001
A-10-28 26CCB	12/20/74	-109.356	34.230	23	8.7	9.3	1.9	110	6.5	6.3	165.7	0.001
A-10-31 29BBD	12/17/74	-109.093	34.239	62	29	270	15	635	24	280	1315	0.009
A-10-22 30ABA	8/5/92	-110.048	34.241	73	28	4.7	1.3	292	5.7	57	461.7	0.002
A-10-21 24DDC	6/14/72	-110.063	34.242	76	28	4.4	1.3	311	6	58	484.7	0.003
A-10-22 20DAD	11/21/72	-110.027	34.246	64	24	6.9	1.6	267	5.4	53	421.9	0.002
A-10-22 20DAD	8/5/92	-110.027	34.246	66	23	5.8	1.3	247	6.9	59	409	0.002
A-10-25 22BBD2	5/9/96	-109.691	34.254	18	9	8.6	2.2	100	9.1	7.2	154.1	0.001
A-10-25 22BBD2	6/17/08	-109.691	34.254	15.8	8.38	8.15	2.41	92	6.39	5.17	138.3	0.001
A-10-27 17DCB	11/21/74	-109.507	34.258	16	10	9.5	4.9	124	3.8	3.2	171.4	0.001
A-10-25 15DAC	7/30/74	-109.679	34.263	27	9.9	8.6	1.3	128	8.3	9.7	192.8	0.001
A-10-29 15BAB	1/16/75	-109.263	34.270	55	100	200	1.3	453	22	590	1421.3	0.003
A-10-29 15ABA	8/12/92	-109.257	34.271	220	0.1	250	0.1	582	280	440	1772.2	0.009
A-10-20 08DAC	4/4/72	-110.238	34.275	84	28	4.8	1.6	314	8.1	80	520.5	0.003
A-10-30 08AAA	3/19/75	-109.185	34.283	11	38	78	10	247	54	79	517	0.002
A-10-28 11BAA	1/16/75	-109.349	34.285	55	41	41	1.3	435	14	16	603.3	0.004
A-10-21 03CCC	6/14/72	-110.111	34.287	67	21	5.7	1.2	291	9.9	18	413.8	0.002
A-10-29 03BCC	8/12/92	-109.269	34.294	250	46	270	19	614	310	490	1999	0.007
A-11-30 35CCA	3/19/75	-109.145	34.302	190	69	380	36	396	460	610	2141	0.004
A-11-26 31DDC	11/22/74	-109.626	34.302	20	15	9.8	4.9	157	3.5	3.8	214	0.001
A-11-27 34CDA	1/8/75	-109.472	34.304	46	22	18	4.2	129	60	47	326.2	0.001
A-11-27 34CDA	8/6/92	-109.472	34.304	40	17	16	4	135	41	28	281	0.001
A-11-31 31CAD	3/19/75	-109.105	34.305	210	64	370	38	411	460	680	2233	0.004
A-11-29 27ACA	1/16/75	-109.257	34.325	320	59	430	29	741	500	740	2819	0.009
A-11-29 27ACA	5/13/75	-109.257	34.325	320	56	410	8	740	430	720	2684	0.009
A-11-26 29BBB	1/14/75	-109.621	34.329	19	13	11	5.9	150	3.2	4.5	206.6	0.001
A-11-27 23CCC	12/20/74	-109.461	34.331	20	13	13	4.3	142	6.6	5.3	204.2	0.001
A-11-23 20DCD	4/6/72	-109.925	34.331	12	7.1	8.5	3.2	95	2	2.9	130.7	0.001
A-11-30 20ACD	3/19/75	-109.188	34.337	320	75	390	35	885	460	590	2755	0.010
A-11-25 23CAB	1/15/75	-109.671	34.337	20	13	13	4.4	106	16	5.4	177.8	0.001
A-11-27 23AAA	12/20/74	-109.444	34.343	130	42	130	13	414	140	220	1089	0.004
A-11-28 21ABA	12/19/74	-109.380	34.343	110	34	100	13	339	120	170	886	0.003
A-11-25 18DCC2	1/15/75	-109.734	34.346	62	21	12	5.2	257	15	36	408.2	0.002
A-11-25 18DCC2	8/3/92	-109.734	34.346	66	29	40	3.2	199	78	84	499.2	0.001
A-11-24 18DDA	12/19/74	-109.833	34.348	49	25	21	3.9	226	28	34	386.9	0.002
A-11-31 17ACD	3/19/75	-109.083	34.353	200	64	400	37	389	490	680	2260	0.004
A-11-26 17ADC	1/14/75	-109.608	34.354	20	12	12	5	141	5.9	4.6	200.5	0.001

sample ID	date	lon	lat	Ca	Mg	Na	K	HCO3	Cl	SO4	TDS	Cext
A-11-22 15ADB	8/12/92	-109.993	34.355	15	9.1	8.4	2.7	111	3.6	4.5	154.3	0.001
A-11-21 17BAC	6/14/72	-110.142	34.355	73	24	7	1.4	267	9.7	74	456.1	0.002
A-11-21 17BAC	7/3/72	-110.142	34.355	73	24	7	1.4	267	9.7	74	456.1	0.002
A-11-28 09DAD	1/17/75	-109.375	34.363	160	59	280	15	296	350	550	1710	0.002
A-11-29 07DBB	1/16/75	-109.312	34.365	250	66	430	32	473	520	800	2571	0.005
A-11-28 09BDA	1/8/75	-109.386	34.368	190	48	200	16	523	220	370	1567	0.006
A-11-29 10ACA	3/19/75	-109.256	34.369	200	90	460	42	363	550	890	2595	0.002
A-11-24 08AAC	12/19/74	-109.816	34.372	41	45	46	6.1	235	93	60	526.1	0.002
A-12-15 36DDC	6/8/72	-110.692	34.375	52	29	2.3	0.7	312	3.1	3.7	402.8	0.003
A-12-15 36DDC	6/22/72	-110.692	34.375	52	29	2.3	0.7	312	3.1	3.7	402.8	0.003
A-11-28 05DBC	3/19/75	-109.401	34.378	99	46	110	14	369	140	200	978	0.004
A-11-30 03CAD	5/20/75	-109.158	34.379	260	75	450	37	530	520	820	2692	0.006
A-11-22 06BCD	8/13/92	-110.056	34.382	59	28	13	4.5	346	7	16	473.5	0.003
A-11-25 05AAA	8/17/66	-109.712	34.387	20	8.8	9	2.3	110	4	12	166.1	0.001
A-12-16 24BBA	6/20/72	-110.554	34.388	48	27	2.7	0.6	273	2.9	5.3	359.5	0.002
A-12-27 35CDA	1/7/75	-109.455	34.390	82	29	55	15	329	69	97	676	0.003
A-12-27 35CDB	1/7/75	-109.455	34.390	39	27	27	4.6	206	60	21	384.6	0.002
A-12-25 34CAB	1/22/75	-109.687	34.394	44	41	32	3.6	287	48	45	500.6	0.002
A-12-29 31BDC2	3/20/75	-109.315	34.397	370	96	370	31	772	450	930	3019	0.009
A-12-22W31BDA	1/12/72	-110.068	34.399	58	31	12	5.9	346	3.3	16	472.2	0.003
A-12-29 35BAB	3/21/75	-109.237	34.402	200	88	480	41	387	560	850	2606	0.003
A-12-28 30DBA	1/7/75	-109.413	34.409	280	61	360	26	741	380	600	2448	0.009
A-12-22W30BCB	1/12/72	-110.070	34.413	41	25	12	5.5	269	3.3	12	367.8	0.002
A-12-30 27ABA	5/20/75	-109.154	34.417	220	110	540	48	541	660	820	2939	0.004
A-12-27 26BAB1	1/7/75	-109.455	34.417	19	15	47	2.7	222	11	19	335.7	0.003
A-12-16 20DBA	8/11/92	-110.660	34.421	67	38	3.8	0.8	378	7.3	16	510.9	0.003
A-12-17 21BCB	6/21/72	-110.549	34.426	58	26	2.5	0.8	279	4.3	20	390.6	0.002
A-12-17 21BCB	8/11/92	-110.549	34.426	56	25	3.5	0.9	281	3.7	18	388.1	0.002
A-12-28 19BAD	3/18/75	-109.418	34.430	290	62	430	31	780	470	610	2673	0.009
A-12-28 19BAD	9/11/75	-109.418	34.430	260	64	460	23	776	470	600	2653	0.010
A-12-28 19BAD	4/15/76	-109.418	34.430	310	68	360	26	764	410	600	2538	0.008
A-12-28 19BAD	9/9/76	-109.418	34.430	240	67	470	25	712	550	510	2574	0.008
A-12-28 19BAD	4/6/77	-109.418	34.430	290	63	390	23	760	410	600	2536	0.009
A-12-28 19BAD	5/11/78	-109.418	34.430	310	69	360	27	610	420	650	2446	0.006
A-12-28 19BAD	3/18/87	-109.418	34.430	280	64	360	25	769	440	600	2538	0.009
A-12-28 19BAD	9/25/87	-109.418	34.430	310	71	370	24	776	360	690	2601	0.009
A-12-28 19BAD	3/17/88	-109.418	34.430	280	61	370	26	744	320	670	2471	0.010
A-12-26 19ABA	10/9/86	-109.630	34.431	13	8.2	7.7	8.5	95	3.2	3.8	139.4	0.001
A-12-26 19ABA	3/17/87	-109.630	34.431	13	8.4	7.7	2.7	102	2.2	2.7	138.7	0.001
A-12-26 19ABA	9/23/87	-109.630	34.431	14	8.6	8	2.7	100	4.5	12	149.8	0.001
A-12-26 19ABA	3/16/88	-109.630	34.431	14	8.7	8.2	3	95	3.5	4.1	136.5	0.001
A-12-17 18DDD	6/20/72	-110.569	34.432	55	26	4.3	1.9	294	3.4	20	404.6	0.003
A-12-26 13DCD	1/16/75	-109.538	34.432	4.7	3.1	200	3.3	226	81	38	556.1	0.004
A-12-26 13DCD	10/8/86	-109.538	34.432	3.7	0.82	210	2.9	342	80	42	681.42	0.006
A-12-25 18CCC2	1/21/75	-109.742	34.433	48	20	11	2.6	164	8.5	81	335.1	0.002
A-12-24 14DCC	4/22/75	-109.769	34.433	28	13	11	3.4	113	9.3	34	211.7	0.001
A-12-28 17CCC	2/26/75	-109.410	34.434	21	10	320	1.7	517	57	280	1206.7	0.008
A-12-28 18DBC	2/26/75	-109.418	34.437	46	24	260	11	587	69	190	1187	0.009
A-12-25 14DBD	1/21/75	-109.666	34.438	27	12	16	2.9	143	9	27	236.9	0.001

sample ID	date	lon	lat	Ca	Mg	Na	K	HCO3	Cl	SO4	TDS	Cext
A-12-26 18CBB	1/22/75	-109.642	34.439	48	15	20	3.9	156	18	100	360.9	0.002
A-12-26 18CBB	8/4/92	-109.642	34.439	31	13	18	2.8	161	20	43	288.8	0.002
A-12-26 15BCC	1/15/75	-109.585	34.440	14	9.4	34	5	164	5	8.8	240.2	0.002
A-12-30 13ACA	3/20/75	-109.119	34.443	220	100	270	38	489	360	630	2107	0.004
A-12-24 11CDA	10/14/74	-109.771	34.448	50	16	18	4.1	185	17	66	356.1	0.002
A-12-28 07CDB	9/10/75	-109.421	34.450	310	61	360	25	1020	420	740	2936	0.014
A-12-28 07DBD	3/21/75	-109.406	34.451	190	49	380	28	723	310	500	2180	0.010
A-12-31 08DBC	5/20/75	-109.085	34.452	300	83	260	34	821	310	590	2398	0.009
A-12-28 12BDA	3/20/75	-109.332	34.458	66	18	57	6.2	266	15	120	548.2	0.003
A-12-29 10ACA	3/20/75	-109.257	34.458	190	100	400	38	327	470	900	2425	0.001
A-12-21 01BBB	1/12/72	-110.086	34.468	57	34	21	5.2	293	8.7	83	501.9	0.003
A-13-21 34CCD	8/10/92	-110.112	34.470	56	26	12	3.8	307	4.1	19	427.9	0.003
A-12-22 02ADB	9/8/72	-109.975	34.471	36	13	14	2.9	38	12	140	255.9	0.000
A-12-26S02BDA	4/15/76	-109.561	34.471	31	25	97	4.1	231	100	51	539.1	0.003
A-12-26S02BDA	5/10/78	-109.561	34.471	28	22	100	4.3	220	91	52	517.3	0.003
A-12-26 04BBC	1/22/75	-109.607	34.475	33	16	22	4.8	164	19	32	290.8	0.002
A-12-28N02CBD	3/18/75	-109.355	34.482	190	68	560	18	353	220	1400	2809	0.003
A-13-19 27CDC	6/23/72	-110.320	34.484	52	21	5.8	1.2	242	5.8	32	359.8	0.002
A-13-29 32DDC	3/20/75	-109.282	34.484	4.2	38	200	27	232	290	51	842.2	0.002
A-13-20 29CCD	6/23/72	-110.253	34.485	44	16	2.4	1	201	2.1	9.1	275.6	0.002
A-13-27 31ABC	1/16/75	-109.515	34.492	29	26	67	3.7	238	39	40	442.7	0.003
A-13-21 25BCB	1/12/72	-110.077	34.494	30	16	13	4.6	175	7.9	33	279.5	0.002
A-13-21 26ADB2	7/8/91	-110.082	34.494	25	13	16	2.6	131	13	35	235.6	0.001
A-13-21 26ADB2	5/20/92	-110.082	34.494	24	13	15	2.8	124	11	31	220.8	0.001
A-13-29 35AAA	3/20/75	-109.227	34.496	330	92	360	35	827	510	640	2794	0.008
A-13-29 35AAA	4/13/76	-109.227	34.496	240	100	400	33	560	500	680	2513	0.005
A-13-29 35AAA	9/9/76	-109.227	34.496	340	94	370	29	873	500	640	2846	0.009
A-13-29 35AAA	4/6/77	-109.227	34.496	340	92	380	28	900	460	730	2930	0.010
A-13-29 35AAA	4/10/79	-109.227	34.496	360	90	370	29	860	490	660	2859	0.008
A-13-29 35AAA	3/18/87	-109.227	34.496	320	85	360	28	842	530	700	2865	0.010
A-13-27 25DCC	2/7/75	-109.426	34.497	100	35	260	19	405	110	490	1419	0.005
A-13-31 30DCD	3/20/75	-109.091	34.499	160	62	240	27	692	180	400	1761	0.009
A-13-28 28DAD	3/18/75	-109.367	34.502	490	200	940	16	480	1500	1600	5226	0.000
A-13-21 23CBC2	8/17/72	-110.096	34.503	56	17	14	3	214	9.8	53	366.8	0.002
A-13-28 29BCD	8/4/92	-109.397	34.504	40	19	310	3.6	696	43	210	1321.6	0.011
A-13-28 29AAD	3/6/75	-109.385	34.509	140	59	740	17	237	630	1000	2823	0.001
A-13-28 27BDC	2/25/75	-109.362	34.506	240	60	240	28	491	350	430	1839	0.004
A-13-27 26AAC	2/7/75	-109.441	34.507	44	11	260	11	510	33	270	1139	0.008
A-13-28 26ACD	3/18/75	-109.337	34.508	230	65	250	31	680	280	440	1976	0.007
A-13-27 25BBD	2/6/75	-109.433	34.508	68	18	280	14	423	49	440	1292	0.006
A-13-28 27BAD	3/18/75	-109.358	34.509	310	90	320	29	750	450	610	2559	0.007
A-13-28 19DCC	3/21/75	-109.408	34.512	17	8.3	250	4.6	463	92	140	974.9	0.007
A-13-24 22BBD	9/12/75	-109.799	34.513	60	19	18	2.7	192	17	87	395.7	0.002
A-13-24 22BBD	4/13/76	-109.799	34.513	62	20	17	2.9	196	22	89	408.9	0.002
A-13-24 22BBD	9/8/76	-109.799	34.513	63	19	18	2.8	184	18	97	401.8	0.002
A-13-24 22BBD	4/5/77	-109.799	34.513	62	19	17	2.6	190	14	83	387.6	0.002
A-13-24 22BBD	9/19/77	-109.799	34.513	60	19	15	2.7	190	17	86	389.7	0.002
A-13-24 22BBD	5/10/78	-109.799	34.513	67	20	15	2.8	190	18	87	399.8	0.002

sample ID	date	lon	lat	Ca	Mg	Na	K	HCO3	Cl	SO4	TDS	Cext
A-13-24 22BBD	9/12/78	-109.799	34.513	63	18	14	2.6	190	15	87	389.6	0.002
A-13-24 22BBD	10/9/86	-109.799	34.513	47	17	16	2.6	146	15	80	323.6	0.001
A-13-24 22BBD	3/18/87	-109.799	34.513	60	18	15	2.4	193	16	85	389.4	0.002
A-13-24 22BBD	3/15/88	-109.799	34.513	62	19	16	2.8	188	15	95	397.8	0.002
A-13-28 20DBC	2/6/75	-109.391	34.516	93	26	420	16	579	180	540	1854	0.008
A-13-28 20ABD	2/25/75	-109.389	34.523	75	33	320	8.1	433	96	500	1465.1	0.006
A-13-22 10CCA	9/5/72	-110.008	34.530	150	45	14	3.2	289	13	350	864.2	0.003
A-13-28 18DAA	9/17/75	-109.402	34.532	130	33	430	18	766	240	480	2097	0.011
A-13-28 17ACA	2/6/75	-109.391	34.535	51	21	300	12	473	94	370	1321	0.007
A-13-27 13A	10/16/86	-109.423	34.538	44	17	280	5.5	569	73	270	1258.5	0.009
A-13-27 13A	3/18/87	-109.423	34.538	44	19	280	7.2	488	77	270	1185.2	0.007
A-13-27 13A	3/16/88	-109.423	34.538	37	16	290	6.1	481	67	260	1157.1	0.007
A-13-26 12DDA	4/7/77	-109.526	34.541	15	16	150	1	280	81	61	604	0.004
A-13-26 12DDA	9/14/78	-109.526	34.541	120	120	330	2.8	260	680	350	1862.8	
A-13-26 12DDA	4/9/79	-109.526	34.541	34	35	190	1.9	270	190	120	840.9	0.003
A-13-26 12DDA	3/18/87	-109.526	34.541	33	37	200	1.8	259	240	140	910.8	0.003
A-13-17 05CAA	6/20/72	-110.567	34.544	56	30	2.5	0.8	310	4.1	18	421.4	0.003
A-13-27 09CAD	2/25/75	-109.483	34.544	110	45	150	13	251	210	310	1089	0.002
A-13-28 06DDD	2/14/75	-109.406	34.556	79	18	750	14	814	440	600	2715	0.013
A-13-30 05DCA	11/20/75	-109.178	34.559	180	39	93	17	545	60	280	1214	0.006
A-14-16 34BCB	6/19/72	-110.644	34.564	56	32	2.5	0.8	330	3.9	8.8	434	0.003
A-14-29 35CDC1	9/17/75	-109.240	34.571	200	46	170	21	654	160	330	1581	0.007
A-14-29 35CDC1	4/14/76	-109.240	34.571	200	42	170	21	660	150	300	1543	0.007
A-14-29 35CDC1	9/9/76	-109.240	34.571	210	45	170	21	653	160	310	1569	0.007
A-14-29 35CDC1	4/7/77	-109.240	34.571	210	43	180	20	650	170	320	1593	0.007
A-14-29 35CDC1	9/20/77	-109.240	34.571	210	46	180	22	650	160	320	1588	0.007
A-14-29 35CDC1	5/11/78	-109.240	34.571	210	46	180	22	640	180	310	1588	0.007
A-14-29 35CDC1	9/13/78	-109.240	34.571	210	42	180	21	640	170	310	1573	0.007
A-14-29 35CDC1	4/10/79	-109.240	34.571	220	44	170	21	620	170	320	1565	0.006
A-14-24 29DCC	4/13/76	-109.835	34.576	60	24	25	3.6	139	44	120	415.6	0.001
A-14-24 29DCC	9/8/76	-109.835	34.576	51	22	21	3.3	156	25	100	378.3	0.001
A-14-24 29DCC	9/19/77	-109.835	34.576	58	24	22	3.3	180	23	110	420.3	0.002
A-14-24 29DCC	5/10/78	-109.835	34.576	61	24	24	3.6	180	27	120	439.6	0.002
A-14-24 29DCC	9/12/78	-109.835	34.576	55	20	18	3.1	170	23	98	387.1	0.002
A-14-24 29DCC	4/10/79	-109.835	34.576	78	23	28	3.7	150	28	170	480.7	0.001
A-14-24 29DCC	10/9/86	-109.835	34.576	67	24	24	3.6	183	24	140	465.6	0.002
A-14-24 29DCC	3/17/87	-109.835	34.576	60	23	21	3.1	195	24	110	436.1	0.002
A-14-24 29DCC	9/24/87	-109.835	34.576	65	23	23	3.2	189	23	130	456.2	0.002
A-14-24 29DCC	3/15/88	-109.835	34.576	72	23	22	3.6	183	22	140	465.6	0.002
A-14-20 30CAA	9/21/72	-110.265	34.577	53	29	290	2.1	219	430	90	1113.1	0.002
A-14-20 30CAA	8/5/92	-110.265	34.577	53	28	270	2	221	430	84	1088	0.002
A-14-27 35BDC	9/12/75	-109.451	34.578	160	43	290	18	514	270	420	1715	0.007
A-14-27 35BDC	4/14/76	-109.451	34.578	64	17	350	10	409	170	400	1420	0.006
A-14-27 35BDC	9/9/76	-109.451	34.578	110	29	310	14	458	210	400	1531	0.006
A-14-27 35BDC	4/7/77	-109.451	34.578	34	8.6	380	7.3	350	140	430	1349.9	0.005
A-14-27 35BDC	9/14/78	-109.451	34.578	62	31	330	15	360	220	410	1428	0.005
A-14-27 35BDC	4/9/79	-109.451	34.578	150	35	300	16	450	240	410	1601	0.006
A-14-27 35BDC	10/8/86	-109.451	34.578	48	12	340	2.1	342	170	430	1344.1	0.005
A-14-27 35BDC	3/18/87	-109.451	34.578	91	25	310	11	420	210	440	1507	0.006

sample ID	date	lon	lat	Ca	Mg	Na	K	HCO3	Cl	SO4	TDS	Cext
A-14-27 35BDC	9/23/87	-109.451	34.578	58	15	350	9.2	350	170	430	1382.2	0.005
A-14-27 35BDC	3/15/88	-109.451	34.578	74	19	350	12	390	180	440	1465	0.006
A-14-27 28DCD	2/24/75	-109.481	34.584	150	76	260	25	300	290	550	1651	0.002
A-14-29 33BBB	3/18/75	-109.278	34.586	220	49	260	25	659	300	400	1913	0.007
A-14-30 26DDB	5/21/75	-109.126	34.589	150	41	100	12	541	70	250	1164	0.006
A-14-27 30BAC	3/17/75	-109.525	34.593	220	63	190	22	549	230	490	1764	0.006
A-14-26 21BCC	5/11/78	-109.600	34.601	43	12	100	6	190	120	47	518	0.002
A-14-26 21BCC	10/10/86	-109.600	34.601	42	12	120	8.2	198	160	54	594.2	0.002
A-14-26 21BCC	9/25/87	-109.600	34.601	69	29	37	4.7	191	42	130	502.7	0.002
A-14-26 21BCC	8/13/92	-109.600	34.601	44	12	110	5.3	192	140	51	554.3	0.002
A-14-26E19BCB	3/5/75	-109.633	34.601	39	14	45	5.5	161	52	59	375.5	0.002
A-14-26E19BCB	8/5/92	-109.633	34.601	38	14	41	4.2	163	47	56	363.2	0.002
A-14-26 19ADA	8/17/66	-109.620	34.602	38	16	10	6.8	188	124	52	434.8	0.002
A-14-25 14CCD	3/5/75	-109.676	34.606	70	24	41	8.1	219	51	120	533.1	0.002
A-14-25 14CCD	9/11/75	-109.676	34.606	63	22	44	4.9	178	51	110	472.9	0.002
A-14-25 14CCD	4/14/76	-109.676	34.606	66	23	37	4.9	199	46	110	485.9	0.002
A-14-25 14CCD	4/8/77	-109.676	34.606	68	26	41	4.9	200	42	140	521.9	0.002
A-14-25 14CCD	9/21/77	-109.676	34.606	62	23	35	4.6	190	39	100	453.6	0.002
A-14-25 14CCD	5/12/78	-109.676	34.606	70	26	37	5.3	200	45	130	513.3	0.002
A-14-25 14CCD	9/14/78	-109.676	34.606	62	22	33	4.8	190	41	110	462.8	0.002
A-14-25 14CCD	4/10/79	-109.676	34.606	72	28	38	5	200	42	130	515	0.002
A-14-25 14CCD	10/10/86	-109.676	34.606	67	29	36	5.1	242	42	120	541.1	0.002
A-14-25 14CCD	3/17/87	-109.676	34.606	66	28	36	4.5	222	48	140	544.5	0.002
A-14-25 14CCD	9/25/87	-109.676	34.606	43	12	110	5.4	231	150	53	604.4	0.003
A-14-25 14CCD	3/15/88	-109.676	34.606	68	29	37	5.1	231	42	120	532.1	0.002
A-14-26E18DDD	8/17/66	-109.618	34.607	38	15	44	5.8	162	42	54	360.8	0.002
A-14-30 21ADB	5/21/75	-109.159	34.613	120	29	210	13	597	110	270	1349	0.008
A-14-30 21ADB	4/7/77	-109.159	34.613	120	30	200	12	590	87	250	1289	0.008
A-14-30 21ADB	9/20/77	-109.159	34.613	120	30	200	11	540	100	250	1251	0.007
A-14-28 13DBD3 unsurv	8/12/75	-109.323	34.619	190	94	610	4.8	334	430	1300	2962.8	0.010
A-14-28 13DBD3 unsurv	8/4/92	-109.323	34.619	180	86	620	4.2	331	430	1300	2951.2	0.002
A-14-27 15BDC	7/2/75	-109.473	34.620	600	230	1200	15	434	2200	1700	6379	
A-14-26 10CDC	3/17/88	-109.577	34.624	230	82	510	21	603	670	660	2776	0.007
A-14-24 10BBB	8/9/66	-109.800	34.633	66	22	32	5.1	171	37	127	460.1	0.002
A-14-27 09BCD	7/2/75	-109.493	34.634	290	80	460	18	610	680	670	2808	0.006
A-14-27 09BCD	8/12/92	-109.493	34.634	290	100	470	16	626	750	740	2992	0.006
A-14-24 04DDA	8/17/66	-109.802	34.635	66	22	33	5.8	165	36	132	459.8	0.002
A-14-26 02DDD	3/17/75	-109.548	34.640	330	86	550	26	689	770	760	3211	0.007
A-14-26 03CBC	3/17/75	-109.580	34.644	270	96	600	24	662	750	660	3062	0.007
A-14-30 07ACA unsurv	5/21/75	-109.196	34.639	65	28	320	17	534	170	300	1434	0.008
A-14-30 07ACA unsurv	8/12/92	-109.196	34.639	110	25	270	14	669	140	260	1488	0.010
A-14-27 01DCD	7/2/75	-109.428	34.645	110	22	1100	6.4	641	1400	420	3699.4	0.010
A-14-25 01ABD	5/12/75	-109.646	34.646	77	25	520	6.3	266	750	180	1824.3	0.003
A-15-16 35AAC	6/23/72	-110.614	34.652	51	28	4.4	9	279	5.2	15	391.6	0.002
A-15-21 36BCB	9/12/72	-110.204	34.655	37	13	74	2.9	180	83	50	439.9	0.002
A-15-24 33BBD	3/23/72	-109.812	34.660	56	17	40	3.9	160	53	110	439.9	0.002
A-15-30 33DAC unsurv	5/21/75	-109.158	34.663	160	38	410	11	515	400	420	1954	0.007
A-15-30 33DAC unsurv	8/7/92	-109.158	34.663	150	30	400	9.6	518	380	400	1887.6	0.007
A-15-24 29CDB unsurv	12/17/71	-109.827	34.666	64	18	45	4.4	156	54	130	471.4	0.002

sample ID	date	lon	lat	Ca	Mg	Na	K	HCO3	Cl	SO4	TDS	Cext
A-15-28 29BDC	7/2/75	-109.399	34.684	55	12	280	2.7	244	300	170	1063.7	0.004
A-15-24 13DAC	3/23/72	-109.749	34.697	410	46	660	8.2	159	1500	360	3143.2	
A-15-30 21AAB	7/31/75	-109.159	34.702	150	34	220	12	430	260	270	1376	0.005
A-15-30 21AAB	4/13/76	-109.159	34.702	150	29	220	11	425	270	260	1365	0.005
A-15-30 21AAB	4/7/77	-109.159	34.702	150	32	230	11	420	260	260	1363	0.005
A-15-30 21AAB	9/20/77	-109.159	34.702	150	34	230	11	410	270	280	1385	0.004
A-15-30 21AAB	8/12/92	-109.159	34.702	150	31	210	10	429	250	270	1350	0.005
A-15-28 13CDD	7/2/75	-109.323	34.705	140	25	200	6	441	74	420	1306	0.006
A-15-31 17ADA	5/21/75	-109.070	34.711	45	12	30	1.6	247	8.8	16	360.4	0.003
A-15-22 10DBA	9/5/72	-110.000	34.711	66	74	59	7.5	204	71	350	831.5	0.000
A-15-17 04D	7/24/69	-110.545	34.719	88	42	910	3.8	152	1400	330	2925.8	0.001
A-15-23 03BBB	12/22/71	-109.902	34.734	100	29	350	7.6	182	580	200	1448.6	0.001
A-16-24 31CCC	12/22/71	-109.851	34.735	110	27	200	13	168	360	190	1068	0.001
A-16-18 28DCC	7/24/69	-110.438	34.747	80	28	940	4.4	217	1500	27	2796.4	0.001
A-16-22 29DDD	9/5/72	-110.157	34.749	56	25	63	3.6	148	75	160	530.6	0.001
A-16-28 35DAD	7/2/75	-109.333	34.750	210	63	2800	26	312	4300	730	8441	0.003
A-16-18 28DCB	7/24/69	-110.438	34.751	80	28	940	4.4	217	1500	27	2796.4	0.001
A-16-17 27BCA	7/24/69	-110.535	34.754	88	42	910	3.8	152	1400	330	2925.8	0.001
A-16-15 13DAB	8/11/92	-110.703	34.774	65	31	22	1.1	240	29	97	485.1	0.002
A-16-25 20BBC	9/17/75	-109.728	34.779	5.7	0.9	370	1.2	771	65	110	1323.8	0.013
A-16-22 17CCD	8/19/92	-110.045	34.779	95	30	88	3.6	229	110	210	765.6	0.002
A-16-30 19DBC2	7/31/75	-109.196	34.781	150	41	210	4	450	81	500	1436	0.006
A-16-29 19ADC	8/13/75	-109.301	34.786	6.1	0.2	230	0.5	262	130	91	719.8	0.004
A-16-22 14ADB	9/12/72	-109.981	34.789	210	51	780	14	364	350	1600	3369	0.004
A-16-20 16BAC	8/20/92	-110.232	34.788	69	37	110	1.9	301	140	120	778.9	0.003
A-16-23 15BAD	12/22/71	-109.896	34.790	96	23	1200	12	331	1800	270	3732	0.004
A-16-17 11DCC	9/27/72	-110.510	34.790	43	25	120	1.3	208	180	68	645.3	0.002
A-16-17 08CAB	9/27/72	-110.567	34.794	41	19	42	1.3	217	56	28	404.3	0.002
A-16-25 15BAC	9/17/75	-109.691	34.794	28	3.3	790	1.8	519	760	300	2402.1	0.008
A-16-18 09ACD1	9/6/72	-110.437	34.799	94	54	1000	3.4	179	1500	370	3200.4	0.001
A-16-30 14BDD	7/31/75	-109.128	34.800	400	100	510	2.2	307	26	2200	3545.2	0.001
A-16-28 18ADB	8/13/75	-109.409	34.800	15	3	130	1.5	193	85	22	449.5	0.003
A-16-24 33CDD	3/23/72	-109.737	34.808	150	23	330	10	264	430	350	1557	0.003
A-17-28 36DDD	8/13/75	-109.317	34.819	19	3.3	120	1.2	288	33	33	497.5	0.004
A-17-28 31BBC	8/13/75	-109.426	34.831	6.1	0.3	130	1.4	126	88	14	365.8	0.002
A-17-28 35BBC	8/13/75	-109.348	34.833	20	4.6	65	2.2	146	41	9.4	288.2	0.002
A-17-29 20CDA	8/13/75	-109.292	34.853	12	6.4	60	1.4	161	9.4	13	263.2	0.002
A-17-19 24DBA	8/17/92	-110.275	34.856	62	33	130	1.9	236	140	120	722.9	0.002
A-17-27 21CBA	8/13/75	-109.476	34.858	7.9	1.4	68	0.9	185	3.2	13	279.4	0.003
A-17-28 21ACA	8/13/75	-109.373	34.861	3.7	0.1	87	0.8	148	19	15	273.6	0.002
A-05-30 01BBC1	3/19/75	-109.225	34.861	14	3.4	27	1.6	95	5.2	22	168.2	0.001
A-17-31 16DBC	7/31/75	-109.056	34.864	200	45	160	4.8	328	100	610	1447.8	0.004
A-17-22 17DDB	8/18/92	-110.025	34.869	140	40	1100	7.2	204	1600	250	3341.2	0.001
A-17-28 13DBD	8/13/75	-109.317	34.872	3.6	0.8	120	0.5	176	26	82	408.9	0.003
A-17-26 13CCD	8/19/75	-109.559	34.883	20	3.3	420	0.7	661	35	140	1280	0.011
A-17-20 11DAC	9/6/72	-110.185	34.884	150	130	170	6.1	240	270	740	1706.1	
A-17-20 10DAC	9/6/72	-110.202	34.884	90	59	94	2.5	240	140	280	905.5	0.002
A-17-19 12BCC	8/17/72	-110.286	34.885	72	43	140	2.5	232	180	230	899.5	0.002
A-17-28 11ACB	8/13/75	-109.337	34.886	21	2.8	34	2.9	150	4.2	10	224.9	0.002

sample ID	date	lon	lat	Ca	Mg	Na	K	HCO3	Cl	SO4	TDS	Cext
A-17-19 12CBD	8/17/72	-110.285	34.885	72	43	140	2.5	232	180	230	899.5	0.002
A-17-20 08BDB	9/12/72	-110.247	34.889	39	26	100	2.1	201	130	83	581.1	0.002
A-17-18 03DDB	7/21/70	-110.417	34.896	74	51	928	3.4	182	1340	225	2803.4	0.001
A-17-29 03DBB	8/20/75	-109.246	34.900	24	4.4	47	2.3	194	9.5	13	294.2	0.003
A-17-20 03BBC	9/13/72	-110.215	34.907	120	46	290	3.1	206	460	300	1425.1	0.001
A-18-20 33DBC	7/26/72	-110.225	34.913	110	47	3.2	330	204	540	280	1514.2	0.001
A-18-26 36AAD1	8/19/75	-109.523	34.914	2.9	0.2	84	0.6	164	19	11	281.7	0.003
A-18-19 33ADA	7/21/70	-110.324	34.919	46	34	140	1.8	228	170	110	729.8	0.002
A-18-17 34ABB	7/6/05	-110.529	34.922	86.8	58.5	790	6.63	245	1280	255	2721.93	0.002
A-18-29 26BDB unsurv	8/12/75	-109.240	34.932	28	5.1	41	2.5	184	5.2	11	276.8	0.002
A-18-29 26BDB unsurv	8/11/92	-109.240	34.932	26	3.5	39	2.5	186	7.6	9.5	274.1	0.002
A-18-28 30BBC	8/13/75	-109.503	34.936	23	6	29	3.2	138	6.8	13	219	0.002
A-18-30 20CDD	8/12/75	-109.183	34.937	37	6.2	20	2.6	170	5.2	9.7	250.7	0.002
A-18-19 22CBB	7/21/70	-110.323	34.944	47	33	610	32	207	860	180	1969	0.002
A-18-28 22ABC	8/13/75	-109.356	34.947	2.8	0.1	110	0.7	82	22	35	252.6	0.001
A-18-27 18CBB	8/19/75	-109.506	34.950	7	1.7	100	1	179	34	17	339.7	0.003
A-18-19 17CBC	8/13/92	-110.358	34.956	57	28	230	2.7	226	320	150	1013.7	0.003
A-18-31 16CAC	8/12/75	-109.059	34.958	52	8.8	13	3.8	148	44	10	279.6	0.001
A-18-19 18DAA	4/21/70	-110.360	34.959	26	26	190	2.9	207	210	120	781.9	0.002
A-18-19 17ADA	6/16/72	-110.342	34.963	63	34	530	3.5	263	780	180	1853.5	0.003
A-18-19 17ADA	8/17/72	-110.342	34.963	64	35	540	3	255	790	180	1867	0.003
A-18-24 16BBB1	12/6/86	-109.806	34.966	10	3.2	590	0.9	827	390	260	2081.1	0.013
A-18-24 08BCB	12/22/71	-109.824	34.978	880	190	24000	37	530	37000	1700	64337	
A-18-24 08BCB	8/6/92	-109.824	34.978	560	210	23000	48	227	37000	2300	63345	
A-18-24 09ABB	7/9/91	-109.798	34.981	25	5.8	320	1.4	540	91	210	1193.2	0.009
A-18-24 09ABB	5/20/92	-109.798	34.981	22	5	300	1.6	522	100	200	1150.6	0.008
A-18-24 09ABB	5/8/96	-109.798	34.981	22	5	310	1.5	532	87	200	1157.5	0.009
A-18-24 09ABB	3/17/05	-109.798	34.981	46.9	13.4	512	2.35	603	331	300	1808.65	0.009
A-18-24 09ABB	8/9/05	-109.798	34.981	40.5	10.9	425	2.03	585	299	284	1646.43	0.009
A-18-24 09ABB	10/26/05	-109.798	34.981	43.8	11.5	450	2.31	634	293	285	1719.61	0.010
A-18-24 08AAA	9/22/75	-109.808	34.982	15	4.9	430	2.6	580	190	240	1462.5	0.009
A-18-16 10CBC2	6/30/05	-110.639	34.983	92.9	65.3	1140	8.58	284	1750	301	3641.78	0.002
A-18-16 10CAC	6/30/05	-110.508	34.971	98.3	68.1	1180	8.86	280	1710	299	3644.26	0.002
A-18-30 04CBC unsurv	8/12/75	-109.173	34.986	45	5.8	12	2.6	175	4.9	6.4	251.7	0.002
A-18-30 04CBC unsurv	8/12/92	-109.173	34.986	29	3.3	29	2.6	173	3.4	9.3	249.6	0.002
A-18-17 06CBB2	8/12/92	-110.590	34.986	80	37	810	6	282	1200	220	2635	0.003
A-18-27 06BCA	8/19/75	-109.520	34.991	16	2.7	87	1.8	180	35	18	340.5	0.003
A-19-23 33DCC	9/13/95	-109.906	34.999	9.1	4.1	440	1.5	421	340	200	1415.7	0.007
A-19-30 36DBA1	7/8/87	-109.108	34.999	30	3.3	24	2.1	159	3.9	7.5	229.8	0.002
A-19-29 35CDB	8/12/75	-109.240	35.000	34	5.3	47	3.6	145	58	9.6	302.5	0.001
A-19-16 36DDB I-40	6/16/72	-110.599	35.001	150	64	1000	7.5	267	1500	52	3040.5	
A-19-23 33DBA	6/17/75	-109.903	35.003	11	2.8	390	1.3	439	240	150	1234.1	0.007
A-19-16 28CCC	2/20/79	-110.661	35.011	93	51	1200	11	200	1800	320	3675	0.001
A-19-15 26DDA	2/8/79	-110.716	35.012	70	38	770	3.9	200	1200	100	2381.9	0.001
A-19-15 26DAC	1/9/79	-110.719	35.014	64	36	850	4.5	230	1300	110	2594.5	0.002
A-19-15 26DAC	8/12/92	-110.719	35.014	70	38	800	2.9	227	1200	130	2467.9	0.002
A-19-25 30BDD	6/17/75	-109.730	35.020	26	4.8	290	1.9	529	79	170	1100.7	0.008
A-19-15 28AAC	11/2/78	-110.753	35.023	92	34	410	2.3	230	670	170	1608.3	0.002
A-19-23 19DCB	6/18/75	-109.939	35.029	81	5.4	1200	4.5	490	890	1100	3770.9	0.008

sample ID	date	lon	lat	Ca	Mg	Na	K	HCO3	Cl	SO4	TDS	Cext
A-19-16 20BCD	2/27/79	-110.677	35.033	79	60	1200	12	190	1800	300	3641	0.001
A-19-25 16CCA	6/17/75	-109.698	35.043	39	4.8	290	3.4	723	42	65	1167.2	0.011
A-19-30 18CAB	8/12/75	-109.203	35.044	35	5.3	15	3.4	157	6.4	6.5	228.6	0.002
A-19-29 09AAC	8/12/75	-109.265	35.065	49	5.6	11	2.3	179	4.5	5.7	257.1	0.002
A-19-16 06CDC	2/21/79	-110.692	35.069	50	24	510	3.8	300	670	190	1747.8	0.004
A-19-25 05ABB	6/17/75	-109.709	35.079	22	6.1	420	1.4	580	190	230	1449.5	0.009
A-19-25 01AAB	6/17/75	-109.632	35.082	65	13	130	1.6	257	42	210	718.6	0.004
A-20-29 35DCD	11/18/75	-109.230	35.085	43	3.3	16	3.6	178	5.6	11	260.5	0.002
A-20-26 32BDD	6/18/75	-109.605	35.091	5.7	3.7	290	2.6	619	59	93	1073	0.010
A-20-28 36AAA1	8/20/75	-109.313	35.096	31	7.4	21	3.2	166	8.2	11	247.8	0.002
A-20-27 36BBB	8/21/75	-109.434	35.096	3.2	0.3	67	1.2	162	5.5	13	252.2	0.003
A-20-30 27DBD	11/18/75	-109.146	35.102	45	3.6	8	1.9	153	7.7	8.3	227.5	0.001
A-20-31 29ADC2	11/18/75	-109.071	35.106	48	3.9	12	1.8	158	10	6.3	240	0.001
A-20-25 28BAA	6/17/75	-109.693	35.111	6.9	0.9	420	1.4	890	20	170	1509.2	0.015
A-20-26 21DCB	8/12/75	-109.585	35.114	25	6.3	260	3.3	461	37	240	1032.6	0.007
A-20-28 19CAC	11/18/75	-109.412	35.116	24	2.6	34	3.1	167	3.3	8.4	242.4	0.002
A-20-27 24BDA1	11/18/75	-109.426	35.121	2.8	0.4	73	1	189	3.1	10	279.3	0.003
A-20-26 13DAC	6/17/75	-109.526	35.130	76	18	170	4.3	561	38	120	987.3	0.008
A-20-25 15BCD	6/17/75	-109.678	35.134	4.9	1.1	340	1.4	653	21	200	1221.4	0.011
A-20-28 14AAB	8/19/75	-109.334	35.140	42	4.8	14	3.1	161	8.9	6.2	240	0.001
A-20-27 09CAD	8/20/75	-109.479	35.145	36	8.1	240	5	485	39	200	1013.1	0.008
A-20-30 12ABD	11/18/75	-109.110	35.149	34	3.2	14	1.9	121	13	7.7	194.8	0.001
A-20-20 09BAC	9/13/95	-110.228	35.154	4.1	1.5	260	1.4	501	35	120	923	0.008
A-20-30 03BBB	8/19/75	-109.156	35.166	41	3.5	17	3.1	142	13	12	231.6	0.001
A-20-27 04BCA	6/18/75	-109.485	35.166	69	21	180	2.6	428	62	190	952.6	0.006
A-21-27 25CCA	11/19/75	-109.437	35.188	100	21	200	4.7	850	38	3.4	1217.1	0.011
A-21-27 26DBD	11/18/75	-109.445	35.189	69	16	210	3.6	503	36	220	1057.6	0.008
18 137-11.07X04.04	8/2/75	-109.197	35.191	44	4.2	17	2.1	158	14	9.9	249.2	0.001
18 137-11.54X03.87	8/20/75	-109.205	35.194	26	2.9	27	2.2	119	11	7.4	195.5	0.001
A-21-28 24CCC	8/22/75	-109.331	35.196	32	6.1	220	9.3	358	110	110	845.4	0.006
A-21-27 25BBD1	11/18/75	-109.436	35.197	4.2	0.6	440	3.8	1010	47	88	1593.6	0.017
A-21-27 25BBD2	11/18/75	-109.436	35.197	6	1.3	430	6.4	930	45	61	1479.7	0.015
A-21-29 22CCA	8/19/75	-109.258	35.199	28	2.9	61	1.7	172	30	18	313.6	0.002
A-21-28 19CCC	11/21/75	-109.421	35.200	92	36	500	20	825	64	640	2177	0.012
A-21-28 20DCA	11/19/75	-109.391	35.201	110	25	140	5.3	478	34	150	942.3	0.006
A-21-28 24BBC	11/20/75	-109.331	35.208	85	15	100	2.7	296	39	170	707.7	0.004
A-21-28 24BBC	8/14/92	-109.331	35.208	98	14	97	2.3	295	45	220	771.3	0.004
A-21-28 14DCA	11/18/75	-109.338	35.215	110	46	52	8.2	361	33	250	860.2	0.004
A-21-28 14DCA	8/11/92	-109.338	35.215	110	46	44	8.1	323	38	250	819.1	0.003
17 139-08.38X02.07	9/19/67	-109.649	35.220	76	7.9	55	4.5	220	18	110	491.4	0.003
A-21-29 07ABB	11/18/75	-109.305	35.239	120	22	38	4.1	315	39	140	678.1	0.003
18 138-04.10X00.65	12/7/72	-109.323	35.240	210	38	4.6	0.8	120	20	520	913.4	0.000
17 126-07.90X14.10	5/14/69	-109.640	35.296	20	5.5	110	2.7	270	35	19	462.2	0.004
18 124-12.38X14.06	11/5/68	-109.219	35.298	95	20	61	1.7	241	40	190	648.7	0.003
17 126-07.87X13.90	5/14/69	-109.639	35.299	18	8.5	89	0.78	240	32	12	400.28	0.003
A-18-15 28AAD avg	8/12/69	-110.752	34.934	88.35	56.3	3390	10.9	328.5	5225	270.5	9369.55	

REFERENCES

Aldrich, M.J., Jr. and Laughlin, A.W., 1984: A model for the tectonic development of the southeastern Colorado Plateau boundary, Journal of Geophysical Research, v. 89, no. B12, p. 10,207-10,218.

Allis, R.G, Chidsey, T., Gwynn, W., Morgan, C., White, S.P., Adams, M., and Moore, J. 2001: Natural CO_2 reservoirs on the Colorado Plateau and Southern Rocky Mountains: candidates for CO_2 sequestration. Proceedings of First National Conference on Carbon Sequestration, May 14-17, 2001, Washington, D.C., DOE/NETL CD DOE/NETL-2001/1144, 19 pp.

Allis, R., Bergfeld, D., Moore, J., McClure, K., Morgan, C., Chidsey, T., Heath, J., and McPherson, B., 2005: Implications of results from CO_2 flux surveys over known CO_2 systems for long-term monitoring, Proceedings of Fourth Annual Conference on Carbon Capture and Sequestration DOE/NETL, 22 pp.

Anders, M.D., Pederson, J.L., Rittenour, T.M., Sharp, W.D., Gosse, J.C., Karlstrom, K.E., Crossey, L.J., Goble, R.J., Stockli, L., and Yang, G., 2005: Pleistocene geomorphology and geochronology of eastern Grand Canyon: linkages of landscape components during climate changes, Quaternary Science Reviews v. 24, p. 2428-2448.

Anderson, O. J., 1994: Geology of the Zuni Salt Lake 7 ½ minute quadrangle, Open-File Report 405, 21 pp.

Anderson, O.J., Chamberlin, R.M., and Roybal, G.H., 1987: Road log from Fence Lake, New Mexico, to Springerville, Arizona, Bulletin - New Mexico Bureau of Mines and Mineral Resources, v.121, pp.26-30.

Anzalone, E., Ferreri, V., Sprovieri, M., and D'Argenio, B., 2007: Travertines as hydrologic archives: The case of the Pontecagnano deposits (southern Italy), Advances in Water Resources, v. 30, issue 10, p. 2159-2175.

Aubele, J.C., Crumpler, L.S., and Shafiquallah, M., 1986: K-Ar ages of late Cenozoic rocks of the central and eastern parts of the Springerville volcanic field, east-central Arizona, Isochron/West, v.46, pp.3-5.

Aubele, J.C., Crumpler, L.S., and Condit, C., 1983: Differentiation in the Springerville volcanic field, Arizona, U. S. Geological Survey Professional Paper, Report: P 1375, pp.142-143.

Baldridge, W.S., Barlov, Y., and Kron, A., 1983: Structural setting of the central Rio Grande Rift; relationship to basement grain in New Mexico and Arizona, Proceedings of the International Conference on Basement Tectonics, v.4, pp.370.

Ballentine, C.J., Schoel, M., Coleman, D., and Cain, B.A., 2000: Magmatic CO_2 in natural gases in the Permian Basin, West Texas: identifying the regional source and filling history, Journal of Geochemical Exploration 69–70 pp. 59–63.

Ballentine, C.J., Lollar, B.S., 2002: Regional groundwater focusing of nitrogen and noble gases into the Hugoton-Panhandle giant gas field, USA: Geochimica et Cosmochimica Acta, v. 66, no. 14, pp. 2483–2497.

Ballentine, C.J., Schoell, M., Coleman, D., and Cain, B.A., 2001: 300-Myr-old magmatic CO_2 in natural gas reservoirs of the west Texas Permian basin: Nature, v. 409, pp. 327-331.

Beaumont, E.C. and Roybal, G.H., 1987: Road log from Springerville to Show Low, Arizona, Bulletin - New Mexico Bureau of Mines and Mineral Resources, v.121, 30 pp.

Bonny, S., and Jones, B., 2003: Relict tufa at Miette Hot Springs, Jasper National Park, Alberta, Canada, Can. J. Earth Sci., v. 40, p. 1459-1481.

Cather, S.M., Chamberlin, R.M., McIntosh, W.C., Witcher, J., Ratte, J.C., and Anderson, O.J., 1994a: Second-day road log from Quemado Lake to Mangas Mountains, Omega, Quemado, Tejana Mesa, and Red Hill, New Mexico, and Springerville and Alpine, Arizona, *in* Chamberlin, R.M., Kues, B.S., Cather, S.M., Barker, J.M., and McIntosh, W.C, eds. NMGS Guidebook, 45th Field Conference, Mogollon Slope, West Central New Mexico and East Central Arizona, p. 47-77.

Cather, S.M., Chamberlin, R.M., and Ratte, J.C., 1994b: Tertiary stratigraphy and nomenclature for western New Mexico and eastern Arizona, *in* Chamberlin, R.M., Kues, B.S., Cather, S.M., Barker, J.M., and McIntosh, W.C., eds, NMGS Guidebook, 45th Field Conference, Mogollon Slope, West Central New Mexico and East Central Arizona,. p. 259-266.

Cather, S.M and McIntosh, W.C., 1994c: The Plio-Pleistocene Quemado Formation of West-Central New Mexico, *in* Chamberlin, R.M., Kues, B.S., Cather, S.M., Barker, J.M., and McIntosh, W.C., eds., NMGS Guidebook, 45th Field Conference, Mogollon Slope, West Central New Mexico and East Central Arizona, p. 279-281.

Cather, S.M. and Johnson, B.D., 1986: Eocene depositional systems and tectonic framework of west-central New Mexico and Eastern Arizona, *in* Peterson, J.A., ed.,

Paleotectonics & Sedimentation in the Rocky Mountain Region, United States, AAPG Memoir 41, p. 623-652.

Cather, S.M. and Johnson, B.D., 1984: Eocene tectonics and depositional setting of west-central New Mexico and eastern Arizona, New Mexico Bureau of Mines and Mineral Resources, circular 192, 30 pp.

Chafetz, H.S. and Folk, R.L., 1984: Travertines: Depositional morphology and the bacterially constructed constituents, Journal of Sedimentary Petrology, v. 54, no. 1, pp. 0289-0316.

Chafetz, H.S., and Guidry, S.A., 2003: Deposition and diagenesis of Mammoth Hot Springs travertine, Yellowstone National Park, Wyoming, U.S.A., Can. J. Earth Sci., v. 40, p. 1514-1529.

Chafetz, H.S., Rush, P.F., and Utech, N.M., 1991: Microenvironmental controls on mineralogy and habit of CaCO3 precipitates: an example from an active travertine system, Sedimentology, v. 38, p. 107-126.

Chamberlin, R.M., Cather, S.M., Anderson, O.J., and Jones, G.E., 1994: Reconnaissance geologic map of the Quemado 30 x 60 minute quadrangle, Catron County, New Mexico, New Mexico Bureau of Mines and Mineral Resources Open-File Report 406, 28 pp.

Cheng, H., Edwards, R.L., Hoff, J., Gallup, C.D., Richards, D.A., and Asmerom, Y., 2000: The half-lives of uranium-234 and thorium-230, Chemical Geology, v. 169, p. 17-33.

Chiodini, G., Frondini, F., and Ponziani, F., 1995: Deep structures and carbon dioxide degassing in central Italy, Geothermics, v. 24, no. 1, pp. 81-94.

Chiodini, G., Frondini, F., Kerrick, D.M., Rogie, J., Parello, F., Peruzzi, L., and Zanzari, A.R., 1999: Quanitfication of deep CO_2 fluxes from central Italy. Examples of carbon balance for regional aquifers and of soil diffuse degassing, Chemical Geology, v. 159, pp 205-222.

Chiodini, G., Frondini, F., Cardellini, C., Parello, F., and Peruzzi, L., 2000: Rate of diffuse carbon dioxide Earth degassing estimated from carbon balance of regional aquifers: The case of central Apennine, Italy, Geophysical Research Letters, pp. 8423-8434.

Chiodini, G., Cardellini, C., Amato, A., Boschi, E., Caliro, S., Frondini, F., and Ventura, G., 2004: Carbon dioxide Earth degassing and seismogenesis in central and southern Italy, Geophysical Research Letters, v. 31, L07615, 4 pp.

COARSE (Consortium for Arizona Reconnaissance Seismic Experiment) microearthquake data, Arizona State University, http://asuarray.asu.edu/coarse

Condit, C.D., Crumpler, L.S., and Aubele, J.C.: 1999, Miscellaneous Investigations Series - U. S. Geological Survey, Report: I-2431, 22 p., 5 sheets.

Condit, C.D. and Connor, C.B.: 1996, Recurrence rates of volcanism in basaltic volcanic fields; an example from the Springerville volcanic field, Arizona, , Geological Society of America Bulletin, v.108, no.10, p.1225-1241.

Condit, C.D.: 1995, DDM-SVF; a prototype dynamic digital map of the Springerville volcanic field, Arizona, , GSA Today, v.5, no.4, p.69, 87-88.

Condit, C D, 1991: Lithologic map of the western part of the Springerville volcanic field, east-central Arizona, Miscellaneous Investigations Series - U. S. Geological Survey, Report: I-1993, 3 sheets.

Condit, C.D., Crumpler, L.S., Aubele, J.C., and Elston, W.E., 1989: Patterns of volcanism along the southern margin of the Colorado Plateau; the Springerville Field, Journal of Geophysical Research, B, Solid Earth and Planets, v.94, no.6, p.7975-7986.

Condit, C.D. and Shafiqullah, M., 1985: K-Ar ages of late Cenozoic rocks of the western part of the Springerville volcanic field, east-central Arizona, Isochron/West, v.44, p.3-5.

Condit, C.D., 1984: The petrogenesis of the western 1/3 of the Springerville volcanic field, east-central Arizona; a first look, Eos, Transactions, American Geophysical Union, v.65, no.45, p.1122.

Condit, C.D., 1984: The geology of the western part of the Springerville volcanic field, east-central Arizona, thesis University of New Mexico, Albuquerque.

Condit, C.D., Crumpler, L.S., and Aubele, J.C., 1980: Basaltic rocks of the Springerville volcanic field, Arizona, U. S. Geological Survey Professional Paper, Report: P 1175, p.79.

Connor, C.B., Condit, C.D., Crumpler, L.S., and Aubele, J.C., 1992: Evidence of regional structural controls on vent distribution; Springerville volcanic field, Arizona, Journal of Geophysical Research, B, Solid Earth and Planets, v.97, no.9, p.12,349-12,359.

Cooley, M.E., Harshbarger, J.W., Akers, J.P. and Hardt, W.F., 1969, Regional hydrogeology of the Navajo and Hopi Indian reservations, Arizona, New Mexico, and Utah: US Geological Survey Professional Paper 521-A, 61 pp.

Cooper, J.L., 1991: The Springerville volcanic field; a case study of crust/mantle evolution and petrogenetic processes in a tectonophysical transition zone, PhD Thesis, Miami University (Ohio), Oxford, OH, 308 pp.

Cooper, J.L. and Hart, W.K., 1990: Mantle sources in the Arizona transition zone and global mantle heterogeneity, Geology (Boulder), v.18, no.11, p.1146-1149.

Cooper, J.L., Aronson, J.L., Condit, C.D. and Hart, W.K., 1990: New K-Ar ages of lavas from the Colorado Plateau-Basin and Range transition zone, east-central Arizona, Isochron/West, v.55, p.28-31.

Cooper, J.L., 1986: Chemical and isotopic variations within late Cenozoic tholeiitic and alkalic basalts in relation to the Colorado Plateau and Basin and Range provinces, east-central Arizona, PhD thesis, Miami University (Ohio), Oxford.

Crossey, L.J., Karlstrom, K.E., Springer, A.E., Newell, D., Hilton, D.R., and Fischer, T., 2009: Degassing of mantle-derived CO2 and He from springs in the southern Colorado Plateau region – Neotectonic connections and implications for groundwater systems. GSA Bulletin, v. 121, no. 7/8, p. 1034-1053.

Crossey, L.J., Fischer, T.P., Patchett, P.J., Karlstrom, K.E., Hilton, D.R., Newell, D.L., Huntoon, P., Reynolds, A.C., and de Leeuw, G.A.M., 2006: Dissected hydrologic system at the Grand Canyon: Interaction between deeply derived fluids and plateau aquifer waters in modern springs and travertine. *Geology*: v. 34, no. 1, p. 25–28.

Crumpler, L.S., Aubele, J.C., and Condit, C.D., 1994: Volcanoes and neotectonic characteristics of the Springerville volcanic field, Arizona, *in* Chamberlin, R.M., Kues, B.S., Cather, S.M., Barker, J.M., and McIntosh, W.C., eds, NMGS Guidebook, 45th Field Conference, Mogollon Slope, West Central New Mexico and East Central Arizona, p. 147-164.

Crumpler, L.S., Aubele, J.C., and Condit, C.D., 1989: Influence of Quaternary tectonic deformation on volcanism in the Springerville volcanic field, Colorado Plateau, USA, Bulletin - New Mexico Bureau of Mines and Mineral Resources, Report: 131, 64 pp.

Dallege, T.A., Ort, M.H., McIntosh, W.C., and Perkins, M.E., 2001: Age and depositional basin morphology of the Bidahochi Formation and implications for the ancestral Upper Colorado River, *in* Young, R.A. and Spamer, E.E., eds., Colorado River origin and evolution, Proceedings of a symposium held at Grand Canyon National Park in June, 2000, p. 47-51.

Drever, J.I., 1997: The geochemistry of natural waters: New Jersey,Prentice Hall, 426 pp.

Dutton, C., 1882: Tertiary history of the Grand Canyon district, U.S. Geological Survey monograph #2, 264 pp.

Eagar, K.C., and Fouch, M.J., 2007: Detection of a unique earthquake swarm in Eastern Arizona, Arizona Geology, v. 37, no. 3, 5 pp.

Edwards, R.L., Gallup, C.D., and Cheng, H., 2003: Uranium-series dating of marine and lacustrine carbonates, Reviews in Mineralogy and Geochemistry 52; p. 363-405, doi: 10.2113/0520363.

Embid, E., Crossey, L. J., Karlstrom, K.E., Eagar, K.C., Fouch, M.J., Crumpler, L.S., Aubele, J.C., 2006: "Chemical volcanoes" in the Springerville area, Arizona; using travertines, springs, and microseismicity to link water quality, paleohydrology and neotectonics: Abstracts with Programs - Geological Society of America, v.38, no.6, pp.10.

Evans, W.C., Bergfeld, D., van Soest, M.C., Huebner, M.A., Fitzpatrick, J., and Revesz, K.M., 2006, Geochemistry of low-temperature springs northwest of Yellowstone caldera: Seeking the link between seismicity, deformation, and fluid flow: Journal of Volcanology and Geothermal Research, v. 154, p. 169 – 180.

Farmer, J.D., 2000: Hydrothermal systems: doorways to early biosphere evolution, GSA Today, v. 10, no. 7, 8 pp.

Faulds, J.E., Feuerbach, D.L., Miller, C.F., and Smith, E.I, 2001: Cenozoic evolution of the Northern Colorado River extensional corridor, Southern Nevada and Northwestern Arizona. Utah Geological Association Publication 30, p. 239-272.

Fouke, B.W., Bonheyo, G.T., Sanzenbacher, B., and Frias-Lopez, J., 2003: Partitioning of bacterial communities between travertine depositional facies at Mammoth Hot Springs, Yellowstone National Park, U.S.A., Can. J. Earth Sci., v. 40, p. 1531-1548.

Fouke, B.W., Farmer, J.D., Des Marais, D.J., Pratt, L., Sturchio, N.C., Burns, P.C., and Discipulo, M.K., 2000: Depositional Facies and Aqueous-Solid Geochemistry

of Travertine-Depositing Hot Springs (Angel Terrace, Mammoth Hot Springs, Yellowstone National Park, U.S.A.), Journal of Sedimentary Research: 70, p. 565 - 585.

Gardner, R.D., Crossey, L.J., Groffman, A., Sterling, J., 1996: Travertine mound springs along the eastern margin of the San Juan basin, Sandoval Co., NM: *in* Goff, F., Kues, B., Rogers, M., McFadden, L., Gardner, J., eds., New Mexico Geological Society Guidebook: Jemez Mtns. Region**,** p.12-13.

Gilfillan, S.M.V., Ballentine, C.J., Holland, G., Blagburn, D., Sherwood Lollar, B., Stevens, S. Schoell, M., and Cassidy, 2008: The noble gas geochemistry of natural CO2 gas reservoirs from the Colorado Plateau and Rocky Mountain provinces, USA, Geochimica et Cosmochimica Acta 72, p. 1174-1198.

Gilfillan, S.M.V., Sherwood Lollar, B., Holland, G., Blagburn, D., Stevens, S., Schoell, M., Cassidy, M., Ding, Z., Zhou, Z., Lacrampe-Couloume, G., and Ballentine, C.J., 2009: Solubility trapping in formation water as dominant CO2 sink in natural gas fields, Nature, v. 458, p. 614-618.

Goff, F. and Shevenell, L., 1987: Travertine deposits of Soda Dam, New Mexico, and their implications for the age and evolution of the Valles caldera hydrothermal system, Geological Society of America Bulletin, v. 99, p. 292-302.

Goldstein, S.J. and Stirling, C.H., 2003: Techniques for measuring Uranium-series nuclides: 1992-2002, Reviews in Mineralogy and Geochemistry 52 (1), p. 23-57, doi: 10.2113/0520023.

Hancock, P.L., Chalmers, R.M.L., Altunel, E., and Cakir, Z., 1999: Travitronics: Using travertine in active fault studies. Journal of Structural Geology, v. 21, p. 903-916, doi: 10.1016/S0191-8141(99)00061-9.

Haszeldine, R.S., Quinn, O., England, G., Wilkenson, M. Graham, C., Shipton, Z., Ballentine, C., Crossey, L., Evans, J., and Heath, J., 2005: Natural geochemical analogues for carbon dioxide storage in deep geological porous reservoirs, a United Kingdom perspective. Oil and Gas Science and Technology, v. 60, p. 33-49.

Holm, R.F., 2001: Pliocene-Pleistocene incision on the Mogollon Slope, Northern Arizona: Response to the developing Grand Canyon, *in* Young, R.A. and Spamer, E.E., eds., Colorado River origin and evolution, Proceedings of a symposium held at Grand Canyon National Park in June, 2000, p.59-63

Gilfillan, S.M.V, Ballentine, C.J., Holland, G., Blagburn, D., Lollar, B.S., Stevens, S., Schoell, M., Cassidy, M., 2008: The noble gas geochemistry of natural CO_2 gas reservoirs from the Colorado Plateau and Rocky Mountain provinces, USA, Geochimica et Cosmochimica Acta, v. 72, p.1174-1198.

Giggenbach, W.F., Sano, Y., and Wakita, H., 1993: Isotopes of He and CO_2 and CH_4 contents in gases produced along the New Zealand part of a convergent plate boundary, Geochimica et Cosmochimica Acta, v. 57, p. 3427-3455.

GIS geologic data, Arizona State Land Department http://www.land.state.az.us/alris

Goff, F. and Shevenell, L, 1987: Travertine deposits of Soda Dam, New Mexico, and their implications for the age and evolution of the Valles caldera hydrothermal system, GEOLOGICAL SOCIETY OF AMERICA Bulletin, v. 99, pp. 292-302.

Harper, R.W. and Anderson, T.W., 1976: Maps showing ground-water conditions in the Concho, St. Johns, and White Mountains areas, Apache and Navajo Counties, Arizona – 1975: USGS Water Resources Investigations 76-104, 4 sheets.

Hazeldine, R.S., Quinn, O., England, G., Wilkenson, M., Graham, C., Shipton, Z., Ballentine, C., Crossey, L., Evans, J., and Heath, J., 2005: Natural geochemical analogues for carbon dioxide storage in deep geological porous reservoirs, a United Kingdom perspective, Oil and Gas Science and Technology, v. 60, p. 33-49.

Hearn, E.H., Kennedy, B.M., and Truesdell, A.H., 1990: Coupled variations in helium isotopes and fluid chemistry: Shoshone Geyser Basin, Yellowstone National Park: Geochimica et Cosmochimica Acta, v. 54, p. 3103-3113.

Karlstrom, K.E., Crow, R.S., Peters, L., McIntosh, W., Raucci, J., Crossey, L.J., Umhoefer, P., Dunbar, N., 2007: 40Ar/39Ar and field studies of Quaternary basalts in Grand Canyon and model for carving Grand Canyon: Quantifying the interaction of river incision and normal faulting across the western edge of the Colorado Plateau, GSA Bulletin, v. 119, no. 11/12, p. 1283-1312.

Laughlin, A.W., Damon, P.E. and Shafiqullah, M., 1980: New K-Ar dates from the Springerville volcanic field, central Jemez Zone, Apache County, Arizona, Isochron/West, no.29, p.3-4.

Laughlin, A.W., Brookins, D.G., Damon, P.E., and Shafiqullah, M.: 1979, Late Cenozoic volcanism of the central Jemez Zone, Arizona-New Mexico, Isochron/West, no.25, p.5-7.

Lu, G., Zheng, C., Donahoe, R.J., and Berry Lyons, W., 2000: Controlling processes in a Ca CO_3 precipitating stream in Huanglong Natural Scenic District, Sichuan, China, J. of Hydrology, v. 230, p. 34-54.

McKee, E.D., and McKee, E.H., 1972: Pliocene uplift of the Grand Canyon Region – Time of drainage adjustment, Geological Society of Americ Bulletin, v. 83, p. 1923-1932.

McIntosh, W.C. and Cather, S.M., 1994: $^{40}Ar/^{39}Ar$ geochronology of basaltic rocks and constraints on late Cenozoic stratigraphy and landscape developments in the Red Hill-Quemado area, New Mexico, New Mexico Geological Society Guidebook, 45th Field Conference, Mogollon Slope, West-Central New Mexico and East-Central Arizona, 1994, p.209-224.

McIntosh, W.C. and Chamberlin, 1994: $^{40}Ar/^{39}Ar$ geochronology of middle to late Cenozoic ignimbrites, mafic lavas, and volcaniclastic rocks in the Quemado region, New Mexico, New Mexico Geological Society Guidebook, 45th Field Conference, Mogollon Slope, West-Central New Mexico and East-Central Arizona, 1994, p.165-185.

Moore, J., Adams, M., Allis, R., Lutz, S., and Rauzi, S., 2005: Mineralogical and geochemical consequences of the long-term presence of CO2 in natural reservoirs; an example from the Springerville-St. Johns field, Arizona, and New Mexico, USA, *In* Geochemical aspects of CO_2 sequestration, Chemical Geology, 217 (3-4), p. 365-385.

Moore, J., Adams, M., Allis, R., Lutz, S., and Rauzi, S., 2003: CO_2 Mobility in Natural Reservoirs Beneath the Colorado Plateau and Southern Rocky Mountains: An Example from the Springerville-St. Johns Field, Arizona and New Mexico, Second Annual Conference on Carbon Sequestration, 22 pp.

Newell, D.L., Crossey, L.J., Karlstrom, K.E., Fischer, T.P., and Hilton, D.R., 2005: Continental-scale links between the mantle and groundwater systems of the western United States: Evidence from travertine springs and regional He isotope data, GSA Today, v.15, no.12, p. 4–10.

O'Brien, G., Kaufman, D., Sharp, W. Atudorei, V., Parnell, R., Crossey, L., 2006: Oxygen isotope composition of modern and mid-Holocene banded travertine, Grand Canyon, Arizona, USA, Quaternary Research, v. 65, p. 366-379.

Parkhurst, D.L., 1995: User's guide to PHREEQC – A computer program for speciation, reaction-path, advective-transport, and inverse geochemical calculations: U.S. Geological Survey Water Resources Investigations Report 2004-5146, 56 pp.

Pedley, M., 2009: Tufas and travertines of the Mediterranean region: a testing ground for freshwater carbonate concepts and developments, Sedimentology, v. 56, p. 221-246.

Potochnik, A.R., 1989: Depositional style and tectonic implications of the Mogollon Rim Formation (Eocene), East-Central Arizona, New Mexico Geological Survey Guidebook, 40th Field Conference, Southeastern Colorado Plateau, 1989, p. 107-118.

Potochnik, A.R., 2001: Paleogeomorphic evolution of the Salt River Region: implications for Cretaceous-Laramide inheritance for Ancestral Colorado River drainage, *in* Young, R.A. and Spamer, E.E., eds., Colorado River origin and evolution, Proceedings of a symposium held at Grand Canyon National Park in June, 2000, p. 17-22.

Putirka, K. and Condit, D.D., 2003: Cross section of a magma conduit system at the margin of the Colorado Plateau, Geology, v. 31, no. 8, p. 706-704.

Putirka, K.D and Condit, C.D., 2002: An interior view of the Springerville volcanic field, AZ, magma plumbing system: Eos, Transactions, American Geophysical Union, v.83, no.47, Suppl., p.1431.

Rauzi, Steven L., 2003: Review of helium production and potential in Arizona, Arizona Geological Survey Open-File Report 03-05, 29 pp.

Rauzi, Steven L., 1999: Carbon Dioxide in the St. Johns-Springerville Area, Apache County, Arizona, Arizona Geological Survey Open-File Report 99-2, 22 p.

Raymo, M.E. and Ruddiman, W.F., 2004: DSDP site 607 isotope data and age models, IGBP PAGE/World Data Center for Paleoclimatology, Data Contribution Series #2004-010, NOAA/NGDC Paleoclimatology Program, Boulder, CO, USA.

Scarborough, R., 2001: Neogene development of Little Colorado River Valley and eastern Grand Canyon: field evidence for an overtopping hypothesis, *in* Young, R.A. and Spamer, E.E., eds., Colorado River origin and evolution, Proceedings of a symposium held at Grand Canyon National Park in June, 2000, p. 207-212.

Shackleton, N.J. and Pisias, N.G., 1985: Atmospheric carbon dioxide, orbital forcing, and climate, In Sundquist, E.T. and Broeker, eds, The carbon cycle and

atmospheric CO_2: natural variations Archaen to present , Geophysical Monograph 32, p. 412-417.

Sirrine, G.K., 1958: Geology of the Springerville-Saint Johns area, Apache County, Arizona, PhD thesis, University of Texas, Austin, 248 pp.

Spence, W. and Gross, R.S., 1990: A tomographic glimpse of the upper mantle source of magmas of the Jemez lineament, New Mexico, Journal of Geophysical Research, v. 95, no. B7, p. 10,829-10,849.

Stone, Claudia, 1979: An overview of the geothermal potential of the Springerville area, Arizona, Arizona Geological Survey Open-File Report 79-2a, 25 pp.

U.S. Geological Survey water quality data, http://waterdata.usgs.gov/nwis/qw

U.S. Geological Survey and Arizona Geological Survey, 2006, Quaternary fault and fold database for the United States, accessed 16 November, 2008 from USGS web site: http//earthquake.usgs.gov/regional/qfaults/.